**UNIVERSITA' VITA-SALUTE SAN RAFFAELE**

**CORSO DI DOTTORATO DI RICERCA INTERNAZIONALE IN MEDICINA MOLECOLARE**

**Curriculum in Neuroscience and Experimental Neurology**

# REPOSITIONING OF NIACIN/NIASPAN® FOR THE THERAPY OF CHARCOT-MARIE-TOOTH NEUROPATHIES WITH FOCAL HYPERMYELINATION

DoS: Prof. Alessandra Bolino

Second Supervisor: Prof. Guido Angelo Cavaletti

Tesi di DOTTORATO di RICERCA di Silvia Cipriani

matr. 015569

Ciclo di dottorato XXXV

SSD BIO/13

Anno Accademico 2021/2022

**CONSULTAZIONE TESI DI DOTTORATO DI RICERCA**

Il/la sottoscritto/*I* SILVIA CIPRIANI

Matricola / *registration number* 015569

nat_ a/ *born at* SANSEPOLCRO (AR)

il/*on* 24/10/1993

autore della tesi di Dottorato di ricerca dal titolo / *author of the PhD Thesis titled*

*REPOSITIONING OF NIASPAN®/NIACIN FOR THE THERAPY OF CHARCOT-MARIE-TOOTH NEUROPATHIES WITH FOCAL HYPERMYELINATION*

X AUTORIZZA la Consultazione della tesi / AUTHORIZES *the public release of the thesis*

□ NON AUTORIZZA la Consultazione della tesi per …… mesi /DOES NOT AUTHORIZE *the publicrelease of the thesis for …… months*

a partire dalla data di conseguimento del titolo e precisamente */ from the PhD thesis date,specifically*

Dal / *from* ……/……/…… Al / *to* ……/……/……Poiché /*because*:

□ l'intera ricerca o parti di essa sono potenzialmente soggette a brevettabilità/ *The wholeproject or part of it might be subject to patentability;*

□ ci sono parti di tesi che sono già state sottoposte a un editore o sono in attesa di pubblicazione/ *Parts of the thesis have been or are being submitted to a publisher or are in press;*

□ la tesi è finanziata da enti esterni che vantano dei diritti su di esse e sulla loro pubblicazione/ *the thesis project is financed by external bodies that have rights over it andon its publication.*



Data /Date 12/10/2022 Firma /Signature

# DECLARATION

This thesis has been composed by myself and has not been used in any previous application for a degree. Throughout the text I use both 'I' and 'We' interchangeably.

All the results presented here were obtained by myself, except for:

1) *Sciatic nerve crush and cut experiments in Mtmr2$^{-/-}$ and Pmp22 $^{+/-}$ mice (paragraph 3.2) were always performed together with Dr. Emanuela Porrello and Dr. Previtali, Neuromuscular Repair Unit, INSPE, San Raffaele Scientific Institute, Milan,Italy.*

2) *Morphological and morphometrical analyses on Pmp22$^{+/-}$ mice after sciatic nerve crush (paragraph 3.2.1) were performed together with Dr. Alessio Gioia, Dr. Emanuela Porrello, Dr. Previtali, Neuromuscular Repair Unit, INSPE, San Raffaele Scientific Institute, Milan,Italy.*

3) *Neurophysiological analyses (paragraphs 3.2.1;3.2.2;3.3.3) were performed by Dr. Ubaldo del Carro, Dr. Francesca Bianchi and Dr. Valenzano Serena, Neurophysiology Unit, San Raffaele Scientific Institute, Milan, Italy.*

4) *Pharmacokinetics studies (paragraphs 3.3.1) were performed by Eurofins, France.*

5) *Niacoat-SR formulation (paragraphs 3.3.1) was performed in collaboration with Prof. Andrea Gazzaniga, Dr. Matteo Cerea and Ottilia Andreola, Department of Pharmaceutical Sciences, University of Milan "La Statale", Milan, Italy.*

6) *Histological analyses on liver,gut and kidney samples (paragraphs 3.3.2; 3.3.3) were performed by Dr. Fiocchi Amleto, Animal Histopathology Unit, San Raffaele Scientific Institute, Milan, Italy. Clinical interpretation of the results was done by Dr. Francesca Sanvito, Pathology Unit, San Raffaele Scientific Institute, Milan, Italy.*

7) *Bio clinical analyses on mice serum (paragraph 3.3.3) were performed by Dr. Michele Raso, Animal Biochemistry Facility, San Raffaele Scientific Institute, Milan, Italy.*

8) *Plasmatic Neurofilament-light chain (NF-L) levels analysis (paragraphs 3.3.3; 3.3.4) was performed by Dr. Amanda Heslegrave, UK Dementia Research Institute, UCL, London, UK.*

9) *Transcriptome analyses on Mtmr2$^{-/-}$ mice (paragraph 3.3.3) were performed by Dr. Puo Duong and Prof. John Svaren, Department of Comparative Biosciences, School of Veterinary Medicine, University of Wisconsin-Madison, USA.*

10) *Niacoat-SR administration in Mtmr2$^{-/-}$ mice (paragraph 3.3.2; 3.3.3) was performed in collaboration with CRL (Charles River Laboratories), San Raffaele Scientific Institute, Milan, Italy.*

11) *Mouse genotyping and morphological analyses on Mtmr2$^{-/-}$ semithin sections (3.3.3) were performed together with Dr. Roberta Di Guardo. Human Inherited Neuropathies Unit, San Raffaele Scientific Institute, Milan, Italy.*

12) *Gpr109a mRFPmice (paragraph 3.1) were provided by Prof. Stephen Offermanns, Department of Pharmacology, Max-Planck-Institute for Heart and Lung Research, Bad Nauheim, Germany.*

13) *Immunostaining protocol on spinal cord sections (paragraph 3.1) was optimized in collaboration with Dr. James Sleigh and Prof. G. Schiavo, UCL Queen Square Institute of Neurology, London, UK.*

14) *Figure 1 pag. 13 permission is currently being processed by the journal permission office (journalpermissions@tandf.co.uk) and it will take weeks to be obtained. I will then display it on this thesis by applying the principle of "fair use" for academic purposes.*

All sources of information are acknowledged by means of reference.

# ACKNOWLEDGEMENTS

First, I would like to thank my DoS Prof. Alessandra Bolino for the opportunity she gave me to join her lab and to do my PhD considering my personal aspirations and interests. I am very happy for everything I have learnt during these years.
I would like to thank also my Second Supervisor Prof. Guido Angelo Cavaletti and my tutor Prof. Angelo Quattrini, for our interesting discussions which supported and helped me in every step of my PhD project.

A special thanks goes to Prof. Stefano Previtali and Dr. Emanuela Porrello for their incredible and continuous support during these years, particularly for their help and know-how in nerve regeneration.

A huge thanks goes to all my actual and former colleagues with whom I shared my lab days: Valeria A., Marta G-V., Federica G., Marianna M., Eleonora C., Francesca S., Claudia L., Stefania Ba., Silvia R., Federica R., Stefania Br., Melissa Z., Roberta D. G.. Each one of them contributed to both my professional and personal growth while helping and supporting me in the achievement of this important goal. A special thanks goes to Roberta D.G., who has been my "wing woman" since the very beginning of this journey.

A friendly and grateful thanks also to all the lab members of the Open Space ($6^{th}$ floor) who have been my big-varied-hilarious family for the past four years. A special thanks goes to Dr. Cristina Rivellini for all her precious advices and help.

Finally, I would like to thank all the people working in the Division of Neuroscience, in the Alembic Facility and in all the other facilities/labs of San Raffaele Hospital, in particular the ones with whom I collaborated with, giving me the opportunity to learn new things every time. I would like to thank FCSR (Fondazione Centro San Raffaele) to have financially supported my PhD with the FCSR-fellowship Fronzaroli assigned together with the PhD position.

I am very grateful to all our external collaborators which contributed to the realization of this project: Prof. A. Gazzaniga and Dr. Matteo Cerea, Prof. G. Schiavo, Prof J. Svaren

and Dr. Puo Duong, Prof. A. Rossor and Dr. Amanda Heslegrave, Prof. S. Offermans, Eurofins (France) and Charles-River Laboratories (CRL). Their specific contributions are described in “Declaration”.

Last (but not least), I am plenty of gratitude for all the people, starting from my family and friends, who never stopped believing in me and in my abilities reminding me who I was, despite all.
If I am here today is also because of them.

# DEDICATION

*To Sally,*

*who believed in me, inspired me and gave me*
*the motivation and strength to begin this journey.*

# ABSTRACT

Charcot-Marie-Tooth (CMT) neuropathies are among the most frequent forms of neuromuscular disorders with a common prevalence of 1:2500 and currently no available treatment (Rossor *et al*., 2016; Nagappa *et al*., 2022). CMTs can be primarily classified in demyelinating or axonal forms based on neurophysiological and clinical criteria. Among demyelinating forms, CMT4B1 with myelin outfoldings and HNPP (Hereditary neuropathy with liability to pressure palsies) with tomacula are two clinical forms characterized by excessive focal myelin.

Axonal Neuregulin 1 (NRG1) type III orchestrates PNS myelination by modulating Schwann cells (SCs) fate to become myelinating or non-myelinating cells and by regulating myelin thickness (Taveggia *et al.*, 2005; Salzer, 2015). NRG1 type III is negatively processed by the axonal TACE secretase (Tumor necrosis factor-alpha converting enzyme), which activity can be enhanced by Niacin (nicotinic acid) (Chen *et al.*, 2007; Chen *et al*., 2009; La Marca *et al*., 2011; Fleck *et al*., 2013).

**We thus hypothesized that Niacin, by enhancing TACE activity and reducing NGR1-mediated myelination signalling, may represent an effective strategy to ameliorate CMT neuropathies with focal hypermyelination.**

We had already demonstrated as proof-of-principle that Niacin/Niaspan® (a FDA-approved, extended-release formulation of Niacin) is able to increase TACE activity and to ameliorate CMT4B1 and HNPP phenotypes in both *in vitro* and *in vivo* models (Bolino *et al*., 2016).

In the perspective of a clinical application of this drug, we aimed at refining the treatment protocol, particularly in a long-term treatment setting. Both CMT4B1 and HNPP are chronic diseases which progress to degeneration and fibres loss with age. Thus, we also tested whether Niacin administration can be beneficial during nerve development, but not detrimental during disease progression, by interfering with the physiological attempt of the nerve to remyelinate and regenerate. Finally, we also tried to elucidate niacin mechanism of action in the PNS by checking GPR109A receptor expression, since it is known to be the principal mediator of niacin effects in other tissues.

Our data indicate that Niacin can mainly exert a neuroprotective effect both when chronically given for 6 months and after nerve injury.

# TABLE OF CONTENTS

# ACRONYMS AND ABBREVIATIONS

| | |
|---|---|
| **2PY** | N-Methyl-2pyridone-5-Carboxamide |
| **4PY** | N-Methyl-4-Pyridone-5-Carboxamide |
| **AAV** | Adeno-associate Virus |
| **ADAM17/22** | A Disintegrin and Metalloprotease 17/22 |
| **AKT** | v-Akt Murne Thymoma Viral Oncogene Homolog |
| **ALT** | Alanine Transferase; |
| **AQP7** | Aquaporin 7 |
| **ARI**A | Acetylcholine Receptor Inducing Activity |
| **ASOs** | Antisense Oligonucleotides |
| **AST** | Aspartate-Amino Transferase |
| **ATP** | Adenosine Triphosphate |
| **BACE1** | BACE-1 β-Secretase |
| **BBB** | Blood-Brain-Barrier |
| **BDNF** | Brain Derived Neurotrophic Factor |
| **BNB** | Blood-Nerve-Barrier |
| **BSA** | Bovine Serum Albumin |
| **c-Myc** | c-Myelocytomatosis Oncogene Product. |
| **CASPR-2** | Contactin asccoiated protein-2 |
| **Caspr-2** | Contactin associated protein-2 |
| **CCL2** | C-C Motif Chemokine Ligand 2 |
| **CCR2** | C-C Motif Chemokine Receptor 2 |
| **ChAT** | Choline Acetyltransferase, alpha-motor neurons marker |
| **cKO** | Conditional Knock-out |
| **CMT** | Charcot-Marie-Tooth |
| **CNS** | Central Nervous System |
| **CSF1** | Colony Stimulating Factor 1 |
| **DAPI** | 4’,6-diamino-2-phenylindole |
| **DGAT2** | Diacylglycerol acyltransferase-2 |
| **DNA** | Deoxyribonucleic Acid |
| **DP(S)NI** | Days Post (Sciatic) Nerve Injury |

| | |
|---|---|
| **DRG** | Dorsal Root Ganglia |
| **E** | Embrionic day |
| **ECL** | Enhanced Chemiluminescence |
| **EGF** | Epithelial Growth Factor |
| **eIF4A** | Eukaryotic Initiation Factor-4A |
| **EMT** | Epithelial-to Mesenchymal Transition |
| **EPHB2** | Ephrin type-B receptor 2 |
| **ER** | Extended-Release |
| **ERBB3/B2** | Erythroblastic Leukaemia Viarl Oncogene Homoplog 2/3 |
| **ERK 1 / 2** | Extracellular Signal-Regulated Kinase 1/2 |
| **FDA** | Food and Drug Administration |
| **FFA** | Free-Fatty Acid |
| **FITC** | Fluorecein Isothiocyanate |
| **FOXD3** | Forkhead Box D3 |
| **GDF10** | Growth Differentiation Factor 10 |
| **GDNF** | Glial Derived Neurotrophic Factor |
| **GFAP** | Glial Fibrillary Acid protein |
| **GGF** | Glial Growth Factor |
| **GPR109a** | G protein-coupled receptor 109a |
| **Hif-α** | Hypoxia-Inducible Factors α |
| **HMSN** | Hereditary Motor And Sensory Neuropathies |
| **HNPP** | Hereditary Neuropathy With Liability To Pressure Palsies |
| **i.p**. | Intraperitoneal Injection |
| **IDL** | Intermediate-Density Lipoprotein |
| **IGF2** | Insulin Growth Factor 2 |
| **Il-1** | Interleukin -1 |
| **ILP** | Intraperiod Lines |
| **IR** | Immediate Release |
| **JAM-C** | Junctional Adhesion Molecule-C |
| **JNK** | C-Jun N-Terminal Kinase |
| **KO** | Knock-out |
| **KROX 20** | Early Growth Response 2 |

| | |
|---|---|
| **L-PGDS** | Prostaglandin D2 Synthase |
| **L1** | Neural Cell Adhesion Molecule L1 |
| **LC3-II/I** | Microtubule-associated protein 1 light chain 3 II and I |
| **LDL** | Low-Density Lipoprotein |
| **LIF** | Leukemia Inhibitory Factor |
| **LIPE** | Lipase E hormone sensitive type |
| **LPA** | Lysophosphatidic acid |
| **LPL** | Lipoprotein lipase |
| **MAG** | Myelin Associated Glycoprotein |
| **MBP** | Myelin Basic Protein |
| **MC** | Methylcellulose |
| **MCP-1** | Monocyte Chemoattractant Protein-1 |
| **MDL** | Major Dense Line |
| **MKK7** | Mitogen-Activated Protein Kinase Kinase 7 |
| **MNA** | N-Methylnicotinamide |
| **MNCV** | Motor Nerve Conduction Velocity |
| **MPZ** | Myelin Protein Zero |
| **MTMR2** | Myotubularin-Related 2 Gene |
| **mTORC 1/2** | Mechanistic Target Of Rapamycin Kinase Complex 1/2 |
| **$NAD^+$** | Nicotinamide Adenine Dinucleotide |
| **NAM** | Nicotinamide |
| **Nav1.X** | Voltage-gated $Na^+$ channels |
| **NBR1** | Neighbor of BRCA1 gene 1 |
| **NCAM 1** | Neural Cell Adhesion Molecule 1 |
| **NCCs** | Neural Crest Cells |
| **NeuN** | Neuronal Nuclear Protein |
| **NF-L** | Neurofilament-Light Chain |
| **NF-M** | Neurofilament Medium Chain |
| **NGF** | Nerve Growth Factor |
| **NGS** | Normal Goat Serum |
| **NMN** | Nicotinamide Mononucleotide |
| **NMNAT2** | Nicotinamide Nucleotide Adenylyltransferase 2 |

| | |
|---|---|
| **NrCAM** | Neural Cell Adhesion Molecule |
| **NRG1** | Neuregulin-1 |
| **NT3** | Neurotrophin 3 |
| **NUA** | Nicotinuric Acid |
| **OLIG 1** | Oligodendrocyte Transcription Factor 1 |
| **P** | Postnatal day |
| **P0** | Protein 0 |
| **P75NTR** | P75 Neurotrophin Receptor |
| **PBS** | Phosphate Buffer Saline |
| **PCR** | Polymerase Chain Reaction |
| **PDG** | L-periaxin-DPR2-dystroglycan complex |
| **PDGFB** | Platelet-derived Growth Factor |
| **PDK1** | 3-Phosphoinositide Dependent Protein Kinase 1 |
| **$PGD_2$** | Prostaglandin D2 |
| **$PGE_2$** | Prostaglandin E2 |
| **$PGJ_2$** | Prostaglandin J2 |
| **$PI(3,5)P_2$** | Phosphatidyilinositol 3,5-biphosphate |
| **PI3K** | Phosphatidyl-Inostitol-3 Kinase class I |
| **PI3P** | Phosphatidyilinositol 3-phosphate |
| **$PIP_2$** | Phosphatidylinositol (4,5)-biphosphate |
| **$PIP_3$** | Phosphatidylinositol (3,4,5)-triphosphate |
| **$PLA_2$** | Phospholipase $A_2$ |
| **PLIN1** | Perilipin 1 |
| **PMP22** | Peripheral Myelin Protein 22 |
| **PNS** | Peripheral Nervous System |
| **PPARγ** | Peroxisome Proliferator-activated Receptor gamma |
| **PRAS 40** | Proline-rich Akt Substrate of 40 KDa |
| **PS6K** | Phospho p70-S6 Kinase |
| **PTEN** | Phosphatase and Tensin Homolog on chromosome 10 |
| **RAG** | Regeneration-associated Genes |
| **RDA** | Daily Recommended Allowance |
| **RFP** | Red Fluorescent Protein |

| | |
|---|---|
| **RNA** | Ribonucleic Acid |
| **S6 rp** | S6 Ribosomal Protein |
| **SARM1** | Sterile Alpha and Toll/interleukin-1 Receptor Motif 1 |
| **SCD1** | Stearoyl-CoA Desaturase |
| **SCPs** | Schwann cells Precursors |
| **SCs** | Schwann Cells |
| **SD** | Standard Deviation |
| **SDS-page** | Sodium Dodecyl Sulphate- polycramide gel electrophoresis |
| **SEM** | Standard Error of Mean |
| **SHH** | Sonic Hedgehog |
| **shRNA** | Short Hairpin RNA |
| **SLI** | Schmidt-Lanterman Incisures |
| **SOX 10** | SRY-Box Transcription Factor 10 |
| **SR** | Sustained-Release |
| **SREBPF1** | Sterol Regulatory Element Binding Transcription Factor 1 |
| **SREBPs** | Sterol Regulatory Element-Binding Proteins |
| **TACE** | Tumor Necrosis Factor- α-Converting-Enzyme |
| **TBC** | Tre-2/Bub2/Cdc16 |
| **TG** | Triglycerides |
| **TLRs** | Toll-like receptors |
| **TNFα** | Tumor Necrosis Factor- α |
| **TRITC** | Tetramethylrhodamine Isothiocyanate |
| **TSC** | Tuberous Sclerosis Complex |
| **UCP1** | Uncoupling protein 1 |
| **VEGF** | Vascular Endothelial Growth Factor |
| **VLDL** | Very Low-Density Lipoproteins |
| **WD** | Wallerian Degeneration |
| **WT** | Wildtype |

# LIST OF FIGURES AND TABLES

# 1.INTRODUCTION

## 1.1 The Peripheral Nervous System (PNS)

### *1.1.1 General structure and organization*

The peripheral nervous system (PNS) is usually defined as the neural tissue branching out the cranial vault and the vertebral canal, which connects, both structurally and functionally, the central nervous system (CNS) with all the peripheral body tissues. Anatomically, it is composed of peripheral nerves and ganglia, which transmit motor and sensory impulses between the two compartments.

Peripheral nerves are classified into cranial nerves (12 pairs) and spinal nerves (31 pairs) according to their physical exit from the CNS. Cranial nerves mostly innervate head and neck regions (except from the *vagus* which also innervates thoracic and abdominal organs) and they can be motor, sensory, or mixed. Spinal nerves are clustered in five different groups (cervical, thoracic, lumbar, sacral, and coccygeal) in relation to their exit level along the spinal cord.

Each spinal nerve is composed of several rootlets that converge in the anterior and the posterior root. The anterior one originates from neurons, whose bodies are placed in the anterior horn of the spinal cord and contains motor fibres (efferent neurons or motor neurons). The posterior one originates from the posterior horn of the spinal cord and contains sensory fibres coming from neuronal bodies located in the dorsal root ganglia (afferent neurons). The anterior and posterior root then merge to form the spinal nerve (mixed nerve), which eventually carries both motor and sensory fibres (Dyck P.J & Thomas P.K., 2005). Accordingly, PNS regulates a variety of functions, ranging from voluntary (e.g., skeletal muscle contraction) and involuntary (e.g., gland secretion) motor responses to sensorial information (e.g., pain, temperature, smell, vision, etc…).

### *1.1.2 Anatomy of a peripheral nerve*

Peripheral nerves are composed of motor and/or sensory fibres trough which they send impulses and information from the CNS towards the periphery and vice versa.

They are externally surrounded by a layer of fibrous connective tissue called *epinerium* and internally organized into fascicles containing multiple axons. Axons can be myelinated by multiple Schwann cells or can be clustered with non-myelinating Schwann

cells to form Remak bundles. Each fascicle is in turn surrounded by another layer of fibrous connective tissue called *perineurium* and, finally, each axon, is surrounded by loose connective tissue called *endoneurium* (**Figure 1**).

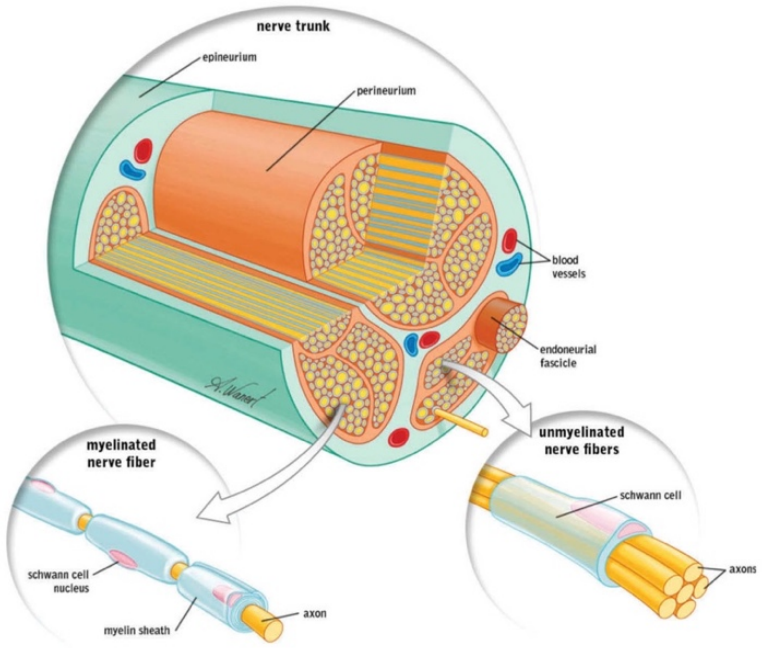


***Figure 1. Anatomy of a peripheral nerve.***
*Internal organization of a peripheral nerve highlighting structural differences between myelinated and unmyelinated fibres (Ilfeld B.M., et al., 2016).*

The *epinerium* contains type I collagen, fibroblasts, adipose tissue, and a vascular network called *vasa nervorum*, which is the main vascular support of the nerve. These vessels enter the *epinerium* and reach the *endoneurium* after crossing the *perineurium.* At the *epinerium* level, vessels are quite permeable whereas starting from the *perineurium,* endothelial cells of arterioles and capillaries interconnect through tight junctions. These complexes create the blood-nerve barrier, which is essential to regulate the homeostasis of the endoneural fluid. The maintenance of the ionic composition and pressure of the fluid allows axons to efficiently conduct the action potential and to have good nerve fibres perfusion. The *perineurium* is composed of multiple layers of perineural cells which mutually interconnect through gap junctions (external layers) and tight junctions (internal layers). Finally, the *endoneurium* mainly consists of longitudinally oriented type I and type II collagen fibres immersed in the endoneural fluid, together with fibroblasts, macrophages, mast cells and small anastomosed capillaries. This fine network of collagen

fibres interacts with both myelinating and non-myelinating Schwann basal lamina, which, in turn, is composed of type IV collagen, fibronectin, laminin and heparan sulfate (Dyck P.J & Thomas P.K., 2005).

### *1.1.3 Structural and functional domains of myelinated axons*

Motor fibres are composed of myelinated axons which are essential for the rapid propagation of action potentials by means of saltatory conduction (Salzer, 2015).

Myelin is a multilamellar membrane, which provides electrical insulation around the axon, while communicating with both neurons and the environment (Bolis *et al*., 2009).

Different structural and functional domains can be defined along a myelinated axon: the internode, the paranode, the juxtaparanode and the node of Ranvier (**Figure 2**).

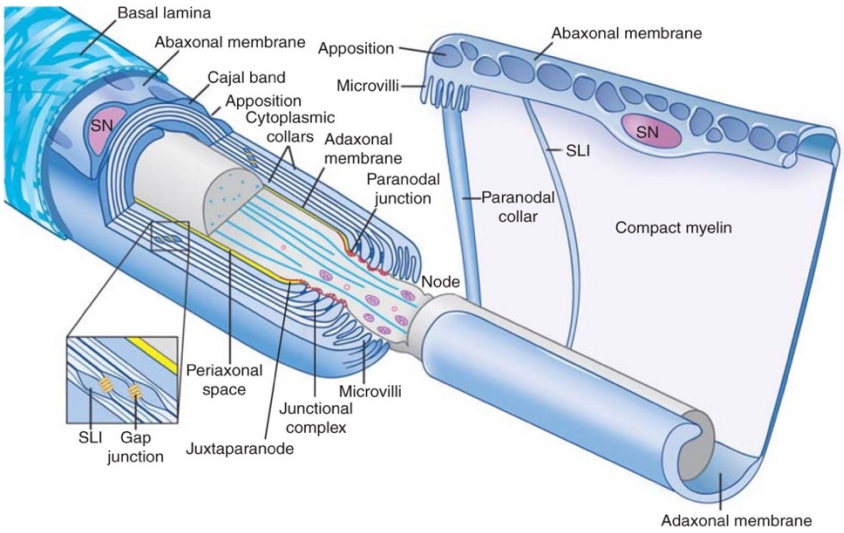


***Figure 2. Microanatomy of a myelinated axon.***
*Schematic representation showing internal compartments formed by Schwann cells wrapping around an axon. On the left: Schwann cell longitudinal section; On the right: unwrapped Schwann cell (Salzer , 2015).*

The myelin internode is on average 0.5mm long and it physically separates two nodes of Ranvier. It can be divided into two domains: 1) non-compact myelin and 2) compact myelin.

**Non-compact myelin** includes all the subdomains containing cytoplasm such as: the inner and outer mesaxon, the microvilli, the Schmidt-Lanterman incisures (SLI), the paranodal loops and the Cajal bands (**Figure 2**). These structures allow communication and cytoplasmic continuity between the outer and the inner portion of the myelin

internode. Specifically, SLI are cytoplasmic channels which traverse compact myelin with a 9 degrees angle from the abaxonal to the adaxonal surface. They are abundant at the perinuclear and paranodal regions and their number is directly proportional to myelin sheath thickness. They mediate ions radial diffusion across the internode through Gap Junctions (Connexin-32, -26, -43), and they probably contribute to myelin formation during early stages because of their role in protein and lipids transport (Salzer, 2003; Trapp & Kidd, 2004).

The paranodal regions constitute the lateral extremities of the myelin internode. They are made up of Schwann cells cytoplasm loops longitudinally disposed and spirally wrapped around the axon (**Figure 2**). Adjacent paranodal loops mutually interact through adherens junctions (E-cadherin, β-catenin, and MAG-Myelin Associated Glycoprotein), and contact the axolemma through specific junctional complexes named septate-like junctions. These structures are composed of axonal Contactin and Caspr, which bind glial Neurofascin 155, thereby becoming the major adhesion points between myelin and axon (Salzer, 2003; Trapp & Kidd, 2004). This tight axo-glial interaction enables to spatially separate $Na^+$ and $K^+$ channels, which is required for proper action potential conduction. $K^+$ channels (Kv1.1 and Kv1.2) are expressed at the juxtaparanodal sites, which extend for 10-15nm before the paranode (Trapp & Kidd, 2004; Nave, 2010; Stassart *et al*, 2018). The presence of adhesion molecules like Caspr-2 (Contactin associated protein-2) contributes to channels localization and clustering, which is essential for potassium outflux during repolarization (Trapp & Kidd, 2004).

Voltage-gated $Na^+$ channels (Nav1.X) are instead positioned in the nodal axolemma, where the saltatory conduction occurs (Nave, 2010; Trapp & Kidd, 2004). Here, channels are stabilized by adhesion molecules such as NrCAM (neural cell adhesion molecule), Neurofascin 186 on the axonal site and gliomedin on glial site, and by the ankyrin G protein, which connects them to the sub membranous cytoskeleton, containing spectrin and f-actin (Trapp & Kidd, 2004).

The node is then a small portion of the axolemma delimited by two internodes. Its length depends on axonal diameter, and normally ranges between 1 to 5μm. In this region, axons are in direct contact with the extracellular matrix and with Schwann cell microvilli, another portion of non-compact myelin coming from the final processes of contiguous myelin segments (Trapp & Kidd, 2004).

Overall, myelinated fibres appear to be both longitudinally and radially polarized structures. The longitudinal polarity is defined in relation to the node of Ranvier, whereas the radial polarity is considered in relation to myelin sheath development from the axon to the basal lamina (**Figure 2**).

Schwann cells (SCs) abaxonal surface interacts with the surrounding basal lamina through integrins, laminins and dystroglicans, which also play an important role during radial sorting (Feltri *et al*., 2016). The abaxonal compartment includes SCs nucleus and Cajal bands, cytoplasmic channels interrupted by periodical appositions of the abaxonal membrane with the outer layer of compact myelin, stabilized by the L-periaxin-DPR2-dystroglycan (PDG) complexes (Trapp & Kidd, 2004; Sherman & Brophy, 2005).

On the other side, Schwann cells adaxonal surface is separated from the axon by a space of around 15nm called periaxonal region (Trapp & Kidd, 2004). In this area, several molecules expressed by both axons and glial cells are involved to establish and maintain their interaction such as MAG and nectin-like proteins (e.g. Necl-1,-2,-4) (Salzer *et al*, 2008; Salzer, 2015).

**Compact myelin** accounts for most of the myelin sheath and it is composed of multiple layers of Schwann cells membrane wrapped around the axon. During compaction, cytoplasm is extruded, thus enabling the formation of insulating units, which prevent ion exchange and dispersion along the axon, and favour saltatory conduction at node sites (Trapp & Kidd, 2004). The apposition between the different extracellular leaflets generates the so called intraperiod lines (IPL), whereas the cytoplasmic membrane leaflets of adjacent lamellae fuse to form the major dense line (MDL).

This organized and periodic structure is maintained by different proteins, which account for the 20-30% of total myelin (the remaining 70-80% are lipids). Among all, P0 and Peripheral Myelin Protein (PMP-22) proteins are responsible for preserving the periodicity of myelin membrane, while Myelin Basic Protein (MBP), together with P0 cytoplasmic segments stabilizes the MDL (**Figure 3**), (Trapp & Kidd, 2004).

P0 protein represents the 70% of all proteins in the PNS. It is a type I transmembrane glycoprotein of 30 kDa with both an extracellular and cytoplasmic domain. Through the extracellular immunoglobulin-like domain, it forms tetramers in cis and interacts with other P0 tetramers in trans (on the opposing plasma membrane) (Trapp & Kidd, 2004).

PMP-22 is a tetraspanin and hydrophilic protein of 22kDa, expressed by myelinating Schwann cells and Dorsal Root Ganglia (DRG) (D'Urso &Müller, 1998). Its expression has also been reported in non-neural tissues, even if its function there remains unknown (Notterperk *et al*., 2001). In addition to its structural role in the maintenance of compact myelin, it also acts as growth arrest protein in myelinating Schwann cells, whereas during development, it promotes tissue differentiation (Trapp & Kidd, 2004).

Finally, MBP is expressed on the cytoplasmic surface, and it is thought to neutralize negatively charged lipids by binding phosphatidylserine residues. It helps the stabilization of the MDL together with P0. (Trapp & Kidd, 2004; Kidd *et al*, 2013; Salzer, 2015).

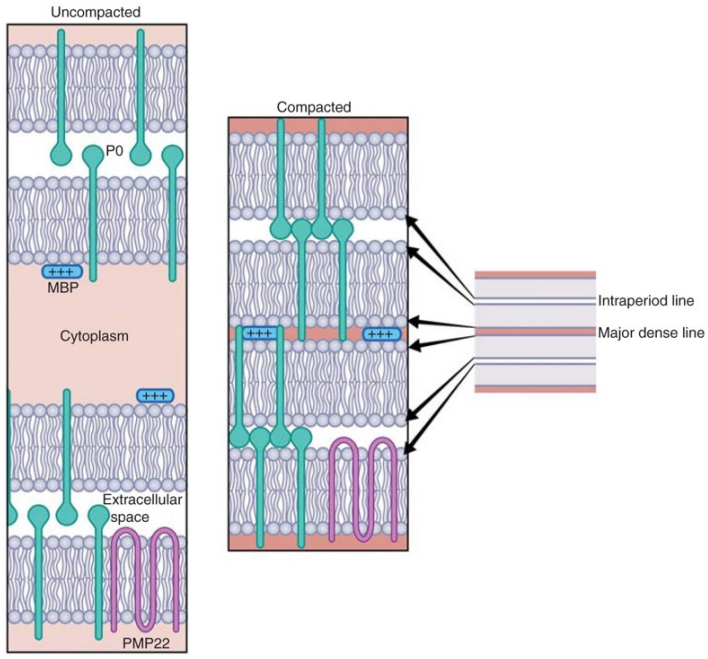


***Figure 3. Structural organization of compact myelin.***
*Schematic representation showing proteins and interactions responsible for the maintenance of myelin sheath structure and periodicity (Salzer et al., 2015).*

## 1.2 The myelination process in the Peripheral Nervous System

### *1.2.1 Schwann cell development: origin and fate towards myelination*

Schwann cells are the most abundant glial cell type in the PNS (Ino & Iino, 2017). During embryonic development, they originate from multipotent neural crest cells (NCCs), which derive from the dorsal portion of the neural tube formed during neurulation. NCCs other than Schwann cells, also give rise to other cell types including melanocytes, fibroblasts, parasympathetic neurons, and smooth muscle cells. It is still not clear how these cells start

to differentiate in one type or another, but it is possibly related to both stochastic events and a combination of several instructive signals (Jessen & Mirsky, 2005;). Particularly, mature Schwann cells formation requires the transition from migrating neural crest cells to two other cell types: Schwann cells precursors (SCPs) and Immature Schwann cells (**Figure 4**). The former group originates from neural crest cells at around embryonic day E12-13 in mice and contains cells at different developmental stages surrounded by the extracellular matrix. Their survival is guaranteed by specific axonal factors such as β-Neuregulin-1 (NRG1). The latter group generates from SCPs at around E13-15 in mice and is composed of cells showing the same developmental potential, which interact with both axons and nascent basal lamina (Jessen & Mirsky, 2005; Jessen *et al*., 2015). Autocrine signals such as insulin-like growth factor 2 (IGF 2), neurotrophin 3 (NT3), platelet-derived growth factor (PDGFB), leukaemia inhibitory factor (LIF) and lysophosphatidic acid (LPA) are responsible for immature Schwann cells survival. This switch from paracrine (axonal) to autocrine (glial) dependence is crucial not only during development but also after nerve injury (Jessen & Mirsky, 2005; Jessen & Mirsky, 2019). During this phase, indeed, denervated Schwann cells (repair Schwann cells) acquire a new phenotype and assure their own survival by means of autocrine signals (e.g., NRG1 type I).

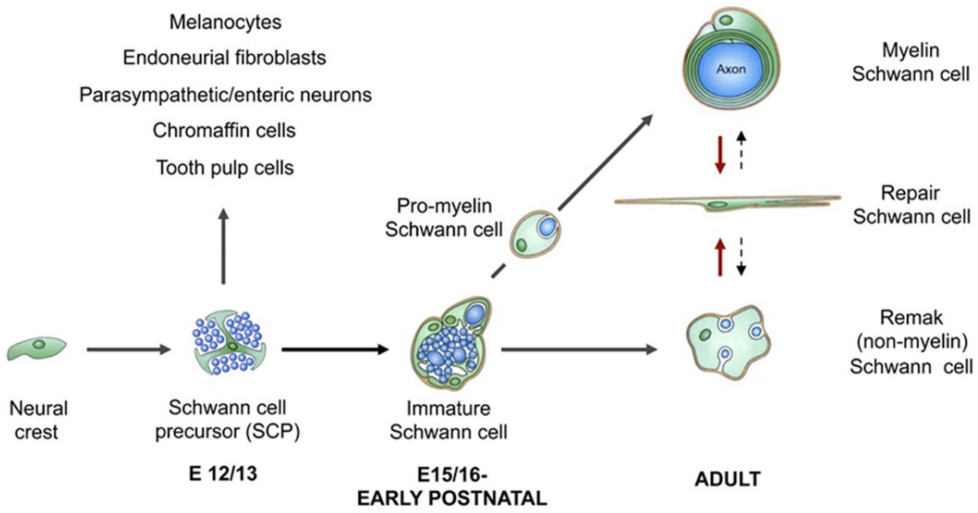


***Figure 4. Schwann cells transitions during development and adulthood.***
*Schematic graph showing the main steps occurring in Schwann cells lineage during development, in adulthood and after nerve damage (Jessen & Mirsky, 2019).*

Around E18-19, immature Schwann cells, together with axons, start to segregate from their original families and undergo a process called radial sorting, which terminates at

post-natal day 10 (P10). During this phase, immature Schwann cells interacting with smaller axons (<1 um diameter) differentiate in non-myelinating Schwann cells to form unmyelinated Remak bundles, whereas the ones interacting with larger axons (>1 um diameter) establish a 1:1 relationship with single axons, thus becoming pro-myelinating Schwann cells (**Figure 4**). To numerically assure the 1:1 match between axons and Schwann cells, a fine regulation of cells proliferation and death also occurs at this point (Jessen & Mirsky, 2005; Pereira *et al*., 2012; Jessen *et al*., 2015). Myelination of large-calibre axons finally starts at birth, thanks to the concurrent activation and inhibition of several pathways.

The progression of embryonic Schwann cells lineage from one state to another is finely regulated by several molecules- including mitogen and differentiation signals as well as transcription factors-, expressed by glial cells, axons, and the surrounding environment. Among all, it is worth to mention the transcription factors SOX10 and FoxD3, which are essential for SCPs generation from neural crest cells, and axonal signals like NRG1 and Notch, which drive SCPs to immature Schwann cells (Jessen *et al.*, 2015).

### *1.2.2 Neuregulin 1 type III-mediated myelination signalling*

The myelin phenotype is then the result of a complex, sequential, feedforward cascade of both intrinsic and extrinsic signals, involving transcriptional and epigenetic factors, receptors, ligands, and different signalling molecules. Among all, the major and best-described extrinsic signal is neuregulin (NRG1) type III, which is expressed on the axonal surface (Jessen *et al.,* 2015). As already mentioned in 1.2.1, NRG1 plays a pivotal role at many stages of Schwann cells lineage during development and postnatally. NRG1 is part of the epidermal growth factor (EGF) superfamily and comprises six major classes (I-VI), which differ in the splicing patterns of the ectodomain. The isoforms I-III are the most abundantly expressed, with type III being the most represented on peripheral axons (Jessen *et al*., 2015). NRG1 type I [also called *heregulin* or acetylcholine receptor-inducing activity (ARIA)] and type II (also called GGF, Glial Growth Factor) are released from the axonal surface, hereby acting as paracrine signals, whereas NRG1 type III is retained on the axonal membrane and acts as a juxtracrine signal (Michailov *et al*., 2004; Nave & Salzer, 2006). Notwithstanding, all of them can interact with the erbB tyrosine-kinase receptors family through the EGF-like domain. Axonal NRG1 type III binds the

ErbB2/ErbB3 heterodimer receptor expressed on Schwann cells surface, thereby activating several second messenger cascades, including the PI3K-Akt-mTOR axis, which is essential for both Schwann cells proliferation and myelination (Taveggia *et al*., 2005; Salzer,2015; Figlia *et al*, 2017). The central role of NRG1 and particularly of NRG1 type III in PNS myelination has been extensively demonstrated in literature. NRG1, ErbB2 and ErbB3 full KO mice are not viable (Wolpowitz *et al*., 2000; Adlkofer *et al*., 2000). Schwann cells/NRG1 type III$^{-/-}$ neurites co-cultures fail to sort into 1:1 relationship and to provide myelination (Taveggia *et al*., 2005). Haploinsufficiency of NRG1 (mainly type III isoform) or conditional inactivation of its receptors results in severe hypomyelination and reduced nerve conduction velocity (Garratt *et al*., 2000; Michailov *et al*., 2004; Taveggia *et al*., 2005; Brinkmann *et al*., 2008), whereas forced expression of NRG1 type III causes hypermyelination (Michailov *et al*., 2004).

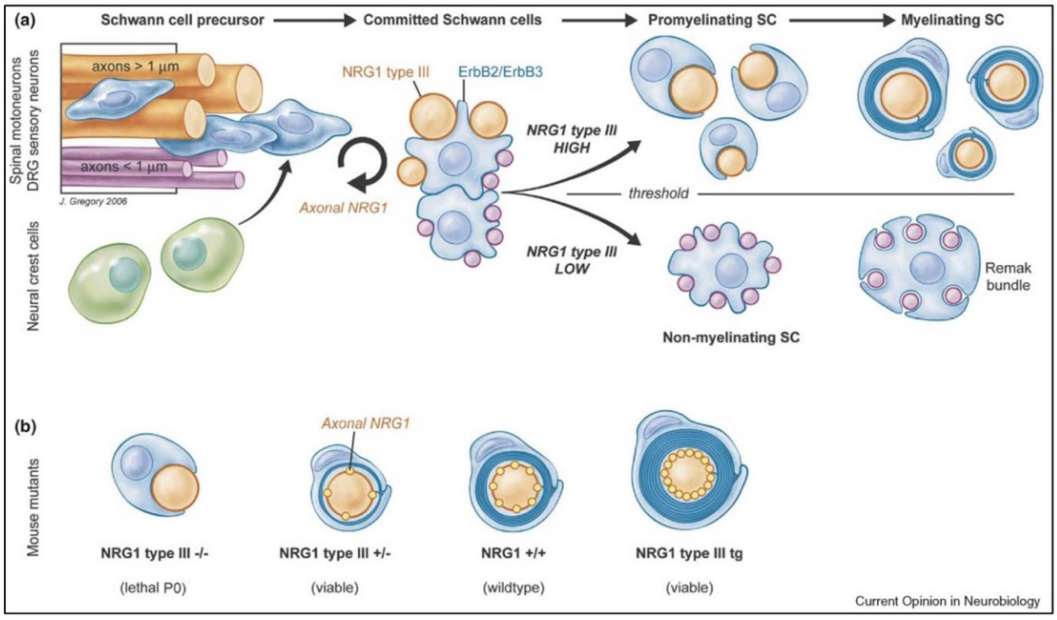


***Figure 5. NRG1 is an instructive signal for PNS myelination.***
*A) Axons expressing high levels of NRG1 type III induce Schwann cells differentiation towards myelination; low levels of NRG1 type III lead Schwann cells to a non-myelinating fate. B) NRG1 type III levels are proportionally related to the quantity of myelin produced (Nave & Salzer, 2006; License number: 5410671441366, Elsevier).*

These findings also suggest that NRG1 type III is an instructive signal, thus meaning that threshold levels stimulate myelination and that above that threshold, the quantity of myelin produced is directly proportional to the amount of NRG1 type III expressed (**Figure 5b**), (Salzer, 2015). Indeed, large-calibre axons expressing high levels of NRG1 type III undergo myelination, whereas small-calibre axons expressing low-levels of

NRG1 type III have a non-myelinating fate (**Figure 5a**), (Taveggia *et al*, 2005). Accordingly, myelin sheath thickness is calculated and expressed with the *g-ratio* value (ratio between the axonal diameter and the myelinated fibre), which physiologically corresponds to 0,68 (Nave & Salzer, 2006). In pathological conditions, *g-ratio* is often altered: in case of hypomyelination the ratio shows higher values (>0,68), whereas in case of hypermyelination they are reduced (<0,68).

### *1.2.3 Modulation of NRG1 type III signal by BACE and TACE secretases*

NRG1 type III is an instructive and essential signal for Schwann cells development and myelination (Nave & Salzer, 2006; Salzer, 2015; Jessen *et al*., 2015). Like the other isoforms, it requires the cleavage of the extracellular ectodomain by metalloproteinases to fully function. However, because of its second amino-terminal hydrophobic sequence (cysteine-rich domain), it is not released as type I and II, but it is retained on the axonal surface and acts as a juxtacrine signal (Falls, 2003; Taveggia *et al*, 2005). Among others (e.g., Nardisilin-1, ADAM22), BACE1 and TACE/ADAM17 are the major secretases acting on NRG1 type III with opposing effects (**Figure 6**).

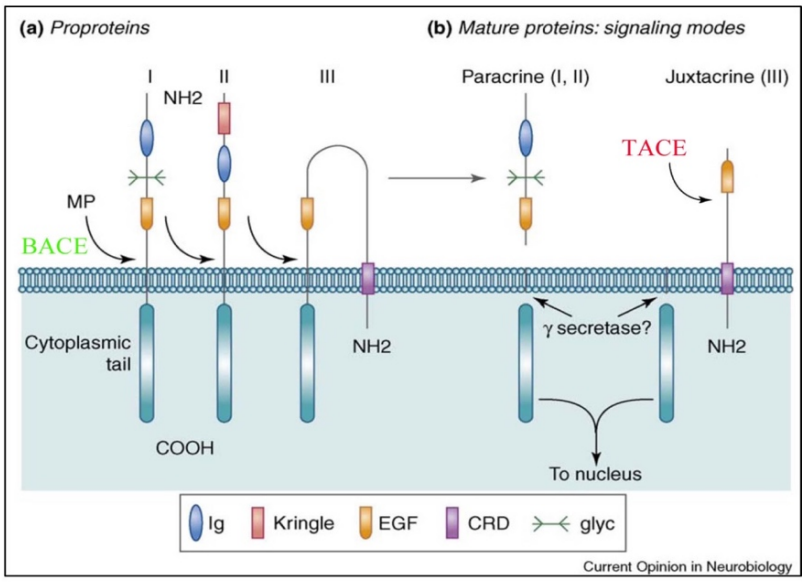


***Figure 6. NRG1 processing by BACE and TACE secretases.***
*Schematic reproduction of the three main NRG1 isoforms (type I, II and III) requiring metalloproteinases cleavage to fully function. NRG1 type I and II are released from the axonal surface and act as paracrine signals; Nrg1 type III is activated by BACE cleavage and acts as juxtracrine signal. TACE secretase cleaves the EGF-like domain and inhibits myelination (Modified from Nave & Salzer, 2006; License number: 5410671441366, Elsevier).*

The β-secretase BACE1 is a positive regulator of myelination and remyelination after injury, whereas TACE/ADAM17 (Tumor necrosis factor α-converting enzyme/a disintegrin and metallopeptidase domain-17) acts as negative regulator of NRG1 type III function (Nave & Salzer, 2006). The balance between BACE1 and TACE/ADAM17 activities is then crucial to regulate the timing and the extent of PNS myelination (Pereira *et al*, 2012; Salzer,2015).

The central role played by these two enzymes on NRG1 Type III modulation and consequently on myelination has been widely demonstrated.

BACE1$^{-/-}$ mice show evident hypomyelination of large-calibre axons and aberrant axonal segregation of small-calibre axons in sciatic nerves at P8. In the CNS, a significant decrease of amino-terminal fragments produced by BACE1 cleavage parallels an increase of unprocessed NRG1 type III, corroborating its role in promoting NRG1 type III activation (Willem *et al*, 2006).

TACE $^{-/-}$ mice are not viable and die at birth (Peschon *et al*., 1998). Conditional KO mice, in which TACE has been specifically deleted in motor neurons (*HB9-Cre; TACE $^{fl/fl}$* ) were generated to investigate axonal TACE activity on NRG1 type III. Ultrastructural analysis of both sciatic nerves and ventral roots at P1 revealed a significant anticipation of the myelination program and a marked hypermyelination of some fibres. Subsequent analyses performed at P7, P15 and P30 confirmed the results obtained at P1. Moreover, the *g-ratio* value was found to be reduced when compared to *wild-type*, supporting the evidence of a hypermyelinated condition (La Marca *et al*., 2011).

Since TACE is expressed by both axons and Schwann cells, to discriminate if the observed aberrant phenotype was the result of an axon-autonomous mechanism or not, the *Mpz-Cre; TACE $^{fl/fl}$* mouse model was generated to specifically delete TACE in Schwann cells. Morphological analysis and *g-ratio* value of sciatic nerves at P7 and P30, as well as detection of MBP and MAG protein levels from sciatic nerve lysates at P15, did not show any differences to *wild-type*. Finally, to further corroborate the inhibitory role of TACE, *Nrg1 type III$^{+/-}$; TACE$^{+/-}$* compound mice have been generated to investigate if a 50% reduction of TACE could be sufficient to restore hypomyelination in *Nrg1 $^{+/-}$* mice. Interestingly, morphological analysis of sciatic nerve sections at P30 confirmed the expected rescue (La Marca *et al*., 2011).

Taken together, these results confirm the role of axonal but not glial TACE in reducing NRG1 type III-mediated myelination signalling and suggest that the modulation of NRG1 signalling through secretases inhibitors or activators could be an efficient therapeutic strategy for different myelin disorders (Salzer, 2015; Bolino *et al*., 2016).

### *1.2.4 The PI3K-Akt-mTOR pathway in PNS myelination*

The PI3K-Akt-mTOR pathway is the main signalling cascade triggering myelination downstream NRG1 type III-ErbB3/ErbB2 interaction (**Figure 7**).

PI3K (phosphatidylinositol 3-kinase class I) converts the $PIP_2$ [phosphatidylinositol (4,5)-biphosphate] in $PIP_3$ [phosphatidylinositol (3,4,5)-triphosphate] to foster Akt activation, whereas PTEN (phosphatase and tensin homolog) catalyses the opposite reaction (Pereira et al., 2012). More precisely, $PIP_3$ recruits Akt to the plasma membrane together with PDK1 (3-phosphoinositide dependent protein kinase 1) and phosphorylates Akt at residue $Thr^{308}$ placed in the catalytic domain (Norrmén & Suter, 2013). Phosphorylation of $Ser^{473}$ by mTORC2 completes Akt activation (Guertin *et al*., 2006; Jacinto *et al*., 2006). Phosphorylated Akt then promotes lipid biosynthesis via SREBPs (sterol regulatory element-binding proteins) and activates mTORC1 complex both directly, through the inactivation of its inhibitors (e.g., PRAS40), and indirectly, through the inactivation of the TSC-TBC complex (Norménn & Suter, 2013; Salzer *et al*., 2015; Figlia *et al*., 2018).

The mammalian target of Rapamycin (mTOR) is one of the main effectors downstream to Akt and it constitutes the catalytic core of mTORC1 and mTORC2 complexes (**Figure 7**). Of note, mTORC1 is widely known for its role in regulating cell metabolism, proliferation, and survival, whereas mTORC2 coordinates cell migration and cytoskeleton remodelling (Norménn & Suter, 2013). Once activated, mTORC1 stimulates lipid and protein production through its downstream effector phospho p70-S6 kinase (PS6K), which in turn phosphorylates S6 ribosomal protein (S6 rp), a member of the 40s ribosomal subunit involved in mRNA translation. Simultaneously, mTORC1 also phosphorylates 4EBP1(eukaryotic initiation factor 4E-binding protein), thereby causing the release of the eIf4 factor (translation initiation factor 4E) and thus further promoting translation (Figlia *et al*., 2018). In addition to SREBPs, mTORC1 stimulates lipid

biosynthesis through the activation of the PPARγ (peroxisome proliferator-activated receptor gamma) transcriptional program, which regulates *de novo* fatty acids synthesis and adipocytes differentiation (Montani *et al*., 2018).

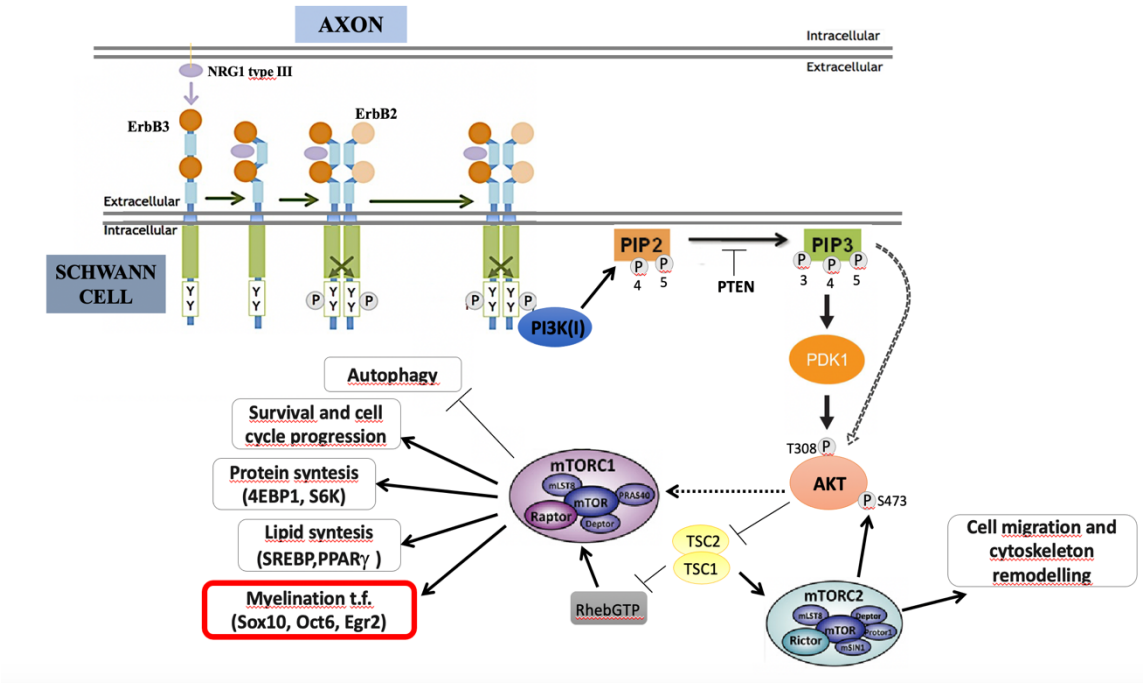


***Figure 7. The PI3K-Akt-mTOR pathway role in PNS myelination.***
*NRG1 type III interaction with its cognate receptors ErB3/B2 activates the PI3K-Akt-mTOR pathway. Schematic overview of the intracellular cascade activating myelination and other cellular mechanisms (Modified from Iwakura & Nawa, 2013).*

Since myelination is a high, biosynthetically demanding metabolic process, it is clear why mTORC1, the gatekeep of anabolism, plays such a pivotal role. During early development, high levels of mTORC1 foster radial sorting and prevent Schwann cells differentiation. When radial sorting is completed, mTORC1 activity decreases to promote myelination and the residual activity is maintained to sustain protein and lipid synthesis during myelin growth (**Figure 8**), (Sherman *et al*., 2012; Figlia *et al*., 2017).
Loss of mTORC1 function in Schwann cells indeed hampers myelination, whereas its hyperactivation not only leads to hypermyelination but, depending on timing and approach, it can result in different phenotypes (Figlia et al., 2017).

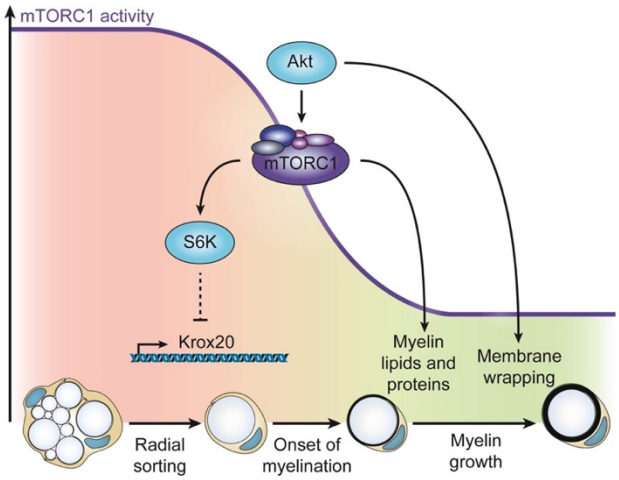


***Figure 8. Dual role of mTORC1 activity in PNS myelination.***
*High levels of mTORC1 stimulate Schwann cells proliferation and radial sorting by inhibiting Krox20 transcription. A decrease in mTORC1 activity allows Schwann cells differentiation and myelination. mTORC1 residual activity is necessary to sustain myelin growth by promoting lipid and proteins production (Figlia et al., 2017).*

## 1.3 PNS response to nerve injury (acute nerve damage in mice)

### *1.3.1 Wallerian degeneration*

Wallerian degeneration (WD) was firstly described in 1850 by August Waller as the degenerating process occurring in the axon distally from the injury site, followed by an active clearance of the debris produced (Stassart *et al*., 2018).

The causes of peripheral nerve degeneration and demyelination have multiple nature: they could be traumatic (nerve compression, neurotmesis or axonotmesis), toxic (diptheric), metabolic (diabetes), infectious (*Mycobacterium leprae*), hereditary (Charcot-Marie-Tooth Neuropathies), immune (Guillame-Barré syndrome, chronic inflammatory demyelinating polyneuropathy CIDP), thermic (hot or cold burn) or ischemic (Tricaud & Park, 2017). While axonotmesis is considered the primary model of acute axonal degeneration (WD), other conditions such as toxic injuries and genetic defects, are more correctly referred to as “dying back axonopathies”. This neuropathological feature has led for many years to the misconception that, differently from WD, degeneration in these disorders progresses retrogradely from the axonal terminus. Ultrastructural analyses have instead revealed that in these conditions, degeneration does not begin from the axonal

terminal but, considering the whole tract, it is most prevalently distal (Stassart *et al*., 2018).

To study nerve degeneration and regeneration in mouse models, axons are usually lesioned in two ways: by nerve cut (neurotmesis) or crush (axonotmesis). After cut, connective tissue and basal lamina sheaths are interrupted, while after crush, the basal lamina remains intact (Jessen & Mirsky, 2016). In both cases, the activation of WD leads to a strictly regulated subcellular self-destruction.

In the very early phase (1-2 days after injury), axons maintain their morphological and metabolic asset, but later they undergo a total structural breakdown. The mechanisms that initiate the process are still quite enigmatic. Recent studies have identified SARM1 as a master executioner of axonal degeneration (Gerdts *et al*.,2015; Sasaki *et al*.,2016; Di Stefano *et al*.,2015,2017; Figley *et al*., 2021). SARM1 (sterile alpha and Toll/interleukin-1 receptor motif-containing 1) is a pro-degenerative molecule which senses the increased NMN/$NAD^+$ ratio caused by both NMNAT2 and/or $NAD^+$ depletion (Figley *et al*., 2021). When an injury occurs, NMNAT2 is degraded, thus leading to an insufficient production of $NAD^+$ molecules, an increased levels of NMN, and axonal degeneration.

In addition, energetic failure caused by both $NAD^+$ and ATP depletion provokes ionic imbalance, including intra-axonal accumulation of calcium. The increased calcium flux, which primarily comes from axonal mitochondria, activates calpain (a calcium-dependent protease) and subsequently leads to neurofilament proteolysis, microtubules destabilization and fragmentation of damaged axons (Gerdts *et al*., 2016; Stassart *et al*., 2018).

### *1.3.2 The "multitasking" role of Schwann cells after nerve injury*

Whilst the starting point of axon degeneration seems to be mainly axon intrinsic, Schwann cells play an active role in the following steps of axonal disintegration and debris clearance, as well as in promoting axon regeneration and remyelination (Stassart & Woodhoo, 2021).

During the first phase after nerve damage, Schwann cells dedifferentiate to a progenitor-like state, which enables them to remodel the environment and make nerve regeneration possible (Klein & Martini, 2016). This is an important feature that distinguish PNS from

CNS, where regeneration is impaired by different intrinsic and extrinsic factors, including oligodendrocytes inability to digest myelin (Rao &Pearse, 2016).

The conversion from differentiated Schwann cells to repair Schwann cells requires a deep modification of the glial phenotypic profile. Expression of myelin genes is downregulated (e.g., MBP, MPZ, periaxin), while an upregulation of genes normally expressed in Remak or developing Schwann cells (e.g., L1, NCAM, GFAP, P75NTR) occurs (Chen *et al*., 2007; Jessen & Mirsky, 2019). In addition, transdifferentiated Schwann cells also express *de novo* genes, like Olig 1 (oligodendrocyte transcription factor 1) and Shh (Sonic Hedgehog) and upregulate a set of neurotrophic factors and surface proteins (e.g., GDNF, BDNF, NT3, NGF, VEGF, N-cadherin) that contribute to neurons survival and axonal regrowth (Jessen & Mirsky, 2016). Even the activation of the immune system is regulated by repair Schwann cells through the release of diverse cytokines and chemokines (e.g., TNFα, Il-1α, LIF, MCP-1), which not only recruit macrophages to the injury site, but also promote nerve regeneration in several ways (see 1.3.3 for details).

Recent evidences also propose the epithelial-to-mesenchymal transition (EMT), as one of the possible processes that Schwann cells undergo during demyelination. After injury, genes like Zeb2 and Snai1, typical of the mesenchymal phenotype, resulted to be upregulated in demyelinating Schwann cells, as well as E-cadherin was found to be replaced by N-cadherin expression (Tricaud & Park, 2017).

During the very early phase of Wallerian degeneration/demyelination (up to 3 days post damage), axons degenerate, and myelin retracts starting from paranodal regions (**Figure 9, points 1-2**).

Myelin sheath then starts to break up into oval-shaped myelin segments, called myelin ovoids, that progressively become small debris (Gomez-Sanchez *et al*., 2015). It has been estimated that about 50% of total myelin is cleared by Schwann cells themselves thanks to the activation of a specific autophagic process called “myelinophagy”, while the rest is later removed by hematogenous macrophages together with antibodies and complement (Gomez-Sanchez *et al*., 2015; Jessen & Mirsky, 2016; Stassart & Woodhoo, 2021). Myelin and axonal fragments are then internalised and delivered to lysosome for degradation (Jung *et al*., 2011), thus enabling the complete clearance within 15 dpni (days post nerve injury), (**Figure 9, points 3-4**).

After that, repair Schwann cells adopt a bipolar, elongated morphology to form columnar tracks (called Bands of Bungner) inside the basal lamina, which support and guide regenerating axons back to their original targets (**Figure 9, points 5-6**), (Jessen & Mirsky, 2016). In case of nerve cut, this step is also supported by regrowing vessels stimulated by macrophage-released VEGF-α (vascular endothelial growth factor alpha) in response to the hypoxic environment (Cattin & Lloyd, 2016). In both cases, once target tissues are reached (around 21dpni), Schwann cells re-differentiate and start to myelinate the regenerated axons following a 1:1 ratio (**Figure 9, point 7**).

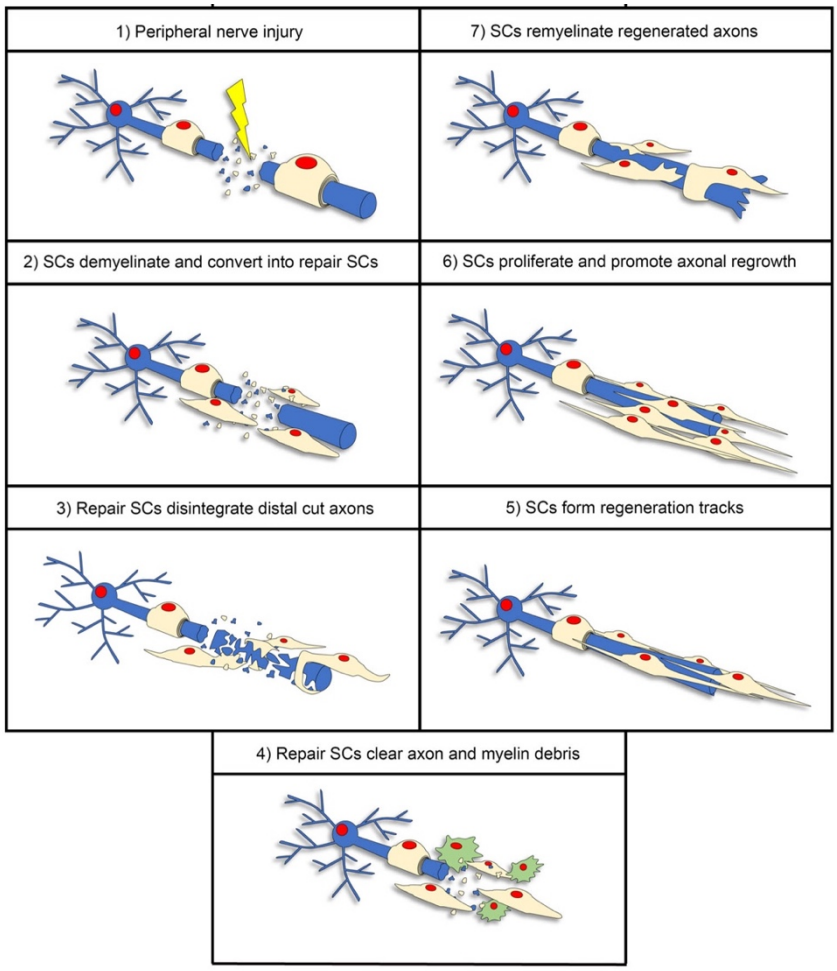


***Figure 9. Main steps of Wallerian Degeneration.***
*1) Injury of a peripheral nerve can have different natures (traumatic, metabolic ,toxic, hereditary) but always results in the activation of the degeneration program; 2)Denervated Schwann cells "transdifferentiate" and become repair Schwann cells; 3-4) Repair Schwann cells together with macrophages remove myelin and axonal debris to allow regeneration; 5) Repair Schwann cells form regeneration tracks (Band of Bunger) to guide new axons back to their original targets;6) Schwann cells proliferate to further help axonal regrowth;7)Once axons have regenerated and reached their targets, Schwann cells can re-differentiate and start the remyelination process. (Nocera &Jacob, 2020).*

It is discreetly evident then that Schwann cells reprogramming after nerve injury does not completely recapitulate embryonic development, but it involves several different mechanisms which have not yet been fully elucidated (Arthur-Farray *et al*., 2012; Jessen & Arthur-Farray, 2019). A central regulator of Schwann cells reprogramming after nerve injury is the JNK/c-jun pathway (Arthur-Farraj *et al*, 2012; Gomez-Sanchez *et al*., 2015). The transcription factor c-jun orchestrates the main steps of injury response, going from the stimulation of trophic and adhesion factors expression to myelin clearance and regeneration. Indeed, inhibition of c-Jun function leads to a missed activation of the repair program and thus, to unsuccessful recovery and neuronal death (Arthur-Farraj *et al*, 2012).

Other studies showed that ErbB2/B3 receptors expressed distally from the injury site, were found to be selectively phosphorylated ten minutes after nerve damage. This activation primarily occurs at Schwann cell microvilli and then spreads along the abaxonal side. Since NRG1 type III is known to trigger ErbB2/B3 phosphorylation, it has been suggested that in addition to its role in survival, proliferation, and myelination, it could also have a role in promoting Schwann cells dedifferentiation (Tricaud & Park, 2017). NRG1-mediated activation of ErbB2/B3 receptors further stimulates within few hours Rac-MKK7-JNK and Ras-MEF-ERK1/2 pathways, which regulate actin polymerization and demyelination, respectively (Napoli *et al*., 2012; Shin *et al*., 2013). Nevertheless, it has been demonstrated that NRG1 can be dispensable during dedifferentiation, whereas it is later required for nerve regeneration (Fricker *&* Bennett, 2011; Stassart *et al*., 2013).

Another candidate for the activation of the repair program in Schwann cells is the Notch pathway. Notch ligands Jagged 1 and 2 were found to be induced within the first two days after nerve injury. Stimulation of the Notch pathway indeed leads Schwann cells reprogramming and demyelination, starting from 4 hours after nerve injury and culminating with the complete disintegration of the myelin sheath two days later (Woodhoo *et al*., 2009; Tricaud & Park, 2017).

### *1.3.3 Macrophages contribution to clearance*

As already mentioned in 1.3.2, macrophages synergically cooperate with Schwann cells to promote myelin and axonal debris removal after nerve injury.

In physiologic conditions, tissue-resident macrophages account for the 2-9% of total cells and their function in a homeostatic condition is still not completely clear (Mueller *et al*., 2001; Cattin & Llyod, 2016). Early after injury, both Schwann cells and resident macrophages proliferate and activate to clear and remodel the environment. From 4 dpni onward, hematogenous macrophages are recruited at the site of damage thanks to specific cytokines and chemokines released by Schwann cells (e.g., CCL2, MCP-1, LIF, TNF-α, IL-6) and fibroblast (e.g. CSF1). Of note, CCL2 binds to CCR2 monocytic receptor and it is thought to be one of the main recruiting factors: genetic disruption of both *Ccl2* or *Ccr2* indeed results in a reduced accumulation of macrophages at the injury site (Cattin & Llyod, 2016; Stassart & Woodhoo, 2021). In addition, products of the degenerating process themselves have been found to trigger the immune response through the interaction with Toll-like receptors (TLRs) expressed by Schwann cells (Martini *et* al., 2008). Finally, it has recently been shown that also neuronal prostaglandin D2 synthase (L-PGDS) is involved in the modulation of macrophage activity, as well as in promoting axonal regeneration and reduction of the inflammatory response in the late phases of WD (Forese *et al*., 2020).

Whilst the first idea about macrophages is usually related to their clearance activity, they play a crucial role in stimulating regeneration as well. In case of nerve cut, they "sense" hypoxia and secrete VEGFA to trigger the formation of new blood vessels (Cattin & Llyod, 2016). Polarised angiogenesis is fundamental not only to restore perfusion, but it also helps Schwann cells to guide regenerating tracks back to target tissues.

Accordingly, macrophages contribute to axonal regeneration both directly, by debris removal, and indirectly, through the release of pro-regenerative factors, such as IL-1β, which stimulates Schwann cells to produce NGF-1 (nerve growth factor 1).

Depending on the type of perturbation- namely WD or inherited demyelinating neuropathy- macrophages contribution can be primarily hematogenous or resident, respectively. In the first case, both axons and myelin are involved, whereas in the second, myelin is wrecked while axons are preserved, suggesting that different mediators are involved in response to the distinct type of damage (Martini *et al*., 2008).

It is evident then that macrophages are incredibly plastic cells, which can show a wide range of activation states in relation to the environment. Using genomics tools, it has been demonstrated that at least 9 subtypes of macrophage-activation patterns exist in response

to different stimuli. Nevertheless, macrophages are usually clustered in two main groups in various tissues, including the nerve: M1 or pro-inflammatory or "classically activated" macrophages and M2 or anti-inflammatory or "alternatively activated" macrophages (Chen *et al*., 2015; Stratton & Shah, 2016). M1-phenotype is predominant within the first 3-4 dpni and stimulates inflammation as well as debris clearance. M2-phenotype also appears early after damage to counteract pro-inflammatory signals but is mostly present later to promote regeneration. This temporal regulation of phenotypic profiles is shared by other tissues, but what really happens in PNS microenvironment is more complex and much still needs to be elucidated (Stratton & Shah, 2016).

Intriguingly, the presence of two spatially and phenotypically distinct subset of macrophages inside a peripheral nerve has been recently described for the first time. In response to nerve injury, these two populations differently react to damage, with a predominant activation of the endoneural (rather than epineural) compartment (Ydens *et al*., 2020).

### *1.3.4 Axons regeneration and remyelination*

The synergic action of Schwann cells and macrophages in promoting clearance of myelin and axonal remnants is the striking point which differentiates PNS from CNS in the ability to regenerate after injury.

In mice, the regenerative program requires 3-4 weeks to be completed, even if remyelination lasts longer (>45 dpni). In humans this process is slower: with a rate of axonal regrowth of around 1 mm/day, it can take more than one year to be over (Höke & Brushart, 2010).

Other than debris removal, axonal regrowth requires the activation of the regeneration-associated gene (RAG) program and an increase in mitochondrial density to energetically support the process. The growth cone starts to elongate from the proximal stump towards periphery, following Schwann cells columnar tracks (Bands of Bungner), which directionally guide and robustly sustain the new forming axons (Stassart & Woodhoo, 2021). This collective migration is also favoured by EphB2 signalling, triggered by fibroblast-expressing Ephrin B, as soon as Schwann cells enter the wound.

Once the target tissue is reached, repair Schwann cells exit the cell cycle, re-differentiate, and start to myelinate new regenerated axons (Stierli *et al*., 2019). Notwithstanding,

remyelination is not as efficient as myelination during development: axonal segments show thinner and shorter ensheathment, which ultimately leads to a partial functional recovery over time (Stassart & Woodhoo, 2021).

The switch from repair to myelinating Schwann cells is determined by the restored expression of NRG1 type III on axonal surface (**Figure 10**). At the beginning of WD, axo-glial interactions are lost, so Schwann cells have no more access to axonal signalling cues. During this phase, denervated Schwann cells start to express NRG1 type I isoform, whose expression is usually inhibited by axonal NRG1 type III. NRG1 type I acts as autocrine signal on Schwann cells themselves, supporting their proliferation and survival in absence of axons. When axons start to regenerate, NRG1 type III expression slowly turns back to normal levels and eventually triggers Schwann cells differentiation and myelination once target reinnervation is complete (Stassart & Woodhoo, 2021).

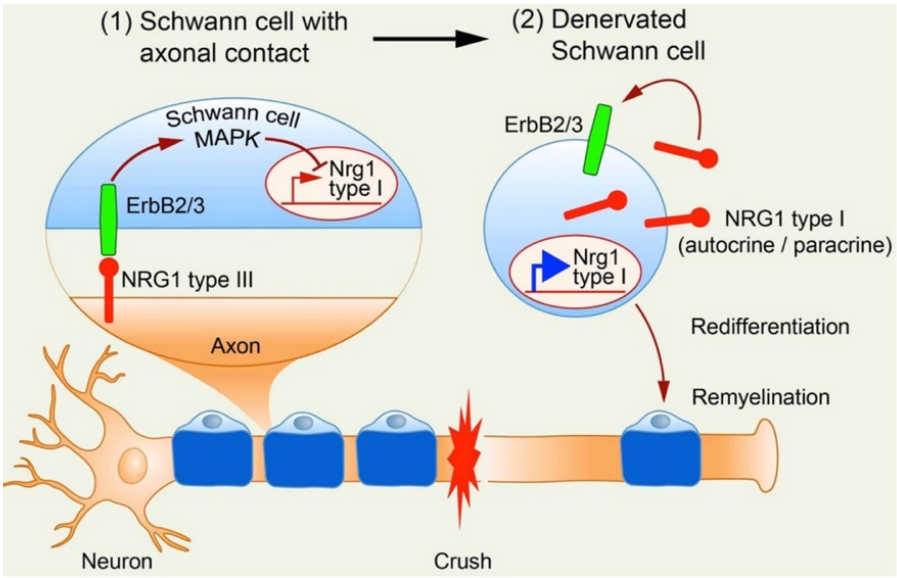


***Figure 10. NRG1 modulation during PNS regeneration and remyelination after injury.***
*In physiological conditions, axons express Nrg1 type III which stimulates myelination and inhibits Nrg1 type I expression in Schwann cells. In case of nerve injury, denervated Schwann cells lose their contact with axons and start to express Nrg1 type I, which acts as autocrine/paracrine signal essential for their proliferation and survival (Mei & Nave, 2014; License number: 5413570128841,Elsevier).*

### *1.3.5 mTORC1 pathway modulation after nerve injury*

As already described in 1.2.4, mTORC1 plays a pivotal role in regulating many aspects of Schwann cells development and PNS myelination in homeostasis and disease. mTORC1 pathway is highly activated before myelination, thereby promoting Schwann

cells proliferation and radial sorting, while at the onset it rapidly declines. The residual activity is however sufficient to promote myelin synthesis and to sustain the elevated metabolic demand (Sherman *et a*l., 2012; Figlia *et al*., 2017).

Recent studies have proposed a transient but consistent reactivation of mTORC1 after nerve injury as one of the main mechanisms regulating Schwann cells dedifferentiation (**Figure 11**). Accordingly, mTORC1 seems to promote c-Jun translation via eIF4A, which is known to be the master regulator of Schwann cells reprogramming after nerve injury. Genetic disruption of mTORC1 activity results indeed in failed c-Jun elevation and in the unsuccessful activation of the repair program (Norrmén, Figlia *et al*., 2018).

Intriguingly, mTORC1 stimulation after damage shows striking parallels with mTORC1 modulation during development. In both cases, high mTORC1 activity limits Schwann cells differentiation and promotes myelin clearance or radial sorting respectively, whereas low activity is necessary for the onset of myelination/remyelination.

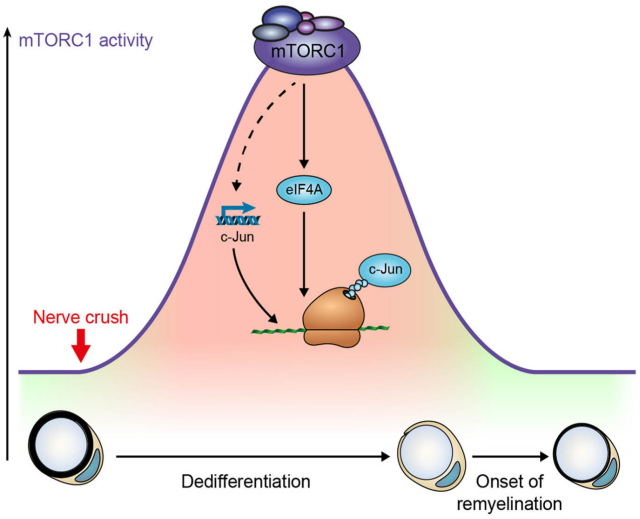


***Figure 11. mTORC1 modulation after nerve injury.***
*mTORC1 reactivation after nerve injury enables Schwann cells dedifferentiation by promoting c-jun expression. (Norrmén, Figlia et al., 2018)*

Moreover, unlike regular autophagy, high levels of mTORC1 after injury have been found not to inhibit myelinophagy, suggesting that a mTOR-independent mechanism occurs during debris clearance. Accordingly, starvation-induced mTORC1 upregulation as well as pharmacological inhibition of mTORC1 by rapamycin does not change the rate of myelin destruction *in vitro* (Gomez-Sanchez *et al*., 2015).

In addition to that, recent findings show that the mTORC1-Hifα /c-Myc axis drives a rapid glycolytic shift in Schwann cells after injury to counteract the energetic failure caused by axonal degeneration (Babetto *et al*., 2020). Schwann cells switch their metabolism from oxidation to glycolysis in order to make a physiological adaptation to the hypoxic environment and protect injured axons from degeneration by pyruvate and lactate delivery as energy supplies.

It is still not completely clear which upstream signals are responsible for mTORC1 activation after injury. Given the role of NRG1 type I in supporting denervated Schwann cells, it is very likely that it could be one of the main factors involved (Norrmén, Figlia *et al*., 2018). This hypothesis is also supported by a consistent phosphorylation of ErbB2/B3 receptors within few minutes after injury, which corroborates the possible link between NRG and mTORC1 also after damage (Tricaud & Park, 2017; Babetto *et al*., 2020).

## 1.4 Charcot-Marie-Tooth (CMT) neuropathies (chronic nerve damage)

### *1.4.1 General classification and definition*

Charcot-Marie-Tooth (CMT) neuropathies, also addressed to as hereditary motor and sensory neuropathies (HMSN), are one of the most frequent forms of inherited neuromuscular disorders with a common prevalence of 1:2500 people (Rossor *et al*., 2016). So far, mutation in more than 100 genes have been found to be disease-causative, suggesting a high genetic and clinical heterogeneity (Pareyson & Marchesi, 2009; Nagappa *et al*., 2022).

The age of onset is between the first and second decade of life, but in the most severe forms it can also be congenital. Genetic transmission can be autosomal dominant, autosomal recessive or X-linked, with the autosomal dominant pattern being the most frequently observed (Nagappa *et al*., 2022).

Patients usually experience progressive muscular weakness and atrophy starting from lower limbs, hands and foot deformities (e.g., *pes cavus*), reduced or absent reflexes, and sensory loss (**Figure 12**).

***Figure 12. Clinical manifestation of Charcot-Marie-Tooth neuropathies.***
*Images of patients showing distal muscular atrophy(A-B) and skeletal deformities affecting hand and foot (C-F), (Pareyson& Marchesi, 2009; License number: 5411370635823, Elsevier).*

This results in a major impairment of normal activities of daily living such as walking, writing, and buttoning. CMTs neuropathies are believed to be non-syndromic disorders, even if other clinical manifestations such as CNS involvement or hearing loss are present in some subtypes (Stavrou *et al*.,2021). Life expectancy is not altered, even if in the most severe forms it is estimated around 40-50 years because of respiratory failure. There are currently no effective treatments available but only clinical attempts to manage and reduce symptoms (Nagappa *et al*., 2022).

CMTs are primarily distinguished on the basis of neurophysiological and clinical criteria into demyelinating or axonal based on whether axons or myelin is the primary site of pathology (Previtali, Quattrini & Bolino, 2007).

Demyelinating forms (CMT1) are determined by a severe reduction of motor nerve conduction velocity (MNCV) to less than 38m/s (in the worst cases nerve responses can also be undetectable), segmental demyelination, hypomyelination, and eventually axonal degeneration. Among them, there is a subgroup of CMTs named “neuropathies with focal

hypermyelination" (e.g., CMT4B1, CMT4B2, CMT4B3, CMT4H, HNPP), because of the presence of aberrant myelin structures (e.g., tomacula and/or myelin outfoldings/infoldings).

Axonal forms (CMT2) are featured by normal or slightly reduced MNCV, decreased action potential amplitude, axonal atrophy, axonal degeneration, and fibres loss. Morphological specimens can also show onion bulbs and clusters of regenerating axons, as an attempt to restore damaged structures.

In addition to axonal and demyelinating CMTs, there is also another group of diseases defined as intermediate CMTs (I-CMT), which show intermediate neurophysiological and morphological profiles between the main two (Previtali, Quattrini & Bolino, 2007).

### *1.4.2 Charcot-Marie-Tooth type 4B1*

Charcot-Marie-Tooth type 4B1 is an autosomal recessive demyelinating neuropathy characterized by focally folded myelin structures called myelin outfoldings/infoldings, firstly identified by Ohnishi in 1989 (Bolino *et al*, 2004; Previtali, Quattrini & Bolino, 2007). Myelin outfoldings are the result of an irregular foldings of myelin arising during postnatal development. They morphologically appear as satellite axons disposed around a main one, with whom they share the same myelin thickness and basal lamina. Myelin infoldings are the corresponding aberrant structures which instead develop inward towards the axon (**Figure 13**). Both myelin outfoldings and infoldings preferentially arise at non-compact regions (e.g., SLI, paranodal regions) and increase in number and complexity with age (Bolino *et al*, 2004).

The disease onset is normally within the first decade of life but, in the most severe conditions, it can also be congenital or neonatal. Patients show reduced MNCV (9-20 m/s or even undetectable in some adults), progressive distal muscular weakness and atrophy, walking difficulties (e.g., walking on tiptoe) and skeletal deformities. Lifespan can be reduced because of respiratory failure, which can occur around the fourth or fifth decade of life (Previtali, Quattrini & Bolino, 2007).

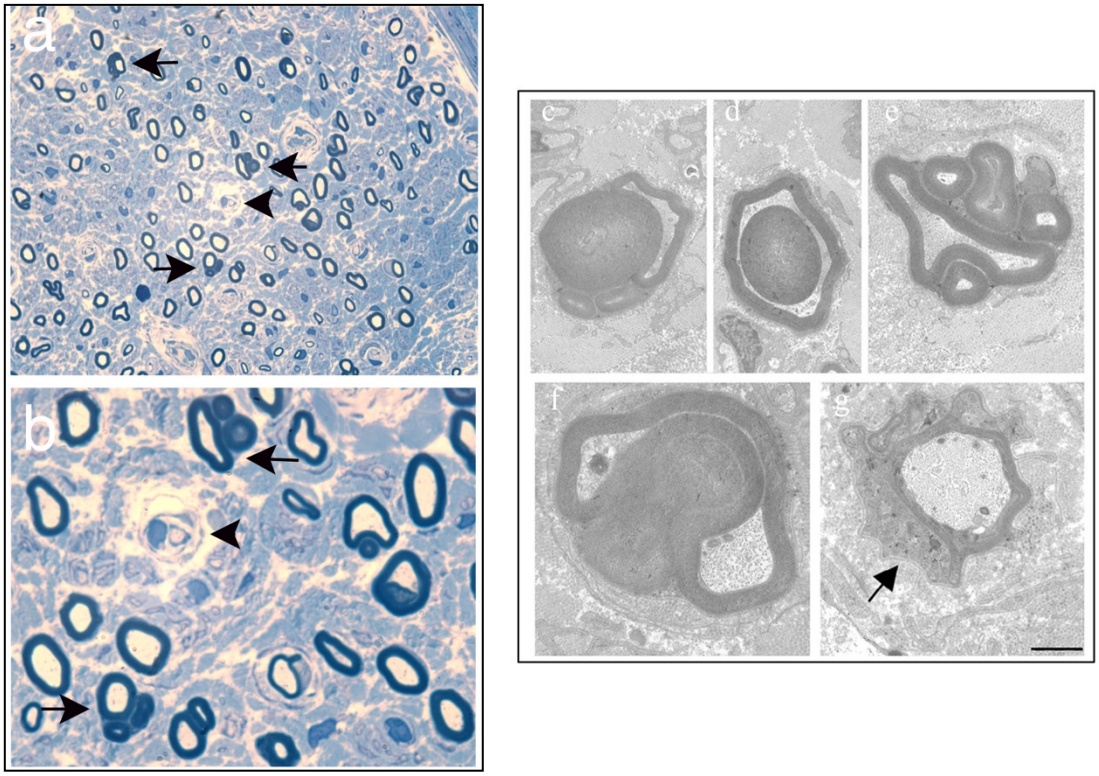


***Figure 13. Myelin outfoldings are the pathological hallmark of CMT4B1.***
*A-B) Transversal nerve sections of sural nerve biopsy showing myelin outfoldings (arrows), onion bulb (arrowhead) and significant axonal loss (modified from Previtali, Quattrini and Bolino, 2007); C-G) Sural nerve biopsy showing myelin outfoldings, infoldings and redundant basal lamina (arrow) at high magnification (Modified from Zambon et al., 2017).*

CMT4B1 is caused by loss-of-function mutations in the myotubularin-related 2 gene (*MTMR2*) encoding for a ubiquitously-expressed, catalytically-active phospholipid phosphatase, which regulates both PI3P and PI(3,5)$P_2$ phosphoinositide levels by removing a phosphate at position D-3 of the inositol ring (Bolino *et al*., 2000; Bolino *et al*., 2002).

Even if the exact pathomechanism of the disease is still unknown, it has recently been demonstrated that myelin outfoldings/infoldings can arise as a consequence of unbalanced PI(3,5)$P_2$ levels due to Mtmr2 loss. The increase in PI(3,5)$P_2$ results in the aberrant modulation of postnatal myelination and cytoskeletal remodelling via mTORC1 and RhoA/Myosin II pathways. Indeed, pharmacological inhibition of both signalling, as well as of PI (3,5)$P_2$ production, is able to partially rescue the phenotype in *in vitro* models (Guerrero-Valero *et al*., 2021).

Studies to understand the molecular basis of the disease and to find possible therapeutical targets have been performed on *Mtmr2*-null mice. In this model, *MTMR2* gene expression was ubiquitously ablated using Cre/loxP technology to remove exon 4 and to efficiently loose Mtmr2 function (Mtmr2 floxed;CMV-Cre). *Mtmr2* KO mice develop normally and have a regular lifespan. As humans, they show morphological alterations in both motor and sensory peripheral nerves from P5 (**Figure14**), reduced MNCV from 6 months and a progressive worsening of the phenotype with age (Bolino *et al*., 2004).

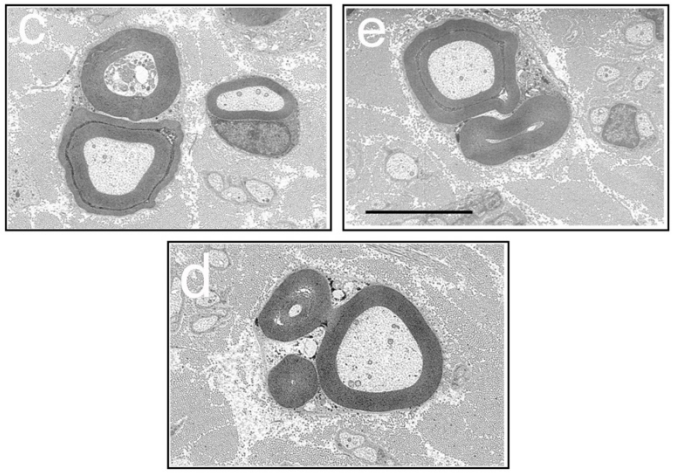


***Figure 14. The Mtmr2 $^{-/-}$ mice (CMT4B1 model) reproduce myelin outfoldings.***
*Sciatic nerve sections showing myelin outfoldings at high magnification. Mtmr2 $^{-/-}$ mice recapitulate the morphological phenotype of CMT4B1 neuropathy; (modified from Previtali, Quattrini and Bolino, 2007).*

Nevertheless, the severity of the disease in *Mtmr2* KO mice is milder than human pathology. This could be due to three main differences between rodents and humans: 1) mice live less, 2) mice have shorter nerves (length-dependent disease), 3) a partial compensation by other myotubularins can occur (Previtali, Quattrini & Bolino, 2007).
To better understand the cell-autonomous role of MTMR2, two conditional knock-out mice in which *Mtmr2* was specifically deleted in Schwann cells (*Mtmr2* floxed; P0-Cre) or motor neurons (*Mtmr2* floxed; HB9-Cre) have been generated. Morphological analyses revealed that Mtmr2-loss in Schwann cells, but not in neurons, was necessary and sufficient to reproduce CMT4B1 neuropathy in mice, suggesting that Schwann cells are the primary target of the disease (Bolis *et al*., 2005).

### *1.4.3 Hereditary neuropathy with liability to pressure palsies (HNPP)*

Hereditary neuropathy with liability to pressure palsies (HNPP) is an autosomal dominant disease characterised by recurrent transient focal mononeuropathies.

The age of onset is normally between the second and third decade of life, but both neonatal and elderly cases (>80 years) have also been reported. Patients experience persistent pressure palsies in single nerves following minor trauma, compression, or physical activities, and recover can take months. Clinically, muscular weakness, atrophy, reduced tendon reflexes, sensory signs and electrophysiological abnormalities also contribute to the diagnosis. Life expectancy is unchanged, even if there are no efficient treatments available (Attarian *et al*., 2020).

HNPP neuropathy is caused by loss-of-function mutations in the *PMP22* gene on chromosome 17p11.2-p12, which encodes for one of the main structural components of compact myelin. *PMP22* haploinsufficiency is sufficient to develop HNPP, whereas its duplication leads to CMT1A neuropathy, suggesting that a correct gene dosage is essential to preserve Pmp22 function (Adlkofer *et al*, 1995).

The histological hallmark of the disease are focally myelin thickenings found along single nerve fibres called “tomacula” (from latin *tomaculum*=sausage*,* sausage-like swellings), which preferentially arise at paranodal regions. These hypermyelinated structures are usually unstable and prone to degeneration (**Figure 15**). Tomacula “compress” the axons, thereby increasing axial resistance and hampering the transmission of the action potential along the nerve (Bai *et al*., 2010). This condition is worsened by an increase in myelin permeability due to the alteration of several junctional complexes requiring Pmp22 for stability. Indeed, Pmp22 interacts with junctional adhesion molecule-C (JAM-C) and myelin-associated glycoprotein (MAG), involved in the regulation of tight/adherens junctions and transmembrane adhesions. Accordingly, mouse models lacking *JAM-C* or *MAG* recapitulate HNPP neuropathy (Guo *et al*., 2014).

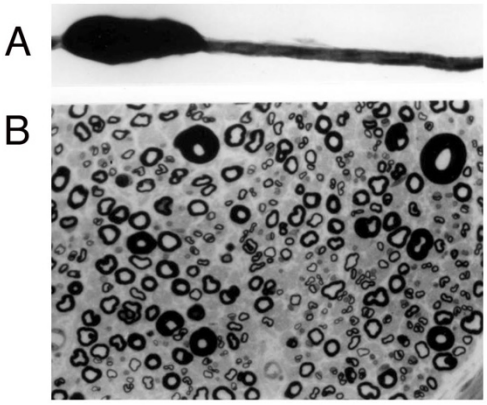


***Figure 15. Tomacula are the pathological hallmark of HNPP.***
*A) Teased nerve fibre from a 23-year-old woman sural nerve biopsy displaying focal hypermeylination; B) Sural nerve semithin section showing multiple fibres with tomacula and myelin aberrant thickenings. Fibres loss is also evident (Modified from Li J. et al., 2013).*

Tomacula have been associated with mTORC1 pathway hyperactivation downstream to NRG1 type III signalling (Goebbels *et al*., 2012). Pharmacological interventions designed to inhibit mTORC1 activity (rapamycin) are indeed able to partially rescue the morphological phenotype of *in vitro* and *in vivo* models of neuropathies with focal hypermyelination (Goebbels *et al*., 2012; Sawade, Grandi *et al*., 2020; Guerrero-Valero *et al*., 2021).

The *Pmp22*$^{+/-}$ mouse model was generated to study the pathomechanisms underlying the HNPP disease (Adlkofer *et al*., 1995; Adlkofer *et al.,* 1997a and b). Morphological and neurophysiological features closely resemble humans' pathological alterations.

Tomacula are already present in 24-days-old mice quadriceps nerves, even if they become prominent at 10 weeks, when almost every Schwann cell shows one. At both 5 and 10 months, hypermyelination is regularly observed in most fibres. At 15 months, myelin stability is lost: major dense line starts to split, onion bulbs and degenerations appear, supporting the fact that tomacula are instable structures with a high predisposition to degenerate (**Figure 16**). Electron microscopy analyses revealed the presence of two classes of tomacula: one characterised by multiple myelin wrappings around the axon and a second one, characterised by redundant myelin loops disposed internally or externally to the axon. Intriguingly, fibres with large-calibre axons were the most affected at all ages, suggesting a major involvement of the motor compartment. Moreover,

electrophysiological analyses showed reduced motor response amplitudes (M-response) of foot muscles starting from 12-14 months (Adlkofer *et al*., 1997).

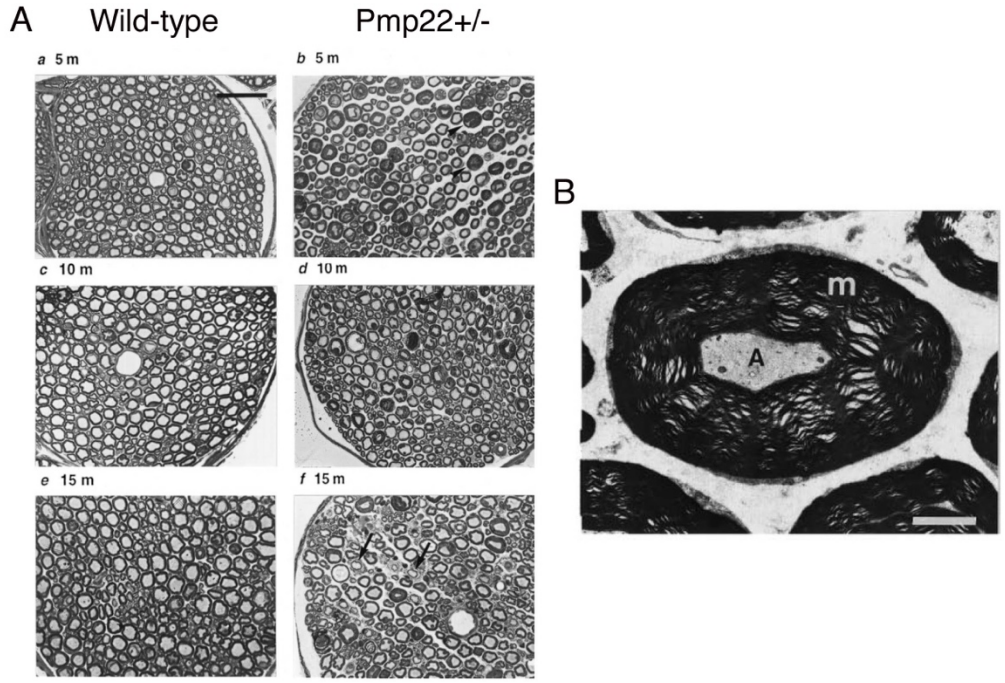


***Figure 16. The Pmp22 +/- mice (HNPP model) reproduce tomacula.***
*A) Quadriceps nerve semithin sections of WT and Pmp22$^{+/-}$ mice at 5, 10 and 15 months of age. Pmp22$^{+/-}$ mice recapitulates the morphological phenotype of HNPP neuropathy. Tomacula and hypermyelinated structures are evident at 5months of age (arrowheads image b). Degenerations and onion bulbs are visible at 15 months (arrows in f);B) Tomaculum at high magnification. (Modified from Adlkofer et al., 1997).*

### *1.4.4 Therapeutical approaches on CMT neuropathies at preclinical levels: Gene therapy (gene replacement and allele correction), Drug repurposing, Drug identification, Molecular therapy (ASO).*

Treating CMTs is then one major unmet clinical need, which urgently requires a solution. In the last decades, thanks to next-generation sequencing, it has been possible to better profile the molecular-genetic signature of each form and find new druggable sites.
New therapies for CMTs neuropathies are currently emerging and they can be divided into: 1) disease-specific, if target is the primary cause of the neuropathy, and 2) non-disease specific, if target is a downstream pathway (Stavrou *et al*.,2021). Concerning this, most non-disease specific strategies seek to counteract axonal degeneration, which is a final, common, disabling condition occurring in both axonal and demyelinating CMTs.

Even if new molecules have been selected to treat different forms of CMTs (e.g., NRG1 type III, PXT3003, curcumin, melatonin, ascorbic acid), repurposing of drugs already used in clinical practice is ongoing as well (e.g., Niaspan). This is of particular importance to quicken drugs approval in clinics and to assure their pharmaceutical production, mainly if addressing different CMT subtypes.

While the identification of small molecules aims to target pathways shared by different disorders, gene therapy is currently the cutting-edge therapeutical approach for precision medicine. Delivery of genetic material by means of viral vectors is a useful way to mitigate the gene-dosage effect by either loss- or gain-of-function mechanisms. CMTs caused by the absence of a functional protein can be treated by delivering the wild-type protein, whereas CMTs caused by toxic gain-of-function mutations or genes overexpression can be fought by gene/allele silencing or gene editing, respectively. Moreover, viral vectors can reach areas often inaccessible for drugs by crossing both BBB (blood-brain-barrier) and BNB (blood-nerve-barrier) and can provide long-lasting effects even after one delivery, thereby avoiding chronic treatments (Stavrou *et al*.,2021). However, other than toxicity and safety, a critical point regarding clinical translation is their biodistribution in the PNS: for demyelinating neuropathies, it means finding the correct conditions to transduce as many Schwann cells as possible.

Other ways to correct mutated gene products or gene overexpression are RNA-interference and antisense oligonucleotides (ASOs). In the first case, by means of short RNA molecules [e.g., microRNA(miRNA), small hairpin RNA (shRNA) or small interfering RNA (siRNA)], specific messenger RNAs (mRNAs) are targeted and degraded. In a similar trend, single-stranded RNA molecules named ASOs cause RNAseH-dependent degradation of selected mRNAs (e.g. *PMP22* mRNA in CMT1A), (Stavrou *et al*.,2021).

Nevertheless, only few treatments have successfully reached the clinical level so far (e.g. AAV1-NT3 or PXT3003 for CMT1A), and often with discouraging results. One of the main problems, other than toxicity, is the absence of valid outcome measures (e.g., biomarkers) that could help in understanding the real efficacy of the experimental approach. Accordingly, a lot of effort has lately been put in finding new accessible biomarkers in addition to clinical exams and neuroimaging.

To mention, plasma neurofilament-light chain (NF-L) and neural cell adhesion molecule 1 (NCAM-1) have been identified as two valuable markers for CMT progression and treatment responsiveness. Interestingly, NF-L, marker of axonal degeneration, has been found to correlate both in humans and mice with disease severity, age, and treatment, suggesting it could be a valid outcome measure also in pre-clinical studies (Rossor & Reilly, 2022).

## 1.5 Drug repurposing: Niacin and disease

### *1.5.1 Niacin functions and metabolism*

Niacin, also referred to as nicotinic acid, nicotinamide, or vitamin B3, is together with nicotinamide riboside and triptophan, a $NAD^+$ precursor, which exerts a crucial role in maintaining cellular homeostasis and metabolism.

The daily recommended allowance (RDA) of vitamin B3 necessary to fulfil the nutritional requirement is around 10-20 mg/Kg *[Institute of Medicine (US) Standing Committee on the Scientific Evaluation of Dietary Reference Intakes and its Panel on Folate, 1998]*. A reduced intake and absorption of niacin or tryptophan results in pellagra.

At higher doses, Niacin has been shown to have different pharmacological effects, which vary in relation to the compound and the dose administered (Mackay *et al*., 2012).

Niacin, as one of the main sources of $NAD^+$, indirectly has the potential to regulate a wide range of cellular activities. $NAD^+$ indeed is involved in many ubiquitous processes such as metabolism, bioenergetics, enzyme regulation, gene expression, DNA repair, cell cycle and calcium signalling (Nikiforov *et al*., 2015). Lately, a tight correlation between $NAD^+$ depletion and axonal degradation has been made, suggesting that energy supply could be an efficient tool to counteract the degenerative process.

Niacin is metabolised in the liver in two different ways: conjugation or amidation (**Figure 17**). Conjugation with glycine is a low-affinity, high-capacity process that converts niacin into nicotinuric acid (NUA), which is then expelled through urine. Amidation is instead a high-affinity, low-capacity process that converts niacin into nicotinamide (NAM) and leads to the production of several oxidative-reductive intermediates, which can exert a hepatotoxic function (e.g., pyrimidine intermediates 2PY and 4PY), (Cooper *et al*., 2015).

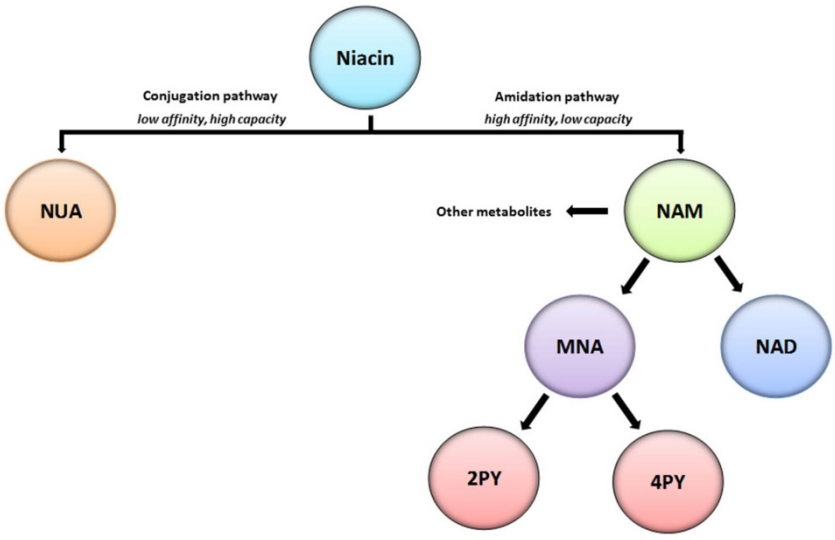


***Figure 17. Niacin metabolism through conjugation and amidation pathways.***
*NUA= nicotinuric acid; NAM= nicotinamide; NAD= nicotinamide adenine dinucleotide; MNA=N-methylnicotinamide; 2PY= N-methyl-2pyridone-5-carboxamide; 4PY= N-methyl-4-pyridone-5-carboxamide (Cooper et al., 2015; License Number 5410680660534, Elsevier).*

It is evident then that both dose and compound formulation can differently influence the metabolism. Specifically, IR (immediate release) formulation rapidly saturate the amidation pathway, thereby forcing conjugation and production of nicotinuric acid. This leads to vasodilatation and flushing, which are among the most common niacin side-effects observed in patients. On the other way, ER (extended-release) and SR (sustained-release) formulations shift the metabolism towards amidation. Since in these cases niacin release is controlled, the amidation pathway can operate on niacin substrates without reaching saturation. However, a prolonged activation of this system leads to a marked hepatic stress, which usually associates with an increase of hepatic biomarkers levels in serum (Cooper *et al*., 2015).

### *1.5.2 Niacin mechanisms of action and GPR109A receptor*

Niacin has been shown to trigger different intracellular pathways.
First, Niacin can limit triglycerides (TG) formation by both reducing free-fatty acid (FFA) availability and inhibiting Diacylglycerol acyltransferase-2 (DGAT2), the central enzyme for lipoprotein synthesis in the liver (**Figure 18A**). Low levels of TG lead to a decreased production of very low-density lipoproteins (VLDL), intermediate-density lipoprotein

(IDL) and low-density lipoprotein (LDL), resulting in an overall reduction of blood circulating lipids (Cooper *et al*., 2015).

In a similar way, niacin activates phospholipase $A_2$ ($PLA_2$) in dermal macrophages (**Figure 18B**). $PLA_2$ liberates arachidonic acid, responsible for vasodilatory prostaglandins production ($PGD_2$ and $PGE_2$) known to induce one of niacin most common side-effects: skin flushing. In addition, $PGD_2$ mediates niacin neuroprotective role both directly, by binding DP1 receptor and indirectly, trough $PGJ_2$ production, which in turn activates PPARγ and inhibits inflammation (Offermanns & Schwaninger, 2015).

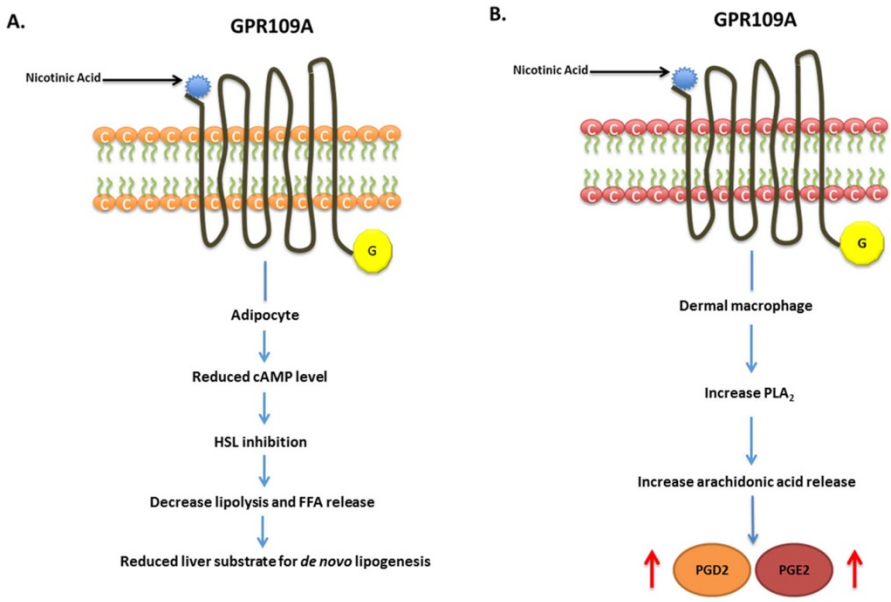


***Figure 18. Gpr109a receptor mediates niacin effects in different tissues***
*A) Gpr109a-mediated niacin mechanism in adipocytes has anti-lipolytic effect; B) Gpr109a-mediated niacin mechanism in macrophages is responsible for skin flushing (Cooper et al., 2015; License Number 5410680660534, Elsevier).*

Despite the variety of mechanisms activated, G protein-coupled receptor 109a (GPR109a) is the main mediator of niacin effects in different tissues. It belongs to the hydroxy carboxylic acid receptor family and it is expressed by adipocytes, keratinocytes, macrophages, and by various immune cells, except lymphocytes (Offermanns & Schwaninger, 2015). Mice lacking this receptor indeed do not show flushing episodes after niacin treatment as well as significant anti-inflammatory and neuroprotective effects (Benyo *et al*., 2005; Offermanns & Schwaninger, 2015).

### *1.5.3 Niacin in clinics: applications and side effects*

Niacin is a water-soluble compound able to regulate lipid metabolism and levels in blood. Several studies have shown that 1-3g/day dose in adults is sufficient to lower circulating triglycerides (TG) and low-density lipoproteins (LDL), while increasing high-density lipoproteins (HDL) (Clark & Holt, 1997; Ito, 2002; Pieper,2003). Accordingly, it is currently used in clinical practice to treat atherosclerosis and dyslipidaemia as well as to prevent cardiovascular disorders (Ganji *et al*., 2003; Brown, 2005; Barter, 2011; Villines *et al*., 2012).

**However, new findings have demonstrated that Niacin has also anti-atherogenic, anti-inflammatory, pro-arteriogenic, and neuroprotective effects, independently from its antilipolytic activity, thus becoming a potential candidate for the treatment of different neurological disorders such as multiple sclerosis, stroke, and psoriasis** (Chen *et al*., 2007; Chen *et al*., 2009; Offermanns & Schwaninger, 2015; Rawji *et al*., 2020). More specifically, neuroprotection may be reached through a direct modulation of BDNF levels or indirectly, by decreasing inflammation. Moreover, by upregulating CD36 expression, Niacin can rejuvenate macrophages and microglia in the CNS, thereby promoting debris clearance and remyelination, both in aging and in chronic pathological conditions (Rawji *et a*l., 2020).

**In addition, it has recently been shown that Niacin can also restore $NAD^+$ levels in degenerative disorders featured by $NAD^+$ depletion and mitochondrial dysfunction (e.g., adult-onset mitochondrial myopathy) as well as in patients with NADX-deficiency (Pirinen *et al*., 2020; Manor *et al*., 2022), thereby widening the spectrum of its clinical applications.**

Despite its beneficial effects, Niacin can also induce adverse reactions (e.g., flushing, abdominal discomfort, headache, nausea), especially at high doses and with immediate release (IR) formulations. This has led to the generation of new compounds, which provide long-lasting release of niacin (ER=extended-release and SR=sustained-release formulations), aiming to limit systemic drug exposure without reducing the dose. To mention, Niaspan® (Abbott) is an orally given, FDA-approved, extended-release formulation of niacin (ER) used to treat dyslipidaemia, which shows a reduced risk of flushing as compared to pure niacin. Nevertheless, both ER and SR formulations are not free of caveats since they shift niacin metabolism towards amidation thereby increasing

the risk of hepatotoxicity. To overcome this issue, identification of new delivery routes- such as transdermal applications or the use of polymeric nanoparticles- have lately emerged because of their biocompatibility, degradation, and low toxicity. Specifically, polymeric nanoparticles are composed of niacin granules encapsulated with ethyl cellulose using a double emulsion solvent diffusion method, which enables drug release over time (Cooper *et al*., 2015).

### *1.5.4 Niacin effect on TACE activity*

Despite its effects on regeneration, neuroprotection and oxidative metabolism, Niacin has emerged as a possible therapeutic approach for some neurological disorders also for its ability to enhance TACE activity.

First evidence of that was found while studying arteriogenesis after stroke: Niaspan® administration was able to increase arterial sprouting and cerebral blood flux partially by activating TACE (Chen *et al.*, 2007; Chen *et al*., 2009).

As already mentioned in 1.2.3, TACE secretase negatively regulates NRG1-mediated myelination signalling in the PNS, thus becoming an interesting therapeutic target also for hypermyelinating neuropathies. Niacin-mediated TACE activation has been found to be an efficient strategy to ameliorate *in vitro* and *in vivo* models of CMT4B1 and HNPP neuropathies (Bolino *et al*., 2016). Specifically, Niaspan® (FDA-approved, long-lasting release formulation of niacin) treatment *in vivo* (160 mg/Kg, by intraperitoneal injection, i.p.) from P15 to P75 in *Mtmr2*$^{-/-}$ mice (CMT4B1 mouse model), and from P15 to P45 in *Pmp22*$^{+/-}$ mice (HNPP mouse model) ameliorated the morphological phenotype. Of note, Niaspan® was able to significantly reduce the percentage of myelin outfoldings and tomacula respectively, without negatively altering the *g-ratio*. It was also demonstrated that Niacin/Niaspan® efficiently increased TACE activity in Schwann cells/Dorsal Root Ganglion *Mtmr2*$^{-/-}$ co-cultures and *in vivo* models of CMT4B1 and HNPP neuropathies.

Finally, to prove that niacin precisely targets TACE, both *Tace*$^{-/-}$ explants and *Mtmr2*$^{-/-}$ co-cultures (in which TACE expression was downregulated by shRNA) were treated with niacin. In both cases, niacin did not rescue myelin alterations (increased number of myelin segments and myelin outfoldings, respectively), supporting the fact that niacin effects on myelination are mediated by TACE and, in its absence, these effects are lost (Bolino *et al.*,2016).

## 2. AIM OF THE PROJECT

Charcot-Marie-Tooth (CMT) neuropathies are genetically and clinically heterogeneous diseases with a prevalence of 1:2500 worldwide and currently untreatable. Because of their wide heterogeneity, the identification of a common treatment strategy or at least a strategy that can be effective for more than one clinical form independently from the specific pathogenetic mechanism would be ideal.

Axonal neuregulin-1 (NRG1) type III plays a crucial role in PNS myelination. Of note, TACE secretase negatively regulates NRG1 type III and its activity can be enhanced by Niacin (nicotinic acid). We thus hypothesized that Niacin, by enhancing TACE activity and reducing NGR1-mediated myelination signalling, may represent an effective strategy to ameliorate CMT neuropathies with excessive myelin, specifically focal hypermyelination. Among demyelinating CMTs, CMT4B1 and HNPP (Hereditary neuropathy with liability to pressure palsies) are indeed neuropathies characterised by the presence of aberrant myelin structures (e.g., myelin outfoldings/infoldings and tomacula), types of focal hypermyelination. Our laboratory recently provided proof-of principle that Niacin/Niaspan®, by increasing TACE activity, reduces aberrant myelin in models of CMT4B1 and HNPP neuropathies (Bolino *et al*., 2016).

**Thus, the aim of my PhD project was to further investigate Niacin/Niaspan® as a therapeutic strategy for CMT neuropathies with focal hypermyelination**.

More precisely, I aimed at unravelling Niacin/Niaspan® *in vivo* effect (both morphological and functional) after long-term treatment. I was also interested in refining the treatment protocol by giving Niacin by gavage to both simulate the human administration *(per os)* and improve the biodistribution of the drug in the nerve over time. Moreover, since 1) both CMT4B1 and HNPP are chronic diseases which progress to degeneration and fiber loss with age, and 2) TACE and NRG1 play a pivotal role in nerve regeneration (Stassart *et al*., 2013), I was interested in evaluating Niacin/Niaspan® impact also after nerve crush injury, a model of nerve damage.

Finally, GPR109A receptor mediates niacin mechanism of action in different tissues, including skin and adipocytes (Offermans & Schwaninger, 2015). Thus, since this process is still unknown in the PNS, I investigated GPR109A receptor expression in both sciatic nerves and spinal cord (motor neurons cell bodies).

# 3. RESULTS

## 3.1 Elucidating Niacin mechanism of action in the Peripheral Nervous System

Niacin is known to bind GPR109A (G-protein coupled receptor 109A) receptor in different tissues including spleen, adipose tissue, and epidermis (Hanson *et al*., 2010). Therefore, we hypothesized that GPR109A may be expressed also in the PNS and it may mediate Niacin-related TACE activation by triggering different subcellular pathways. Since TACE is expressed by both axons and glial cells, but axonal TACE is involved in regulating NRG1-mediated myelination signalling (La Marca *et al*., 2011), we decided to perform immunofluorescent (IF) analyses of GPR109A expression in motor neurons, both in the PNS (axons) and CNS (cellular body) compartments. To this aim, we used the *Gpr109a*$^{mRFP}$ transgenic mice line (provided by Prof. Stephan Offermanns, Department of Pharmacology, Max-Planck-Institute for Heart and Lung Research, Bad Nauheim, Germany), in which RFP (red fluorescent protein) expression is under the control of GPR109A promoter. For all the experiments we used spleen as RFP positive control, since it is known that GPR109A receptor is highly expressed by monocyte/macrophages.

### *3.1.1 GPR109A receptor is not expressed in the Peripheral Nervous System*

To detect GPR109A expression in the PNS, we performed IF analysis on transversal sciatic nerve sections of *Gpr109a*$^{mRFP}$ transgenic mice at P30 **(Figure 20A)** and P60 **(Figure 20B)**. Spleen was always used as positive control **(Figure 19).**

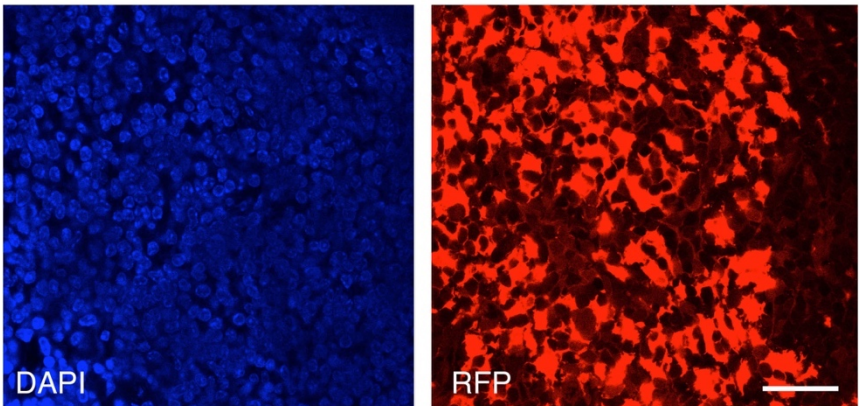


***Figure 19. RFP is highly expressed in Gpr109a$^{mRFP}$ mice spleen.***
*Representative confocal images showing RFP expression in the spleen of Gpr109a$^{mRFP}$ mice. Spleen was used as positive control in all the experiments performed at both P30 and P60. Magnification is 63x. Bar is 45µm.*

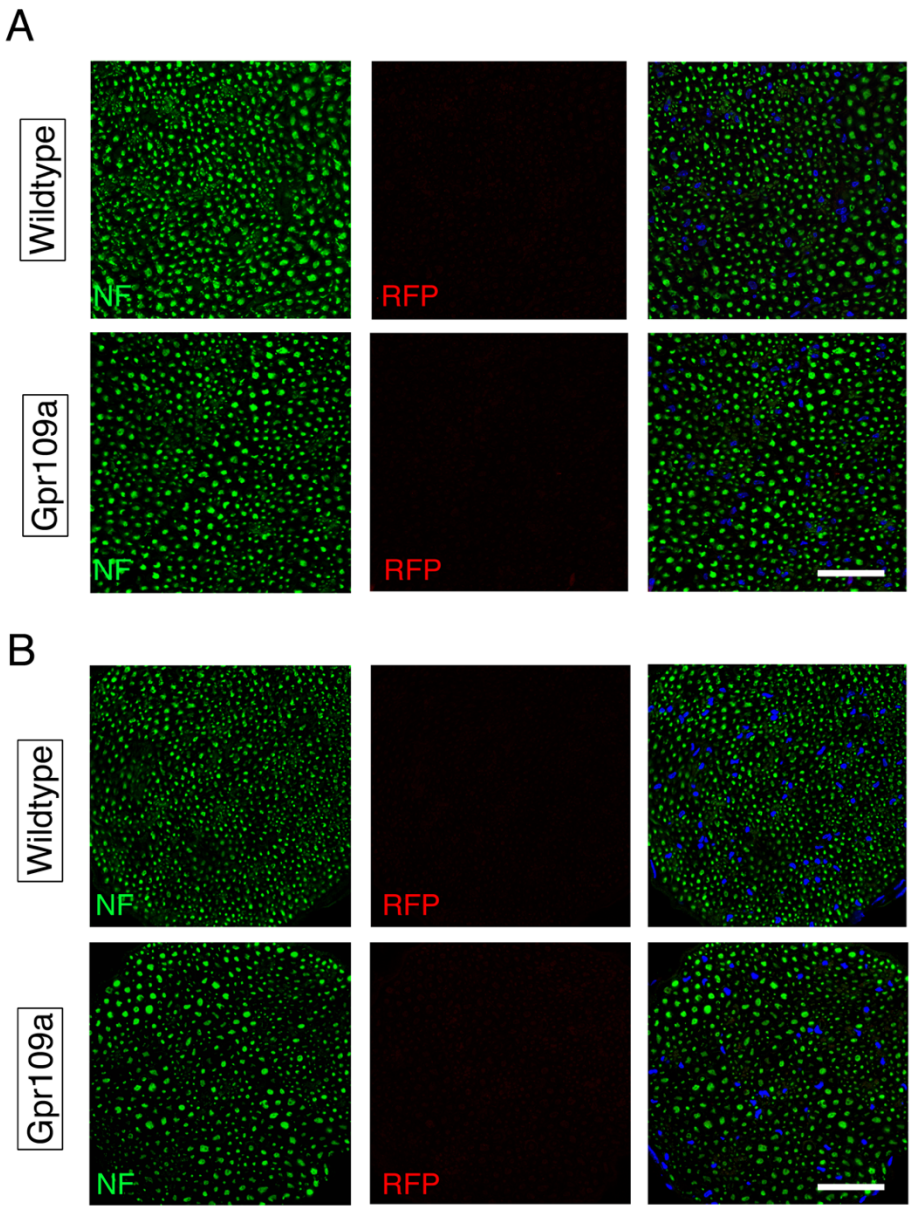


***Figure 20. GPR109A receptor is not expressed in the PNS at both P30 and P60.***
*A-B) Representative confocal images of transversal sciatic nerve sections showing RFP expression at P30(A) and P60(B). No RFP signal was found in the PNS at both ages. Magnification is 63x. Bar in A and B is 45μm. N=3 WT and n=3 Gpr109a$^{mRFP}$. Results of three independent experiments.*

No RFP$^{+}$ cells have been found in the sciatic nerve at both P30 and P60, indicating that GPR109A receptor is not expressed in the PNS at least at these time points which are relevant for the treatment protocol.

### *3.1.2 GPR109A receptor is not expressed in motoneuronal cellular bodies*

Since we did not find any positive signal in the axonal portion of motor neurons (sciatic nerve, PNS), we decided to monitor GPR109A expression in neuronal cellular bodies (spinal cord, CNS). To this aim, we labelled motor neurons using NeuN (Neuronal Nuclear Protein, pan-neurons marker, **Figure 21A)** or ChAT (Choline Acetyltransferase, alpha-motor neurons marker, **Figure 21B)** staining combined with RFP.
Spleen was always used as positive control **(Figure 19).**

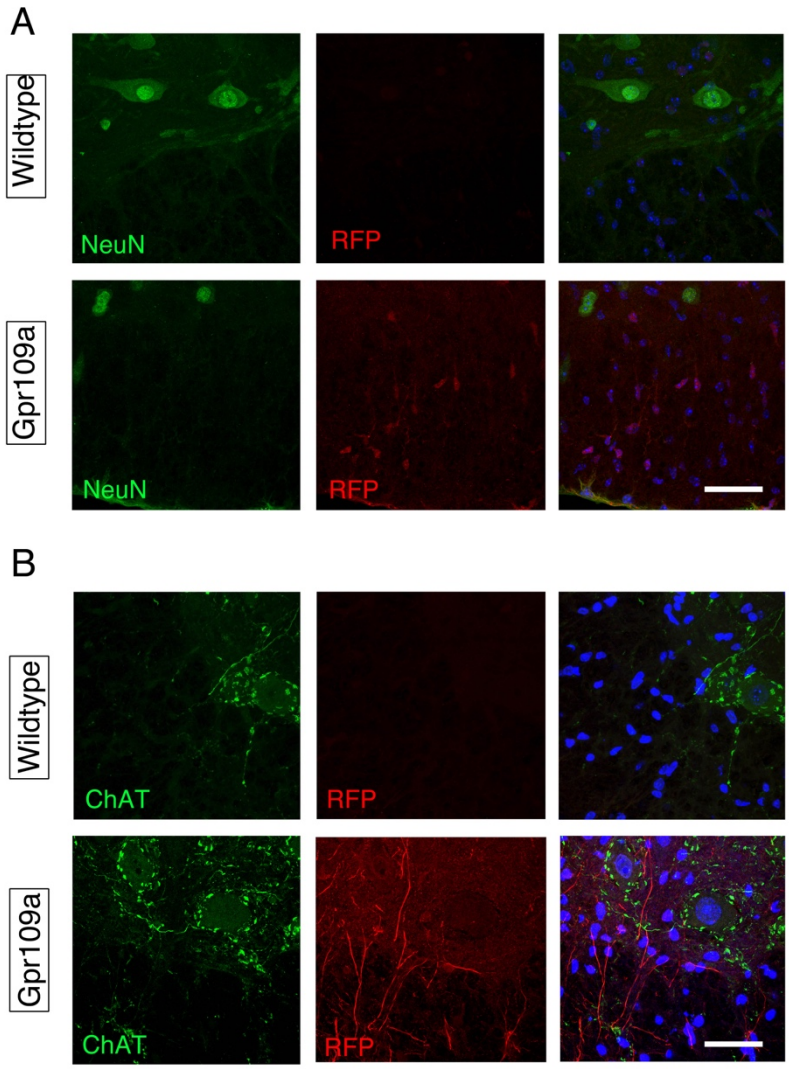


***Figure 21. GPR109A receptor is not expressed in motoneuronal cellular bodies at P60.***
*A-B) Representative confocal images of transversal spinal cord sections showing RFP expression at P60 co-stained with NeuN (A) or ChAT (B) markers in green. ChAT was used to specifically depict alpha-motor neurons while NeuN to detect all neuronal bodies. Magnification is 63x. Stacks are 10 µm. Bar in A and B is 43 µm. N=3 WT and n=3 Gpr109a$^{mRFP}$. Results of three independent experiment.*

In both cases, we found some $RFP^+$ cells (mainly in the white matter) which resulted not to be motor neurons nor other neuronal population, but probably some glial-like cells and/or their projections.

Altogether these results suggest that GPR109A receptor is not expressed by motor neurons in both PNS and CNS compartment and that some other receptors/mechanisms may be involved in mediating niacin signalling in the PNS.

## 3.2 Unravelling the effect of Niaspan® /Niacin treatment in peripheral nerve regeneration

Both CMT4B1 and HNPP are chronic diseases which progress to degeneration and fibres loss with age. Since we know that 1) nerve regeneration is possible in the PNS, 2) NRG1 plays a pivotal role also in nerve regeneration and 3) Niacin acts on myelination by regulating NRG1 type III levels through TACE, we asked whether Niacin treatment could interfere with the physiological attempt of PNS to regenerate and remyelinate after damage.

### *3.2.1 Niacin administration after nerve crush is not detrimental in Pmp22$^{+/-}$ mice*

TACE is expressed by both axons and Schwann cells, but only axonal TACE is involved in NRG1 type III modulation and myelination during development (La Marca *et al*, 2011). On the other hand, TACE expressed by Schwann cells (likely acting on NRG1 type I) is dispensable during development, as mice lacking TACE specifically in Schwann cells display normal myelin (La Marca *et al*, 2011).

During nerve regeneration after damage, instead, the role of Schwann cell derived NRG1 type I is crucial during the first one-two weeks after damage when Schwann cells are present and axons are lost. Subsequently, when axons regenerate, NRG1 type III takes place and inhibits NRG1 type I expression in Schwann cells.

To evaluate the effects of Niacin administration in nerve regeneration, we performed crush nerve injury, a model of nerve damage, first in the *Pmp22*+/- mouse, a model of the HNPP neuropathy. We set up different protocols of Niacin administration, to explore the effects of Niacin-mediated TACE inhibition when Schwann cells only are present (T0-T7/T10) and when axons regrowth after T14 (**Figure 22**).

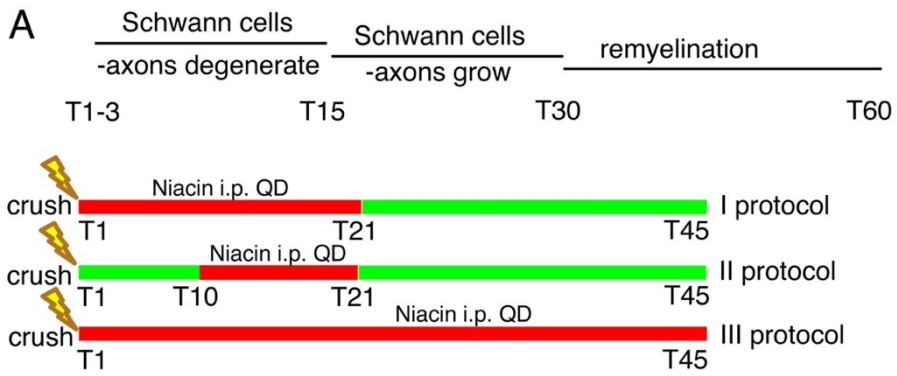


***Figure 22. Study design for Niacin administration after nerve crush.***
*Schematic representation showing different protocols for niacin treatment after nerve crush in relation to the regenerative process.*

First, we confirmed the increase of TACE activity in the nerve following Niacin administration. To this aim, in collaboration with Dr. Stefano Previtali's group (Neuromuscular Repair Unit, INSPE, San Raffaele Hospital, Milan), we crushed adult WT and *Pmp22*$^{+/-}$ mice and we treated them with **Niacin (120 mg/Kg, by i.p.)** for 7 days starting from the day after damage (T1). In parallel, we also treated a group of uncrushed adult WT and *Pmp22*$^{+/-}$ mice. We found that TACE activity was increased in uncrushed nerves of both WT and *Pmp22*$^{+/-}$ mice after one week of treatment, as expected, whereas TACE activity was barely detectable in crushed nerves from both genotypes **(Figure 23).**

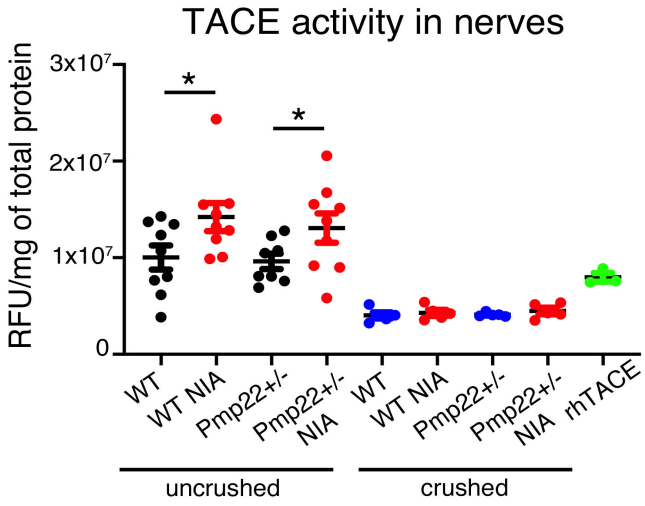


***Figure 23. Niacin increases TACE activity only in uncrushed nerves of WT and Pmp22$^{+/-}$ mice.***
*Quantification of TACE activity in WT and Pmp22$^{+/-}$ sciatic nerves in physiological conditions (uncrushed) and after sciatic nerve crush followed by Niacin administration via i.p. for seven*

*days after injury; rh (recombinant human) TACE was loaded as internal positive control of the experiment.*
*Uncrushed animals: n=9 WT saline, n=9 WT niacin, n=8 Pmp22$^{+/-}$ saline, n=9 Pmp22$^{+/-}$ niacin. Crushed animals: n=5 WT saline, n=5 WT niacin, n=5 Pmp22$^{+/-}$ saline, n=5 Pmp22$^{+/-}$ niacin. WT saline vs. WT Niacin uncrushed: *p= 0.0385, non-parametric Mann-Whitney, T-test; Pmp22$^{+/-}$ saline vs. Pmp22$^{+/-}$ Niacin uncrushed: *p= 0.0464, Non-parametric Mann-Whitney, T-test. The Mann-Whitney test was used instead of ANOVA because we were not interested in evaluating differences between WT and PMP22$^{+/-}$ mice (both saline and niacin-treated) but only after treatment in both genotypes. Data have all been shown in the same graph for simplicity and clarity. Data represent Mean± SEM.*

These results suggest that: 1) Niacin treatment increases TACE activity in uncrushed, intact nerves, confirming previous results; 2) Niacin treatment does not increase TACE activity when axons are lost and only Schwann cells are present, as in the case of crushed nerves from T1 to T7. Thus, only TACE expressed by axons but not Schwann cells likely responds to Niacin.

Then, we crushed adult WT and *Pmp22$^{+/-}$* mice and we treated them **from T1 to T21** with **Niacin (120 mg/Kg, by i.p., QD)**. Electrophysiological and morphological analyses were performed at T45 dpsni, a time when regeneration is almost achieved (**Figure 24-26**).

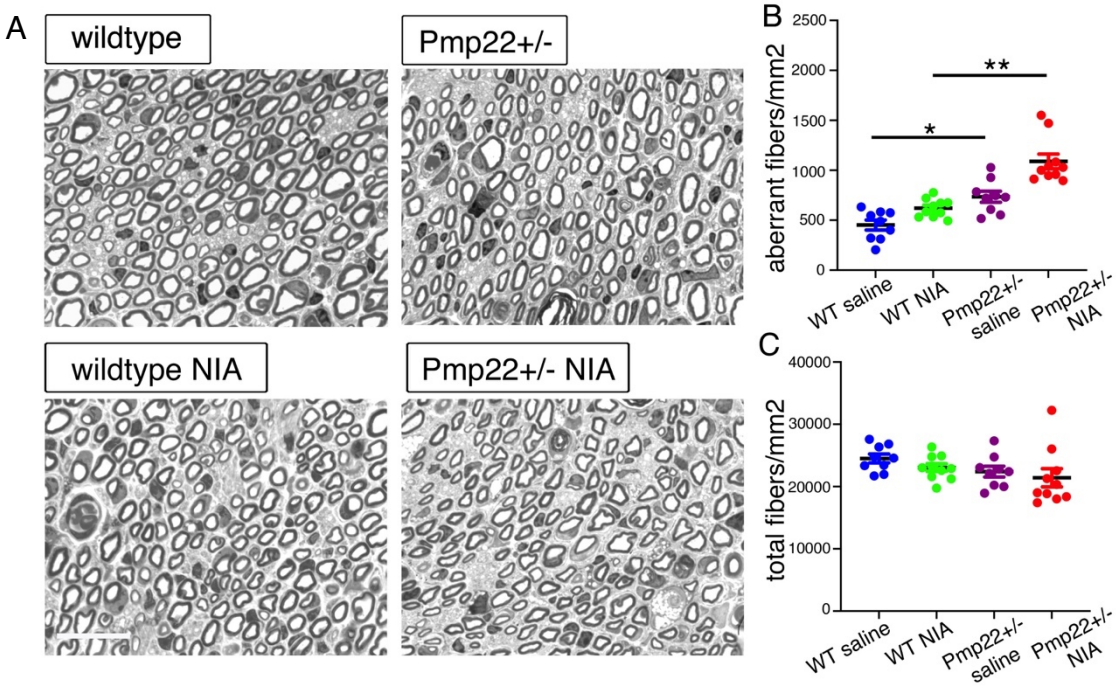


***Figure 24. Niacin treatment from T1 to T21 after crush does not negatively impact on nerve regeneration in both WT and Pmp22$^{+/-}$ mice.***
*A) Representative images of sciatic nerve semithin sections analysis of both vehicle and niacin-treated WT and Pmp22$^{+/-}$ mice at T45dspni; n=10 WT saline, n=10 WT niacin, n=9 Pmp22$^{+/-}$ saline, n=10 Pmp22$^{+/-}$ niacin; Scale Bar is 18,6μm; B) Quantification of fibres displaying*

*aberrant myelin structures on sciatic nerve area ($mm^2$); *p=0.0386; **p=0.0019; non-parametric ANOVA followed by Dunn's multiple comparison test. C) Quantification of total fibres on sciatic nerve area ($mm^2$); p>0.05; Non-parametric ANOVA followed by Dunn's multiple comparison test. Data represent mean± SEM.*

Morphological analyses on sciatic nerve semithin sections revealed that niacin treatment from T1 to T21 did not negatively influence nerve regeneration nor remyelination.

In particular, we did not find any difference in the number of aberrant myelinated fibres (tomacula) nor of total fibres after niacin administration (**Figure 24B ABERRANT FIBRES**: WT saline *vs.* WT niacin p=0.5085 and *Pmp22*$^{+/-}$ saline *vs. Pmp22*$^{+/-}$ niacin p=0.0908; **Figure 24C TOTAL FIBRES**: p>0.05, non-parametric ANOVA followed by Dunn's multiple comparisons test). Of note, mutant mice displayed a significant number of aberrant fibres (tomacula), thus suggesting that the pathological phenotype was efficiently reproduced also after nerve injury (**Figure 24B ABERRANT FIBRES**: WT saline *vs. Pmp22*$^{+/-}$ saline *p=0.0386 and WT niacin *vs. Pmp22*$^{+/-}$ niacin **p=0.0019, non-parametric ANOVA followed by Dunn's multiple comparisons test). The number of total fibres between the four groups was not significantly changed (**Figure 24C**).

In addition, *g-ratio* (calculated as the ratio between axonal diameter and fiber diameter) was analysed to evaluate remyelination (**Figure 25A).**

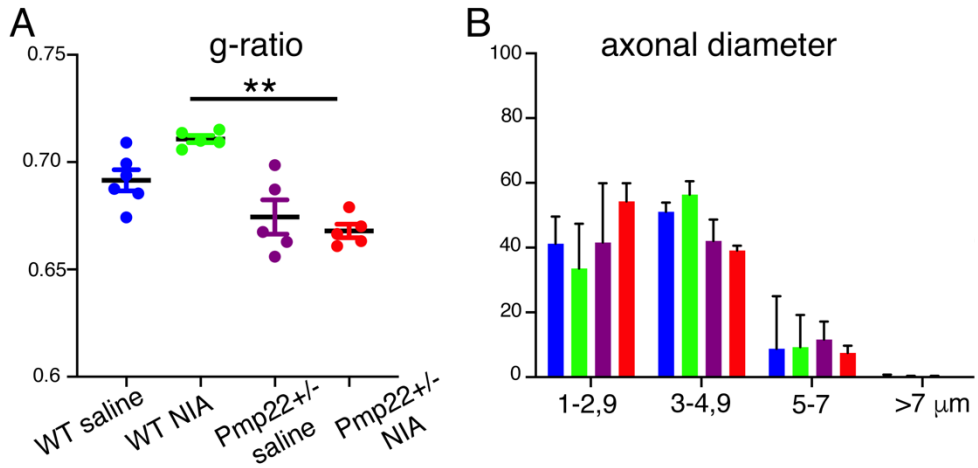


***Figure 25. Niacin treatment from T1 to T21 after crush does not negatively impact nerve remyelination in both WT and Pmp22$^{+/-}$ mice.***

*A) Quantification of g-ratio analysis at T45dpsni. WT saline 0.69±0.004; WT niacin 0,71±0.001; Pmp22$^{+/-}$ saline 0.67±0.007; Pmp22$^{+/-}$ niacin 0,66±0.003; n=5 animals per group; **p=0.0026; non-parametric ANOVA followed by Dunn's multiple comparison test. Data represent mean± SEM B) Quantification of axonal diameter distribution at T45dpsni; n=5 animals per group; p>0.05; Non-parametric ANOVA followed by Dunn's multiple comparison test. Data represent median with range.*

As expected since *Pmp22*+/- nerves are characterized by a hypermyelination phenotype, with both increased myelin thickness and focal thickening of myelin-tomacula, we noticed a significant reduction of the *g-ratio* value between WT-treated and *Pmp22*$^{+/-}$ -treated mice (**Figure 25A G-RATIO**: WT niacin *vs.* *Pmp22*$^{+/-}$ niacin **p=0.0026, n=5 animals per group, non-parametric ANOVA followed by Dunn's multiple comparisons test), but no differences were observed after treatment in both genotypes.

Axonal diameter distribution was also calculated to complement *g-ratio* results: no significant differences have been found among all groups (**Figure 25B AXONAL DIAMETER DISTRIBUTION**: p>0.05, n=5 animals per group, non-parametric ANOVA followed by Dunn's multiple comparisons test), suggesting that niacin treatment from T1 to T21 did not negatively impact on nerve remyelination.

Finally, to evaluate niacin impact from a functional point of view, we decided to perform neurophysiological analyses at T45dpsni in collaboration with Dr. Ubaldo del Carro and Dr. Francesca Bianchi (Neurophysiology Unit, INSPE, San Raffaele Hospital, Milan) **(Figure 26).**

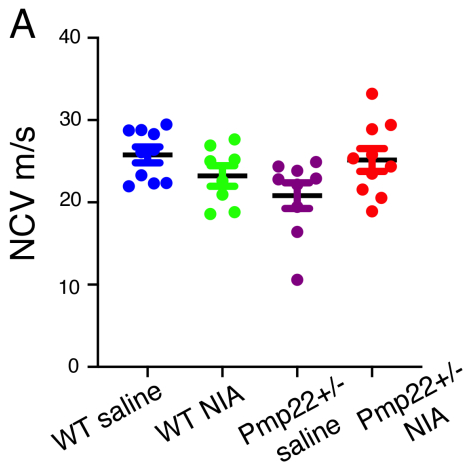


| | NCV (m/s) |
|---|---|
| **WT Saline** | 25,77±0,96 |
| **WT Niacin** | 23,21±1,24 |
| ***Pmp22*+/- Saline** | 20,82±1,56 |
| ***Pmp22*+/-Niacin** | 25,15±1,39 |

***Figure 26. Niacin treatment from T1 to T21 after crush does not negatively alter NCV.***
*A) Quantification of NCV values of WT and Pmp22*$^{+/-}$ *mice at T45dpsni after niacin treatment from T1 to T21. n=10 animals per group; p>0.05; Non-parametric ANOVA followed by Dunn's multiple comparison test. On the right, table showing NCV values. Data represent mean± SEM.*

Our results indicate that *Pmp22*$^{+/-}$ mice have a trend for reduction in nerve conduction velocity (NCV) when compared to WT (**Figure 26A NCV**: WT saline 25,77±0,96 m/s *vs.* *Pmp22*$^{+/-}$ saline 20,82 ± 1,56 m/s, p=0.0876; non-parametric ANOVA followed by

Dunn's multiple comparisons test) and that Niacin treatment has not a detrimental effect on nerve physiology of both WT and *Pmp22*$^{+/-}$ mice (**Figure 26A NCV**: WT saline 25,77± 0,96 m/s *vs.* WT niacin 23,21± 1,24 m/s, p= 0,6894*;* *Pmp22*$^{+/-}$ saline 20,82 ± 1,56 m/s *vs.* *Pmp22*$^{+/-}$ niacin 25,15± 1,39 m/s, p=0.2631, non-parametric ANOVA followed by Dunn's multiple comparisons test).

Taken together, these results indicate that niacin treatment from T1 to T21 did not negatively interfere with Schwann cell-expressed NRG1 type I activity and then with nerve regeneration/remyelination after crush. Moreover, our findings highlighted the presence of a possible degeneration defect in *Pmp22*$^{+/-}$ mice, which has not been previously reported.

Our second step was to evaluate whether niacin influences specifically on axonal NRG1 type III-mediated signalling, which is essential to remyelinate newly regenerated axons. To this purpose, we crushed adult WT and *Pmp22*$^{+/-}$ mice and we treated them from **T10 to T21** with **Niacin (120 mg/Kg, by i.p., QD)**, a time when axons regrowth after damage and express both TACE and NRG1 type III. Electrophysiological and morphological analyses were performed at T45dpsni (**Figure 27-29**).

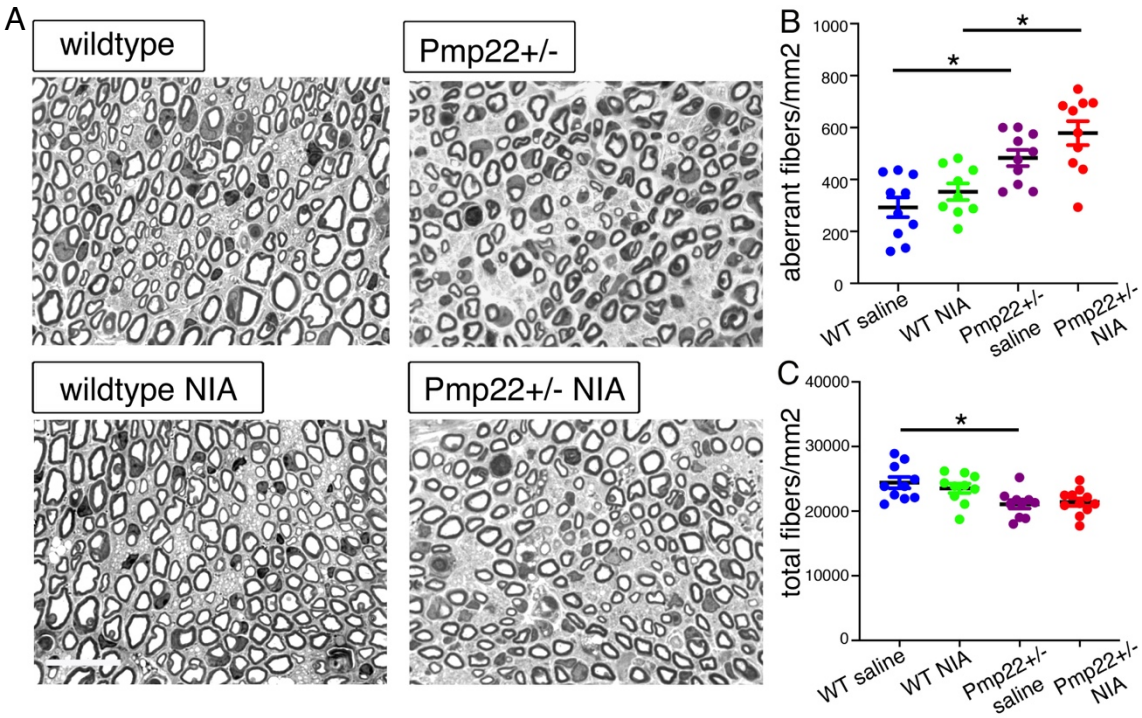


***Figure 27. Niacin treatment from T10 to T21 after crush does not negatively impact nerve regeneration in both WT and Pmp22$^{+/-}$ mice.***

*A) Representative images of sciatic nerve semithin sections analysis of both vehicle and niacin-treated WT and Pmp22$^{+/-}$ mice at T45dspni; n=10 WT saline, n=10 WT niacin, n=10 Pmp22$^{+/-}$*

*saline, n=11 Pmp22$^{+/-}$ niacin; Scale Bar is 18,6μm; B) Quantification of fibres displaying aberrant myelin structures on sciatic nerve area (mm$^2$); WT saline vs. Pmp22$^{+/-}$ saline *p=0.0250 and WT niacin vs. Pmp22$^{+/-}$ niacin *p=0.0248; non-parametric ANOVA followed by Dunn's multiple comparison test. C) Quantification of total fibres on sciatic nerve area (mm$^2$); WT saline vs Pmp22$^{+/-}$ saline *p=0.0304; Non-parametric ANOVA followed by Dunn's multiple comparison test. Data represent mean± SEM.*

Morphological analyses on sciatic nerve semithin sections showed that niacin treatment from T10 to T21 did not negatively influence nerve regeneration nor remyelination.

More specifically, we did not find any difference in the number of aberrant myelinated fibres nor of total fibres after niacin administration (**Figure 27B**: **ABERRANT FIBRES**: WT saline *vs.* WT niacin p=0.7909 and *Pmp22*$^{+/-}$ saline *vs. Pmp22*$^{+/-}$ niacin p=0.8367; **Figure 27C TOTAL FIBRES**: WT saline *vs.* WT niacin p>0.999 and *Pmp22*$^{+/-}$ saline *vs. Pmp22*$^{+/-}$ niacin p>0.999, non-parametric ANOVA followed by Dunn's multiple comparisons test). In addition, mutant mice displayed a significant number of aberrant fibres (tomacula), thus confirming again, as in the first experiment performed, that the pathological phenotype was efficiently reproduced also after nerve injury (**Figure 27B ABERRANT FIBRES**: WT saline *vs. Pmp22*$^{+/-}$ saline *p=0.0250 and WT niacin *vs. Pmp22*$^{+/-}$ niacin *p=0.0248, non-parametric ANOVA followed by Dunn's multiple comparisons test). We also found a significant reduction in the number of total fibres between WT and *Pmp22*$^{+/-}$ mice (**Figure 27C TOTAL FIBRES**: WT saline *vs Pmp22*$^{+/-}$ saline *p=0.0304, non-parametric ANOVA followed by Dunn's multiple comparisons test), suggesting that *Pmp22*$^{+/-}$ mice have a defect in nerve regeneration.

G-*ratio* and axonal diameter distribution were also assessed to evaluate remyelination (**Figure 28).**

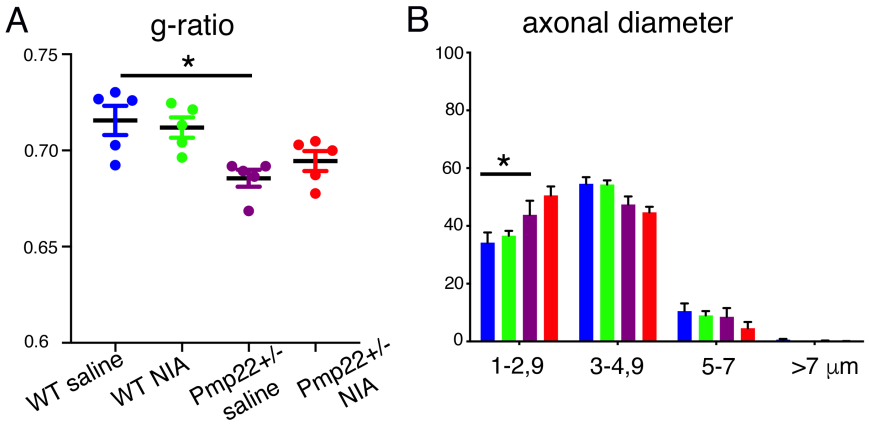


***Figure 28. Niacin treatment from T10 to T21 after crush does not negatively impact nerve remyelination in both WT and Pmp22$^{+/-}$ mice.***

*A) Quantification of g-ratio analysis at T45dpsni. WT saline 0.71±0.007; WT niacin 0,71±0.051; Pmp22$^{+/-}$ saline 0.68± 0.004; Pmp22$^{+/-}$ niacin 0,69± 0.005; n=5 animals per group; *p=0.0156; non-parametric ANOVA followed by Dunn's multiple comparison test. Data represent mean± SEM B) Quantification of axonal diameter distribution at T45dpsni; n=5 animals per group; *p>0.05; Non-parametric ANOVA followed by Dunn's multiple comparison test. Data represent median with range.*

As expected, we confirmed the significant reduction of the *g-ratio* value between WT and *Pmp22*$^{+/-}$ mice as observed in the first protocol (**Figure 28A G-RATIO**: WT saline *vs.* *Pmp22*$^{+/-}$ saline *p=0.0156, n=5 animals per group, non-parametric ANOVA followed by Dunn's multiple comparisons test), but no differences were observed after treatment in both genotypes, suggesting that niacin treatment from T10 to T21 did not negatively impact on nerve remyelination.

Axonal diameter distribution was also calculated to corroborate *g-ratio* results: no significant differences have been found among all groups, except an increase in the 1-2,9µm range between WT saline and *Pmp22*$^{+/-}$ saline mice (**Figure 28B AXONAL DIAMETER DISTRIBUTION**: WT saline *vs.* *Pmp22*$^{+/-}$ saline *p<0.05, n=5 animals per group, non-parametric ANOVA followed by Dunn's multiple comparisons test), which was not considered as relevant since it is not consistent in all fiber size ranges.

To evaluate niacin impact from a functional point of view, neurophysiological analyses were performed as previously done at T45dpsni (**Figure 29).**

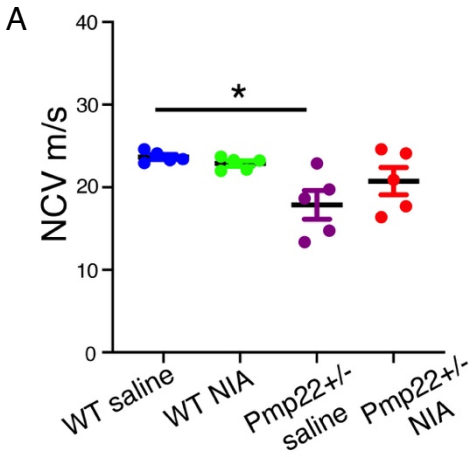


| | NCV (m/s) |
|---|---|
| **WT Saline** | 23,5±0,38 |
| **WT Niacin** | 23,93±1,51 |
| ***Pmp22*+/- Saline** | 17,88±1,74 |
| ***Pmp22*+/-Niacin** | 21,66±1,50 |

***Figure 29. Niacin treatment from T10 to T21 after crush does not negatively alter NCV Pmp22$^{+/-}$ mice.***

*A) Quantification of NCV values of WT and Pmp22$^{+/-}$ mice at T45dpsni after niacin treatment from T10 to T21. n=5 animals per group;*p=0.0199; Non-parametric ANOVA followed by Dunn's multiple comparison test. On the right, table showing specific NCV values. Data represent mean± SEM.*

Our data consistently reproduced the NCV reduction observed in the first protocol between WT and *Pmp22*$^{+/-}$ mice (**Figure 29A NCV**: WT saline 23,5±0,38 m/s *vs.* *Pmp22*$^{+/-}$ saline 17,88±1,74 m/s, *p=0.0199, non-parametric ANOVA followed by Dunn's multiple comparisons test) and the absence of a detrimental effect of niacin treatment on nerve physiology (**Figure 29A NCV**: WT saline 23,5± 0,38 m/s *vs.* WT niacin 23,93± 1,51 m/s, p>0,999; *Pmp22*$^{+/-}$ saline 17,88±1,74 m/s *vs.* *Pmp22*$^{+/-}$ niacin 21,66 ±1,50 m/s, p=0.594, non-parametric ANOVA followed by Dunn's multiple comparisons test).

Taken together, these findings suggest that niacin administration from T1 to T21 (Schwann cells are present which express TACE and NRG1 type I) and from T10 to T21(also axons are present which express TACE and NRG1 type III) is not detrimental for nerve regeneration nor remyelination in both WT and *Pmp22*$^{+/-}$ mice.

Moreover, we found a nerve regeneration defect in *Pmp22*$^{+/-}$ mice which had never been described before.

### *3.2.2 Niacin administration after nerve crush is not detrimental in Mtmr2*$^{-/-}$ *mice*

Since niacin was given for a short period of time after crush injury (T1-T21 or T10-T21) and analyses were performed at T45dpsni, we asked whether this may have led us to underestimate its effects. Thus, we decided to treat mice **continuously for 45 days after injury.** Since NRG1 type I and III modulation is crucial within 21dpsni and we already had information of niacin effects on *Pmp22*$^{+/-}$ mice during this phase, we decided to test this protocol directly in another mouse model of hypermyelinating neuropathy: the *Mtmr2*$^{-/-}$ mouse (CMT4B1 mouse model with myelin outfoldings). This is indeed the second model we used to obtain proof-of-principle data of efficacy of niacin (Bolino *et al*., 2016).

To this aim, we crushed adult WT and *Mtmr2*$^{-/-}$ mice and we treated them with **Niacin (120 mg/Kg, by i.p., QD)** from **T1 to T45**. Electrophysiological and morphological analyses were performed as before at T45 (**Figure 30-32)**.

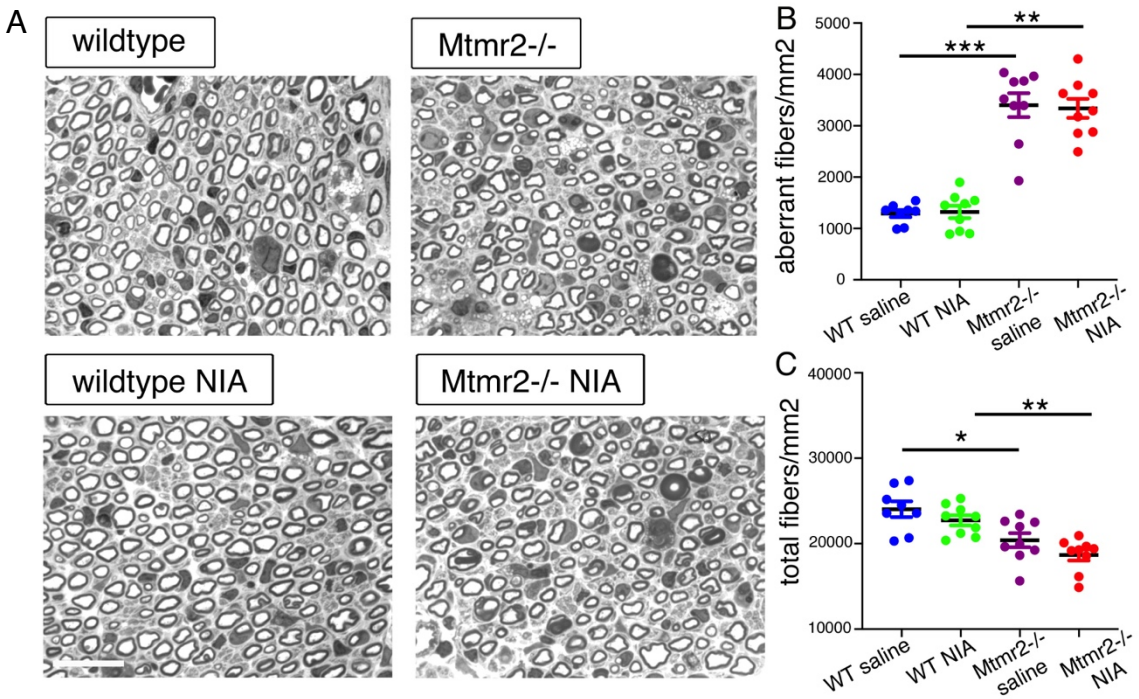


***Figure 30. Niacin treatment from T1 to T45 after crush does not negatively impact nerve regeneration in both WT and Mtmr2$^{-/-}$ mice.***
*A) Representative images of sciatic nerve semithin sections analysis of both vehicle and niacin-treated WT and Mtmr2$^{-/-}$ mice at T45dspni; n=8 WT saline, n=9 WT niacin, n=9 Mtmr2$^{-/-}$ saline, n=9 Mtmr2$^{-/-}$ niacin; Scale Bar is 18,6μm; B) Quantification of fibres displaying aberrant myelin structures on sciatic nerve area (mm$^2$); WT saline vs. Mtmr2$^{-/-}$ saline ***p=0.0006 and WT niacin vs. Mtmr2$^{-/-}$ niacin **p=0.0031; non-parametric ANOVA followed by Dunn's multiple comparison test. C) Quantification of total fibres on sciatic nerve area (mm$^2$); WT saline vs Mtmr2$^{-/-}$ saline *p=0.0411; WT niacin vs. Mtmr2$^{-/-}$ niacin **p=0.0051; Non-parametric ANOVA followed by Dunn's multiple comparison test. Data represent mean± SEM.*

Morphological analyses on sciatic nerve semithin sections revealed that niacin treatment did not negatively influence nerve regeneration nor remyelination, even when chronically administered from T1 to T45.

More specifically, we did not find any difference in the number of aberrant myelinated fibres nor of total fibres after niacin administration (**Figure 30B**: **ABERRANT FIBRES**: WT saline *vs.* WT niacin p>0.999 and *Mtmr2*$^{-/-}$ saline *vs. Mtmr2*$^{-/-}$ niacin p>0.999; **Figure 30C TOTAL FIBRES**: WT saline *vs.* WT niacin p>0.999 and *Mtmr2*$^{-/-}$saline *vs. Mtmr2*$^{-/-}$ niacin p=0.823, non-parametric ANOVA followed by Dunn's multiple comparisons test). However, mutant mice showed a significant number of aberrant fibres (myelin

outfoldings/infoldings) compared to WT, thus suggesting that the pathological phenotype was efficiently reproduced also after nerve injury (**Figure 30B ABERRANT FIBERS**: WT saline *vs. Mtmr2*$^{-/-}$ saline ***p=0.0006 and WT niacin *vs. Mtmr2*$^{-/-}$ niacin **p=0.0031, non-parametric ANOVA followed by Dunn's multiple comparisons test).

In addition, we found a significant reduction in the number of total fibres between WT and *Mtmr2*$^{-/-}$ mice (**Figure 30C TOTAL FIBRES**: WT saline *vs Mtmr2*$^{-/-}$ saline *p=0.0411; WT niacin *vs Mtmr2*$^{-/-}$ niacin **p=0.0051, non-parametric ANOVA followed by Dunn's multiple comparisons test), which suggests that *Mtmr2*$^{-/-}$ mice have a defect in nerve regeneration.

To evaluate remyelination, we calculated g-*ratio* and axonal diameter distribution as previously done for *Pmp22*$^{+/-}$ mice **(Figure 31).**

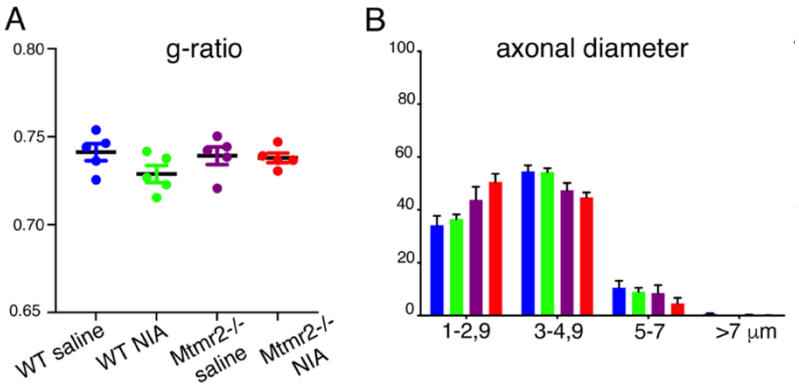


***Figure 31. Niacin treatment from T1 to T45 after crush does not negatively impact nerve remyelination in both WT and Mtmr2$^{-/-}$ mice.***

*A) Quantification of g-ratio analysis at T45dpsni. WT saline 0.741± 0.0048; WT niacin 0,72± 0.0048; Mtmr2$^{-/-}$ saline 0.739± 0.0050; Mtmr2$^{-/-}$ niacin 0,737± 0.0026; n=5 animals per group; non-parametric ANOVA followed by Dunn's multiple comparison test. Data represent mean± SEM B) Quantification of axonal diameter distribution at T45dpsni; n=5 animals per group; p>0.05; Non-parametric ANOVA followed by Dunn's multiple comparison test. Data represent median with range.*

As expected, we did not find any difference in the *g-ratio* value between WT and mutant mice (not altered in this model) and in both genotypes after treatment **(Figure 31A**: n=5 animal per group, p>0.05, non-parametric ANOVA followed by Dunn's multiple comparisons test), suggesting that niacin administration for 45 dpsni did not hinder remyelination. Axonal diameter distribution was also calculated to complement *g-ratio* results: no significant differences have been found among all groups **(Figure 31B**: n=5 animal per group, p>0.05, non-parametric ANOVA followed by Dunn's multiple comparisons test).

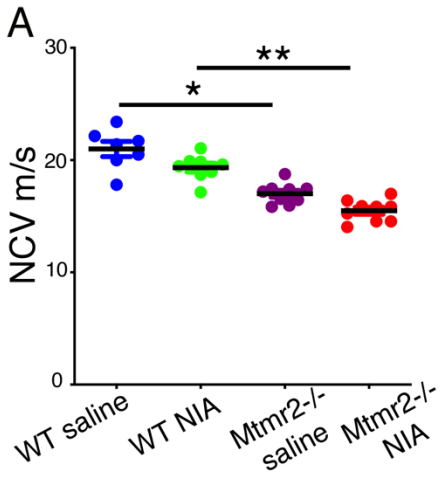


| | NCV (m/s) |
|---|---|
| **WT Saline** | 20,99 ±0,67 |
| **WT Niacin** | 19,33 ±0,39 |
| ***Mtmr2* -/- Saline** | 17,01 ±0,30 |
| ***Mtmr2* -/- Niacin** | 15,61±0,33 |

***Figure 32. Niacin treatment from T1 to T45 after crush does not negatively impact on NCV in Mtmr2$^{-/-}$ mice.***
*A) Quantification of NCV values of WT and Mtmr2$^{-/-}$ mice at T45dpsni after niacin treatment from T1 to T45 (n=5 animals per group;*p=0.0103, **p=0.0012; Non-parametric ANOVA followed by Dunn's multiple comparison test.*
*On the right, table showing specific NCV values. Data represent mean± SEM.*

Finally, neurophysiological analyses revealed that NCV was significantly reduced in *Mtmr2*$^{-/-}$ mice, as in uncrushed nerves in this mutant **(Figure 32A NCV**: WT saline 20,99 ±0,67 m/s *vs. Mtmr2*$^{-/-}$ saline 17,01 ±0,30 m/s; *p=0.0103; WT niacin 19,33 ±0,39 m/s *vs. Mtmr2*$^{-/-}$ niacin 15,61±0,33 m/s; **p=0.0012, non-parametric ANOVA followed by Dunn's multiple comparisons test). However, no significant differences have been observed after treatment, suggesting that chronic administration of niacin had no effects on it.

Altogether, these data suggest that niacin is not detrimental for nerve regeneration nor remyelination, also when chronically given for 45 days after nerve injury. We also report here for the first time that *Mtmr2*$^{-/-}$ mice have a defect in nerve regeneration after injury.

### *3.2.3 The Mtmr2$^{-/-}$ mice show nerve regeneration defect after nerve injury*

Our analyses have shown that *Mtmr2*$^{-/-}$ mice have a defect in nerve regeneration that has not been previously described. Thus, we decided to further investigate this finding.

To this aim, we crushed adult WT and *Mtmr2*$^{-/-}$ mice and performed immunofluorescence (IF) analyses on both transversal **(Figure 33A)** and longitudinal **(Figure 33B)** sciatic

nerve sections using MBP (myelin basic protein) to detect myelin. NF-M (neurofilament medium chain) was used to mark axons.

In both cases, MBP staining revealed that myelin ovoids, which normally appear during myelin degeneration, were more abundant in *Mtmr2*$^{-/-}$ mice when compared to WT, suggesting a delay in clearance, which can be at the basis of the regeneration defect. We then decided to confirm this result by performing MBP fluorescence signal quantification using the Image J software. Our analyses confirmed that MBP signal was significantly higher in *Mtmr2*$^{-/-}$ mice when compared to WT (**Figure 33A'** WT vs. *Mtmr2*$^{-/-}$ mice *p=0.0209 and **Figure 33B'** WT vs. *Mtmr2*$^{-/-}$ mice **p=0.0043, One-sample student's T test, Ctrl set to 1), suggesting that *Mtmr2*$^{-/-}$ mice may have an altered process of myelin clearance.

Myelin clearance following damage is dependent on autophagy induction in Schwann cells and clearance by macrophages, both resident cells and cells deriving from the blood stream once the nerve blood barrier is broken after damage. Interestingly, MTMR2 is a phosphoinositide phosphatase acting on PI(3,5)P2 which is important for late endosomal-lysosomal associated functions, such as autophagy. Moreover, our laboratory recently suggested that MTMR2 and PI (3,5)P2 may control cytoskeleton remodelling through RhoA activation, a process that is relevant for cell migration. Thus, we decided to investigate whether the myelin clearance defect observed in Mtmr2-/- crushed nerves can be associated with 1) altered macrophage migration to the nerve and/or 2) impaired autophagy activation in mutant Schwann cells.

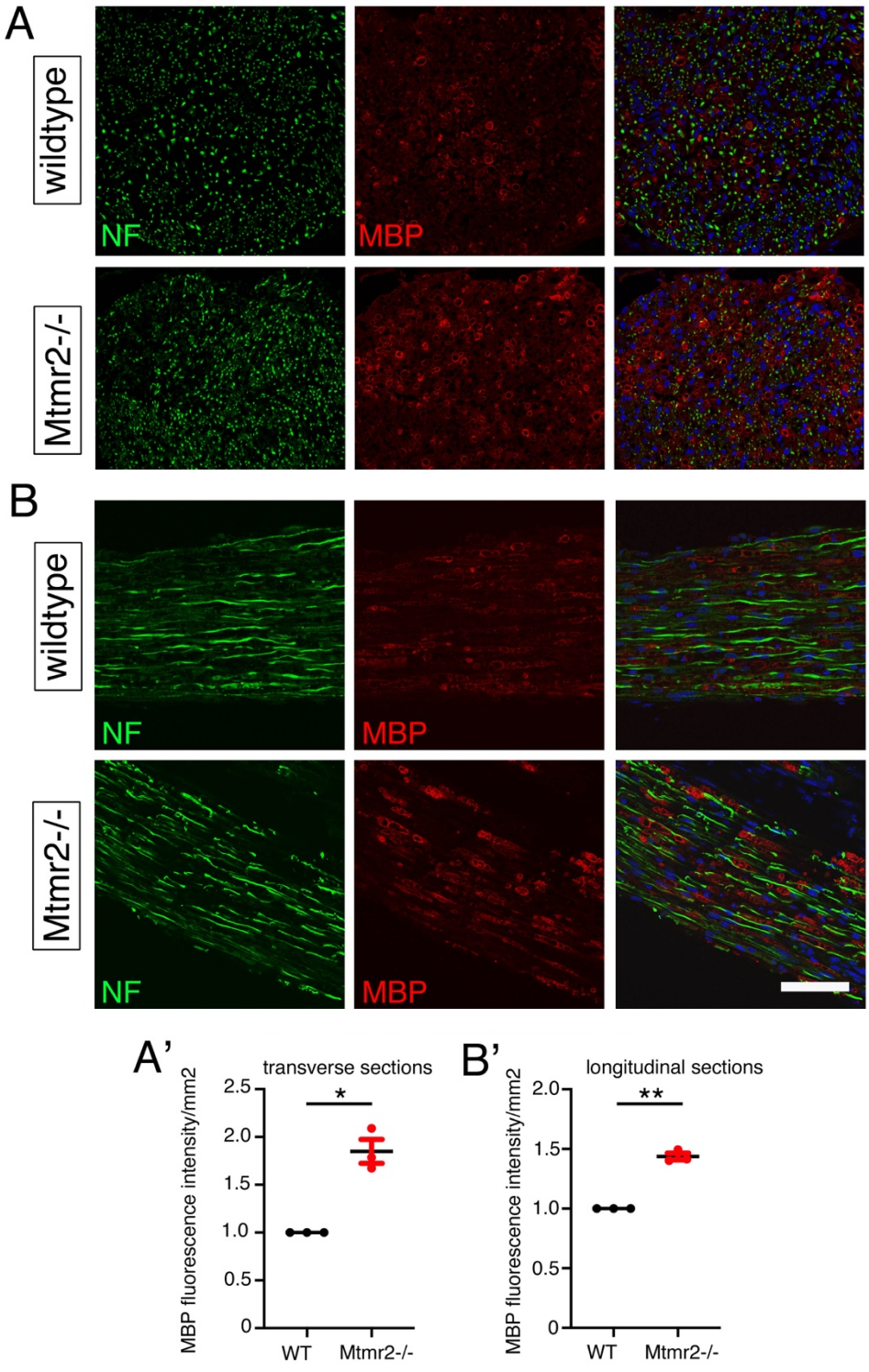


***Figure 33. Mtmr2 $^{-/-}$ mice show increased myelin accumulation at 7dpsni.***
*A-B) Representative confocal images of transversal (A) and longitudinal (B)sciatic nerve sections showing myelin accumulation in Mtmr2 $^{-/-}$ mice in relation to WT at 7dpsni. Magnification is 40x. Bar in A is 114μm and in B is110 μm. A'-B') Quantification of MBP fluorescence intensity in n=3 WT and n=3 Mtmr2 $^{-/-}$, *p=0.0209 and **p=0.0043, One-sample student's T-test, Ctrl is set to 1. Results of three independent experiments, where three mice per genotype were used in each experiment. Data represent mean± SEM.*

### *3.2.3.1 Macrophages-mediated autophagy in Mtmr2$^{-/-}$ mice after nerve injury*

We already knew that the RhoA pathway, which regulates cellular motility through the cytoskeleton, is dysregulated in *Mtmr2*$^{-/-}$ mice (Guerrero-Valero et al., 2021). Since our mouse model is a full KO, we asked whether *Mtmr2* loss in macrophages could affect their ability to reach the injury site. To this aim, we crushed adult WT and *Mtmr2*$^{-/-}$ mice and counted the number of total macrophages present at 7dpsni. More specifically, we performed IF analyses on longitudinal sciatic nerve sections using F4/80 (macrophages cytoplasmic marker) to visualize macrophages **(Figure 34)**.

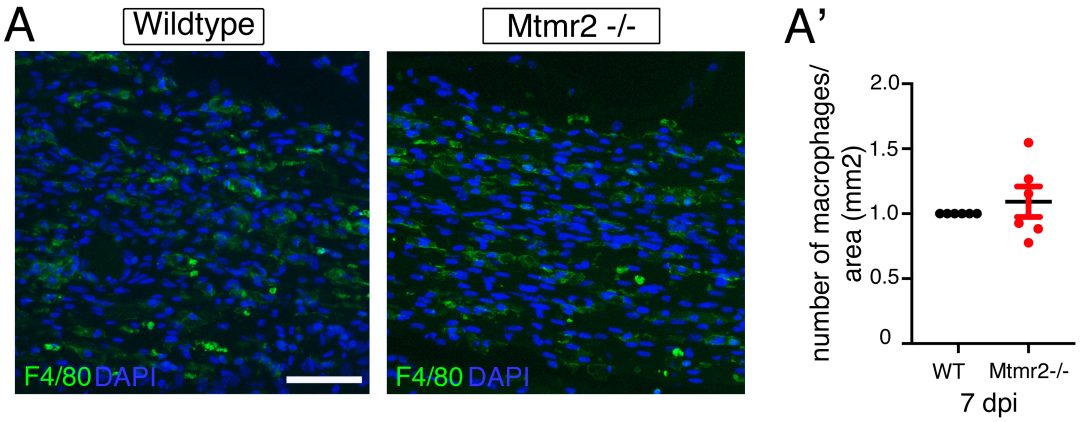


***Figure 34. Macrophages recruitment at injury site is not altered in Mtmr2 $^{-/-}$ mice at 7dpsni.*** *A) Representative fluorescence images of longitudinal sciatic nerve section showing macrophages (F4/80$^{+}$ cells). Magnification is 40x. Bar in A is 48 µm. A') Quantification of total F4/80$^{+}$cells/area for each nerve analysed, n=6 WT and n=6 Mtmr2 $^{-/-}$. WT vs Mtmr2 $^{-/-}$ p=0.4675, One-sample student's T-test, Ctrl is set to 1. Results of six independent experiments. Data represent mean± SEM*

Quantitation of F4/80$^{+}$ cells showed no significant differences between WT and *Mtmr2*$^{-/-}$ mice at 7dpsni (**Figure 34A'**: n=6 mice for each genotype, WT vs. *Mtmr2*$^{-/-}$ mice, p=0.4675, One-sample student's T-test, Ctrl set to 1. Results from six independent experiments), suggesting that macrophages recruitment at injury site is not altered in *Mtmr2*$^{-/-}$ mice and likely not related to myelin accumulation.

### *3.2.3.2 Schwann cells-mediated autophagy in Mtmr2$^{-/-}$ mice after nerve injury*

Other than macrophages, Schwann cells are known to be essential for clearance after injury. During the very early phases of Wallerian degeneration, they undergo a "transdifferentiaton" process, which, among all, enables them to remove their own myelin (Gomez-Sanchez *et al*., 2015). Accordingly, we asked whether the accumulation of

myelin observed in our *Mtmr2*$^{-/-}$ mice could be the result of a defective Schwann cells-mediated autophagy, particularly because MTMR2 controls PI (3,5)P2 levels, a phosphoinositide which is crucial for late endosomal-lysosomal function.

To this aim, we performed Western Blot analyses to investigate the levels of LC3-II/I (Microtubule-associated protein 1 light chain 3 isoform II and I) and NBR1(Neighbour of BRCA1 gene 1) in WT and *Mtmr2*$^{-/-}$ mice at 7 days after sciatic nerve crush **(Figure 35).** In case of autophagy induction and blockage, we expected to observe an accumulation of both LC3 II and NBR1.

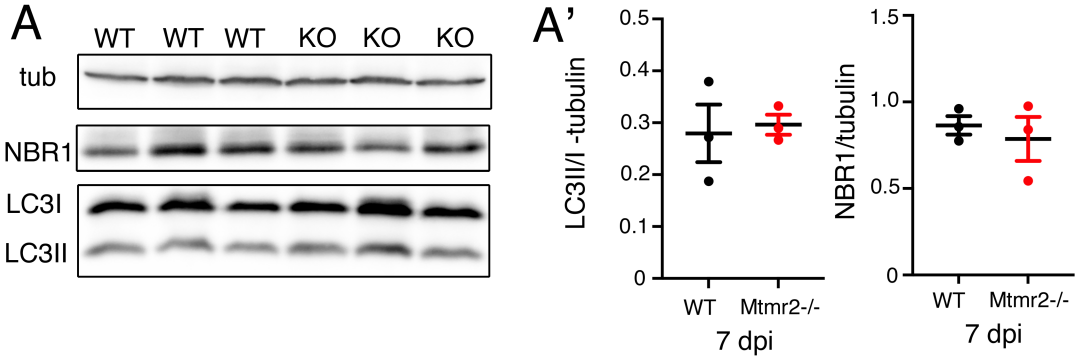


***Figure 35. Autophagy is normally activated in Mtmr2*** $^{-/-}$ ***mice at 7dpsni.***
*A) Immunoblot of LC3 II/I and NBR1 at 7dpsni. Tubulin was used as loading control.*
*A') Quantification of LC3II/I (p>0.999) and NBR1 (p>0.999) at 7dpsni, n=3WT and n=3 Mtmr2* $^{-/-}$*, Two-tailed non-parametric Mann-Whitney student T-test. Result of one single experiment. Data represent mean± SEM.*

Immunoblot analysis revealed no significant differences between WT and *Mtmr2*$^{-/-}$ mice in both LC3 II/I and NBR1 levels (n=3 WT and n=3 *Mtmr2*$^{-/-}$ mice, p>0.999, Two-tailed non-parametric Mann-Whitney, Student T-test), suggesting that the autophagic process is normal in *Mtmr2*$^{-/-}$ mice at 7dpsni **(Figure 35A').**

However, since autophagy is activated within 3 and 7dpsni (Gomez-Sanchez *et al*.,2015), we asked whether an earlier time point could be more informative. For this reason, we repeated the experiment at 3 dpsni **(Figure 36).**

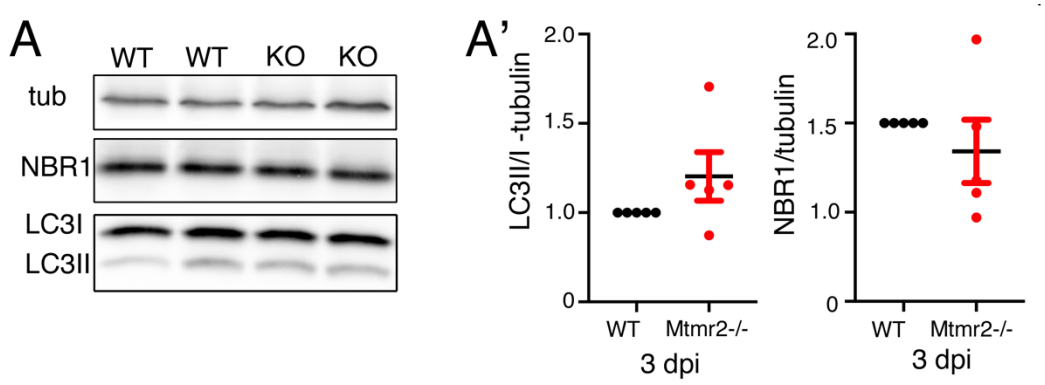


***Figure 36. Autophagy is normally activated in Mtmr2 $^{-/-}$ mice at 3dpsni.***
*A) Representative immunoblot of LC3 II/I and NBR1 at 3dpsni. Tubulin was used as loading control. A') Quantification of LC3II/I (p=0.2112) and NBR1 (p=0.422) at 3dpsni, n=5 WT and n=5 Mtmr2 $^{-/-}$, One-sample Student T-test, Ctrl set to 1. Results of two independent experiments. Data represent mean± SEM.*

Immunoblot results showed no significant differences between WT and *Mtmr2*$^{-/-}$ mice (n=5 WT and n=5 *Mtmr2* $^{-/-}$, LC3II/I (p=0.2112) and NBR1 (p=0.422), One-sample Student T-test, Ctrl set to 1), confirming that autophagy in not altered in mutant mice after injury **(Figure 36 A').**

Taken together, these results suggest that myelin accumulation observed in *Mtmr2*$^{-/-}$ mice at 7dpsni is not likely due to alterations in macrophages recruitment at injury site and also probably not related to a defect in Schwann cells-mediated autophagy.

### *3.2.3.3 mTORC1 activation in Mtmr2$^{-/-}$ mice after nerve injury*

New protective mechanisms have recently been proposed as attempts to prevent axonal degeneration after injury. To mention, mTORC1 activation after injury induces a glycolytic shift in SCs to counteract axonal energy depletion and limit axonal degeneration (Babetto *et al*.,2020).

Since 1) mTORC1 pathway is dysregulated in our *Mtmr2*$^{-/-}$ mouse model during development (Guerrero-Valero *et al*., 2021) and 2) mTORC1 activation after injury peaks between 36 and 72 hours after nerve cut (Babetto *et al*.,2020), we asked whether the defect observed in *Mtmr2*$^{-/-}$ regeneration could be related to a perturbed modulation of mTORC1 also after nerve injury.

To this aim, we performed sciatic nerve cut in adult WT and *Mtmr2*$^{-/-}$ mice. Sciatic nerves were collected at 36 and 72 hours after injury and processed for both IF and Western Blot analyses **(Figure 37).**

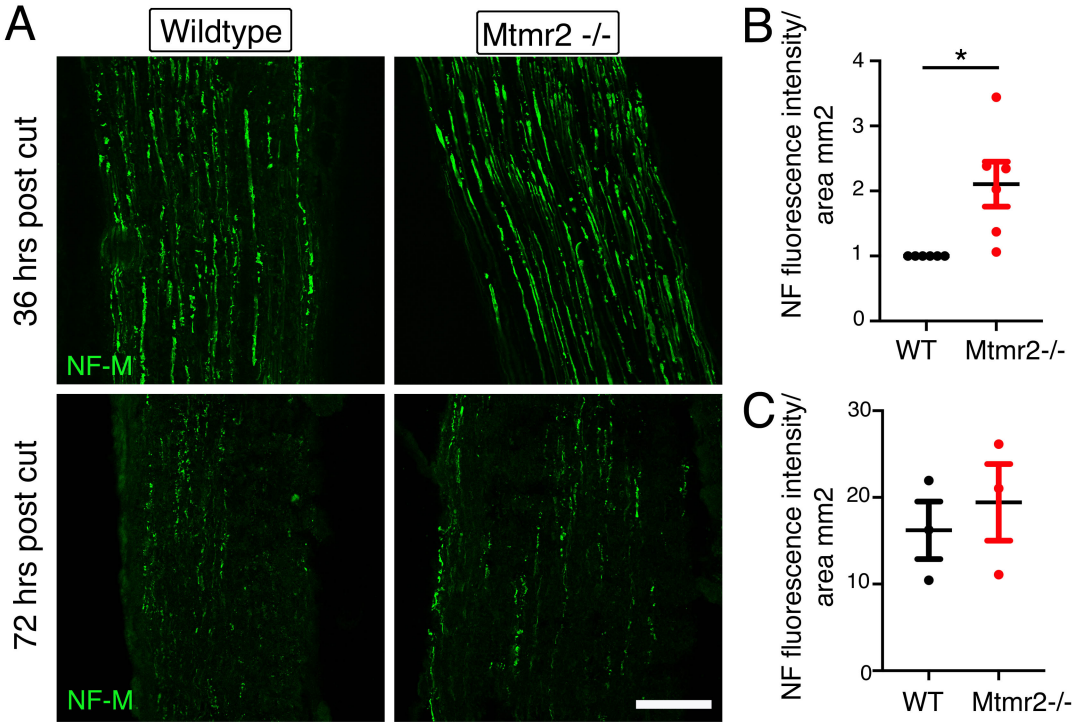


***Figure 37. Mtmr2*** $^{-/-}$ ***mice show higher preservation of axonal structure at 36hrs post cut.***
*A) Representative confocal images of longitudinal sciatic nerve section at 36 and 72hrs post cut showing higher preservation of axons in Mtmr2* $^{-/-}$ *mice at 36hrs post cut. Magnification is 20x. Bar in A is 120 µm. B) Quantification of NF-M fluorescence intensity in WT and Mtmr2* $^{-/-}$ *at 36hrs post cut, n=6 WT and n=6 Mtmr2* $^{-/-}$*, *p=0.0237, One-sample student's T-test, Ctrl is set to 1. Results of six independent experiments; C) Quantification of NF-M fluorescence intensity in WT and Mtmr2* $^{-/-}$ *at 72hrs post cut, n=3 WT and n=3 Mtmr2*$^{-/-}$*, p=0.7, Non-parametric Mann-Whitney student T-test, Results of three independent experiments. Data represent mean± SEM*

IF analyses on longitudinal sciatic nerves sections stained for NF-M (neurofilament-medium chain) showed evident preservation of axonal structure in *Mtmr2*$^{-/-}$ mice as compared to WT at 36 but not at 72hrs post cut (**Figure 37A**).

Quantification of NF-M signal confirmed the presence of an increased fluorescence intensity in *Mtmr2*$^{-/-}$ mice at 36 hrs (**Figure 37B**, n=6 WT and n=6 *Mtmr2*$^{-/-}$, *p=0.0237, One-sample Student's T-test, Ctrl set to 1. Results of six independent experiments), but not at 72hrs post cut (**Figure 37C**: n=3 WT and n=3 *Mtmr2*$^{-/-}$, p=0.7, Non-parametric Mann-Whitney student T test. Results of three independent experiments), suggesting that axonal disruption may be transiently delayed in *Mtmr2*$^{-/-}$ mice, in line with our previous observation in delay of clearance.

To better understand this, we decided to analyse P-S6 levels (phosphorylated form of S6 ribosomal protein, downstream effector of mTORC1) at 36hrs post cut (**Figure 38**).

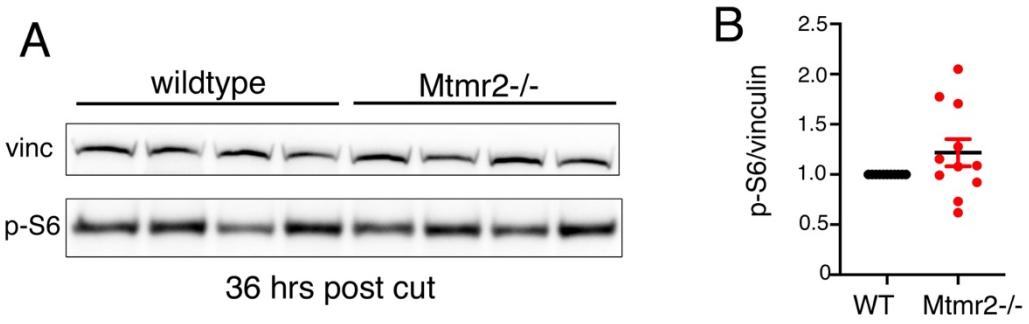


***Figure 38. mTORC1 activation is not altered in Mtmr2$^{-/-}$ mice at 36 hrs post sciatic nerve cut.*** *A) Representative immunoblot showing P-S6 levels at 36hrs post sciatic nerve cut. Vinculin was used as loading control. B) Quantification of P-S6 levels showed no significant differences between WT and Mtmr2 $^{-/-}$ mice levels at 36hrs post cut, n=11 WT and n=11 Mtmr2 $^{-/-}$, p=0.1406, One-sample Student T-test, Ctrl set to 1. Results of three independent experiments. Data represent mean± SEM*

Immunoblot results showed no significant differences between WT and *Mtmr2*$^{-/-}$ mice (**Figure 38B**: n=11 WT and n=11 *Mtmr2*$^{-/-}$, p=0.1406, One-sample Student's T-test, Ctrl set to 1. Results of three independent experiments) indicating that mTORC1 is not perturbed in mutant mice at 36hrs after injury.

Altogether, these results demonstrate that: 1) *Mtmr2*$^{-/-}$ mice have an initial, transient, delayed activation of axonal degeneration which is no more evident at 72hrs post cut; 2) mTORC1 activation after injury is not altered, and likely not contributing to the delay in degeneration and regeneration defect observed in Mtmr2-/- mice.

## 3.3 Refinement of Niacin treatment protocol in *Mtmr2*$^{-/-}$ mice

Our previous results demonstrated that Niaspan® (a FDA-approved, long-lasting release formulation of niacin, ABBVIE) **i.p. treatment** from P15 to P75 in *Mtmr2*$^{-/-}$ mice (CMT4B1 mouse model) and from P15 to P45 in *Pmp22*$^{+/-}$ mice (HNPP mouse model) was able to ameliorate the morphological phenotype of both models (Bolino *et al*., 2016). However, since Niaspan® is commercially available in tablets, we had to manually crush them before giving to mice, thereby causing the loss of the long-lasting release, and reducing Niaspan® to act as niacin, the active molecule. Thus, we decided to set up a collaboration with a group of pharmacologists of the University of Milan "La statale" (Prof. Andrea Gazzinga and Dr. Matteo Cerea) to produce a new long-lasting formulation of niacin (called Niacoat-SR) which could be given to mice by gavage.

In this way, we aimed at: 1) mimic Niaspan® human **administration *per os***; *2)* reproduce Niaspan® human kinetics in 24hrs (long-lasting release); 3) sustain niacin concentration in the nerve.

### *3.3.1 Generation of a new long-lasting release formulation of niacin (Niacoat-SR)*

To produce a new long-lasting release formulation of niacin, suitable for gavage administration ***per os***, we performed several pharmacokinetics studies in collaboration with Eurofins, France. First, since we knew that the dose of 160mg/kg, 5 mg/ml of Niaspan® (which corresponds to 120mg/kg, 5 mg/ml of pure niacin) ameliorated nerve morphology in our mouse models **administered i.p.** (Bolino *et al*., 2016), we aimed at finding the right **oral dose** of niacin able to recapitulate the same kinetics in nerve and plasma. For this purpose, we daily treated 5 groups of WT 129sv/Pas mice from P30 to P37 with different doses of niacin as reported in **Table 1**.

| ANIMALS | GENOTYPE | STRAIN | AGE | TREATEMENT(NIACIN) |
|---|---|---|---|---|
| 15 | WT | 129sv/Pas | P30 | 120mg/Kg, 5 mg/ml, IP |
| 15 | WT | 129sv/Pas | P30 | 120mg/Kg, 15mg/ml,IP |
| 15 | WT | 129sv/Pas | P30 | 120mg/Kg, 15mg/ml, Gavage |
| 15 | WT | 129sv/Pas | P30 | 240mg/Kg, 15mg/ml,Gavage |
| 15 | WT | 129sv/Pas | P30 | 480mg/Kg, 15mg/ml,Gavage |

***Table 1. Table showing the total number of animals involved in the pharmacokinetics study divided by type of treatment and dose.***

Nerves and plasma (n=3 animals for each time-point) were collected at T0h, T30mins, T2h, T4h, T6h after last administration and sent to Eurofins (France).

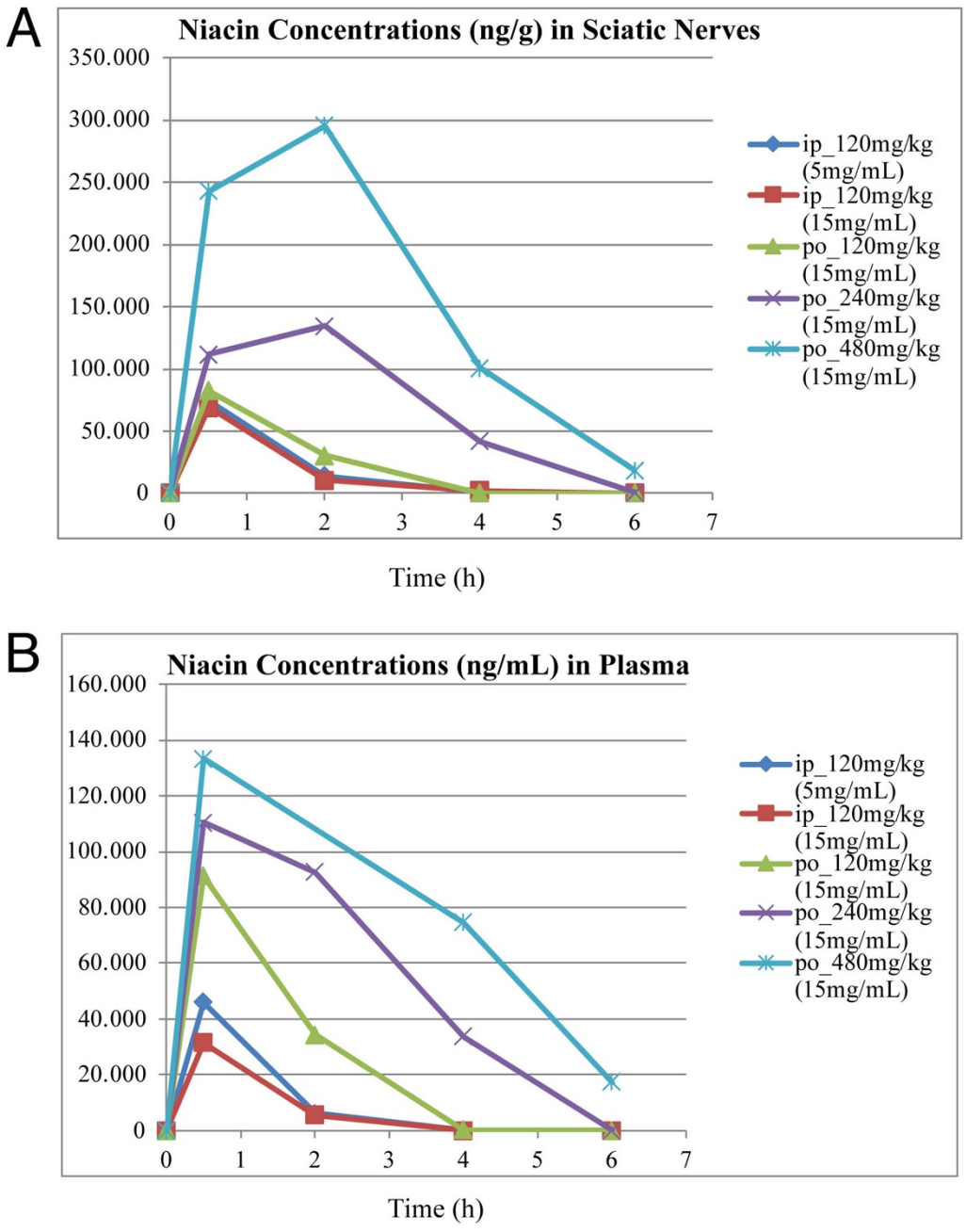


***Figure 39. Niacin pharmacokinetics curves in plasma and nerves.***
*Graph showing niacin concentration (ng/mL) in sciatic nerves(A) and plasma(B) at fixed time-points after last administration performed per os or by i.p. The 120 mg/Kg, 15mg/ml dose of niacin given per os reproduced the kinetics of 120 mg/Kg, 5mg/ml dose given by i.p.; n=3 WT 129 sv/Pas animals per time-point for each condition.*

The analyses indicated that the oral dose of 120 mg/kg, 15mg/ml (in green) was able to reproduce the kinetics curve of 120mg/kg, 5 mg/ml dose given by i.p.(in blue) in sciatic nerves but not in plasma samples **(Figure 39A and 39B).** Here, niacin concentration resulted to be higher when compared to i.p. treatments, indicating that oral administration increases the systemic bioavailability of the compound. However, since 1) niacin was eliminated from plasma after 4hrs as well as i.p. administration and 2) our aim was to produce an extended-release formulation which naturally modulates the overall systemic exposure, we considered that as not a major issue.

Based on these data, Niacoat-SR was produced as described in 5.5 (Materials and Methods section) by Prof. Gazzinga's group and tests were made with the predicted dose of 960 mg/Kg. For this purpose, we treated n=24 WT 129 sv/Pas animals from P30 to P37 to observe Niacoat-SR kinetics in 24hrs (n=3 animals per time-point. Time-points analysed: T0,T1h, T3h, T6h, T9h, T12h, T24h),**(Figure 40).**

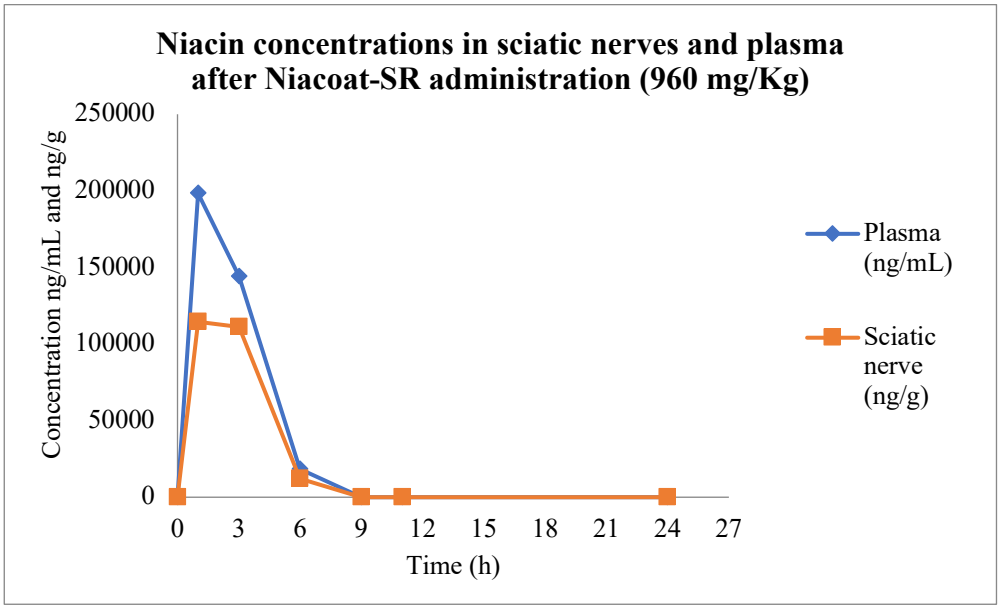


***Figure 40. Niacoat-SR pharmacokinetics in 24hours.***
*Graph showing niacin concentration in sciatic nerve (ng/mL) and plasma (ng/mL) at fixed time-points after Niacoat-SR administration (960 mg/Kg). Niacin concentration peaks after 1hour and remains stable until 3hrs. Niacin is still detectable in nerves also after 9 hrs from last administration. n=3 WT 129 sv/Pas animals per time-point.*

The dose of 960 mg/Kg of Niacoat-SR was able to sustain niacin concentration in the nerve until 9hrs, whereas pure niacin is usually undetectable after 4 hrs from last treatment (**Figure 41**). Moreover, between 1h and 3hrs niacin concentration in nerves reached a plateau, suggesting that it can remain stable for at least two hours at high levels (**Figures**

**40-41**). On the contrary, when pure niacin was given (either by gavage or by i.p), we noticed a peak after 30mins, which abruptly decreased between 1 and 2hrs after last administration (**Figure 41**). When looking at the total concentration of niacin in the nerve between the higher dose of pure niacin 480mg/Kg, gavage and Niacoat-SR 960mg/Kg, gavage (AUC-Area Under Curve: Niacoat-SR 960mg/Kg AUCnerve= 487339,33 ng*mL/h; niacin 480 mg/Kg, gavage AUCnerve= 980943 ng*mL/h), we found it to be lower in Niacoat-SR samples. However, we did not consider that as a main issue since our main goal was to demonstrate the long-lasting release effect and not to increase niacin concentration in the nerve.

Niacin concentration in plasma showed instead a similar trend to pure niacin, with a peak after 1h followed by a progressive reduction, but higher AUC values (Niacoat-SR 960mg/Kg AUCplasma= 713075,4 ng*mL/h; niacin 480 mg/Kg, gavage AUCplasma= 489674,75 ng*mL/h). This was expected considering the higher dose given and the different formulation used. Lowering of niacin plasma levels indeed occurred less rapidly with Niacoat-SR as compared to pure niacin, thus suggesting a correlation between the formulation used and the overall systemic and tissue-specific exposure to the compound.

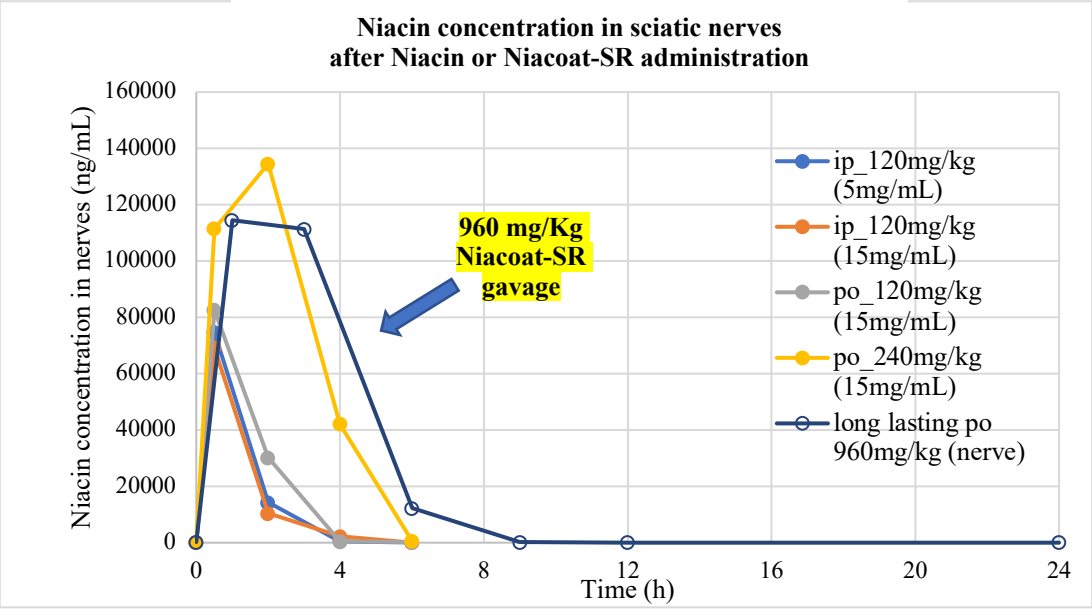


***Figure 41. Comparison between Niacin and Niacoat-SR pharmacokinetics.***
*Graph showing niacin concentration in the sciatic nerve (ng/mL) at fixed time-points after Niacin or Niacoat-SR administration. The 960mg/Kg dose of Niacoat-SR clearly shows sustained niacin concentration in the nerve compared to pure niacin. N=3 WT 129 sv/Pas animals per time-point for each condition.*

Taken together, these results indicate that Niacoat-SR is a reliable new long-lasting release formulation of niacin suitable for gavage administration in mice.

### *3.3.2 Niacoat-SR: safety and target engagement experiments in mice*

Before administering to mice in a long-term treatment setting, we aimed at assessing Niacoat-SR safety and tolerability in mice during development. To this aim, we daily treated n=20 WT mice 129 sv/Pas (n=10 WT vehicle and n=10 WT Niacoat-SR 960mg/Kg, with sex equally distributed within groups) from P21 to P51. Animals were monitored for weight and clinical signs every day, without showing any abnormalities. Moreover, since 1) niacin is known to act as lipid modulator and 2) it is metabolized by both kidney and liver, we performed histological analyses of liver, gut, and kidney (in collaboration with Dr. Fiocchi A., Animal histopathology Unit, HSR, Milan), to evaluate the presence of signs of tissue alterations or inflammation **(Figure 42).** Hematoxylin-eosin sections were clinically analysed by Dr. Francesca Sanvito (MD, Pathology Unit, HSR, Milan): no gross abnormalities were found, suggesting that Niacoat-SR was not toxic and well-tolerated by mice.

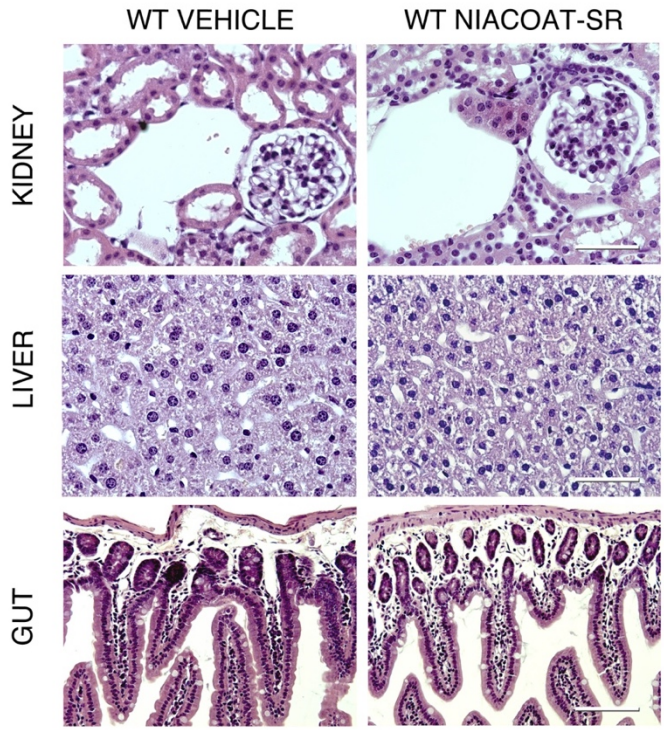


***Figure 42. Niacoat-SR is not toxic and is well-tolerated by mice during development.***
*Representative images acquired at bright-field microscope showing kidney, liver, and gut sections stained with haematoxylin-eosin staining protocol, n=3 WT animals per condition analysed. No*

*alterations have been found. Kidney and liver magnification is 40x, gut's is 20x. Bar in Kidney and Liver sections is 49µm; bar in Gut sections is 98µm.*

Once Niacoat-SR safety was assessed, we decided to prove its efficacy by performing target engagement experiments.

First, since niacin is a TACE activator, we decided to test if also Niacoat-SR was able to efficiently increase TACE activity. For this purpose, we treated n=30 WT 129sv/Pas by gavage (n=10 WT vehicle, n=10 WT niacin 120mg/Kg, n=10 WT Niacoat-SR 960 mg/kg) from P30 to P37. Sciatic nerves were collected 1h after last administration and biochemically analyzed for TACE activity **(Figure 43).**

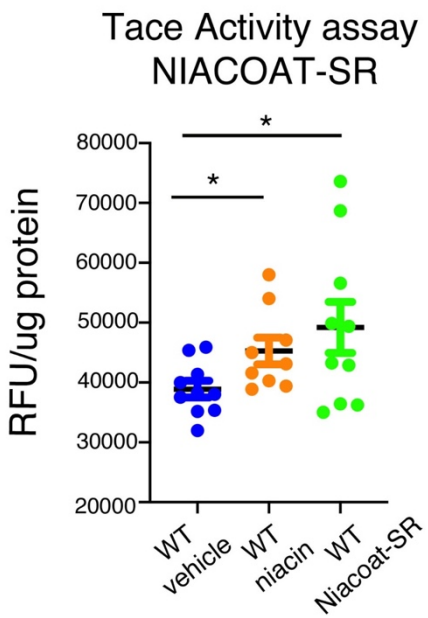


***Figure 43. Niacoat-SR significantly increases TACE activity.***
*Quantification of three independent experiments showing Niacoat-SR effect on TACE activity. Niacin samples were used as internal positive control of the assay. n=10 WT vehicle, n=10 WT niacin, n=10 WT Niacoat-SR; Non-parametric one-way ANOVA followed by Dunn's multiple comparison test; WT vehicle vs. WT Niacin: *p= 0.0471; WT vehicle vs. WT Niacoat-SR: *p=0,0405. Data represent Mean± SEM.*

Our results indicated that Niacoat-SR treatment for one week (960 mg/Kg, gavage, QD) was able to significantly increase TACE activity, even more than pure niacin (n=10 per condition; WT vehicle vs. WT Niacin: *p= 0.0471; WT vehicle vs. WT Niacoat-SR: *p=0,0405; Non-parametric one-way ANOVA followed by Dunn's multiple comparison test).

Second, to further investigate Niacoat-SR functioning on predicted targets, in collaboration with Prof. John Svaren (Department of Comparative Bioscences, School of

Veterinary Medicine, University of Wisconsin-Madison, USA), we analysed the transcriptomic profile of *Mtmr2*$^{-/-}$ mice after Niacoat-SR treatment (**Figure 44**). More precisely, n=4 WT vehicle, n=4 *Mtmr2*$^{-/-}$ vehicle and n=4 *Mtmr2*$^{-/-}$ Niacoat-SR were treated from P10 to P21 by i.p. (with Saline or Niacin 120 mg/Kg, i.p., QD) and from P21 to P30 by gavage (with Methilcellulose or Niacoat-SR 960 mg/Kg, gavage, QD). Sciatic nerves were collected at P30 within 1h after last administration and fast-frozen in Trizol.

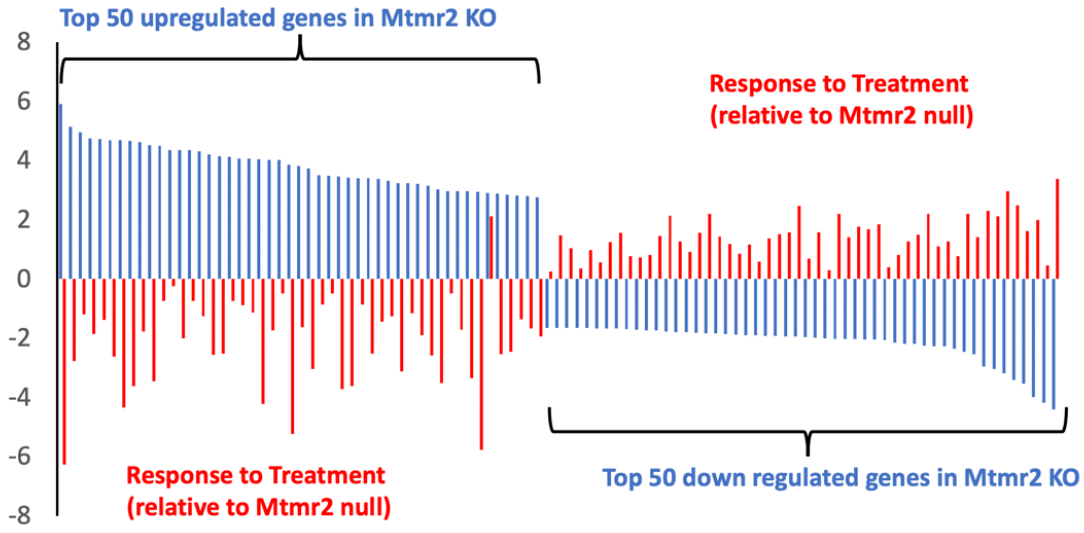


***Figure 44. Niacin normalizes gene expression changes in CMT4B1 mouse model.***
*In blue, selection of top 50 upregulated (left) and downregulated (right) genes in Mtmr2*$^{-/-}$ *mice. In red, the same genes showing to be responsive to the treatment with Niacoat-SR.*
*N=4 animals for each condition (n=4 WT vehicle, n=4 Mtmr2*$^{-/-}$ *vehicle and n=4 Mtmr2*$^{-/-}$ *Niacoat-SR).*

Transcriptomic analyses identified different genes expressed in *Mtmr2*$^{-/-}$ mice when compared to WT. A set of top 50 upregulated and downregulated genes were selected **(Figure 44 in blue)**, which resulted responsive to Niacin/Niacoat-SR treatment **(Figure 44 in red)**. Among others, higher-modulated genes resulted to be involved in lipid metabolism (e.g., SREBF1, SCD1, PLIN1, LIPE, LPL) and in the regulation of adipose tissue from adipogenesis to adipocyte differentiation and functioning (e.g., AQP7, PPARγ, GDF10, UCP1). Considering that niacin effects on lipids regulation are widely known and already applied in clinics to treat dyslipidemia, our data demonstrate Niacoat-SR efficacy in the modulation of niacin predicted targets.

### *3.3.3 Niacoat-SR long-term treatment protocol on Mtmr2$^{-/-}$ mice*

Since our preliminary results on Niacoat-SR efficacy and tolerability were particularly promising, we considered to set-up a long-term pre-clinical trial on *Mtmr2*$^{-/-}$ mice to score morphological and functional outcome measures in the perspective of a potential clinical application of the drug.

To do that, we enrolled 64 animals (n=10 WT vehicle, n=10 WT Niacoat-SR, n=24 *Mtmr2*$^{-/-}$ vehicle, n=20 *Mtmr2*$^{-/-}$ Niacoat-SR, with sex equally distributed within each group) and we treated them from P10 to P21 with Niacin (120 mg/Kg, i.p., QD) and from P21 to P170 (nearly 6 months) with Niacoat-SR (960 mg/Kg, gavage, QD) in collaboration with CRL (Charles River Laboratories). Of note, we performed i.p. administration from P10 to P21 to act as preventively as possible, since previous results showed that the morphological phenotype is already present in our model at P5.

Animals were daily checked for weight and clinical signs, but no abnormalities were reported. Morphological, functional, and biochemical outcome measures were scored at P170 to assess Niacoat-SR effects on *Mtmr2*$^{-/-}$ mice (**Figure 45-49**).

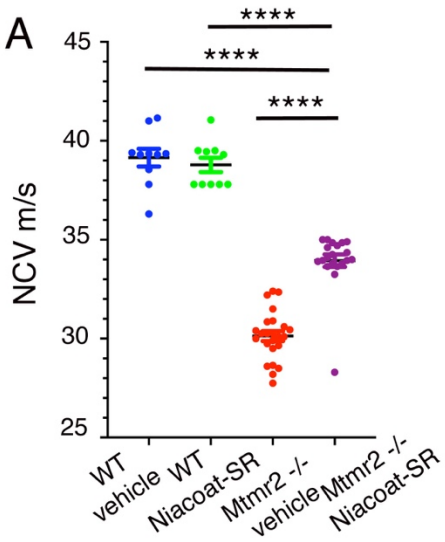


| | NCV (m/s) |
|---|---|
| **WT vehicle** | 39,15±0,44 |
| **WT Niacoat-SR** | 38,78±0,36 |
| ***Mtmr2*** $^{-/-}$ **vehicle** | 30,13±0,25 |
| ***Mtmr2*** $^{-/-}$ **Niacoat-SR** | 33,94±0,31 |

***Figure 45. Niacoat-SR treatment from P21 to p170 ameliorates NCV in Mtmr2$^{-/-}$ mice.***
*A) Quantification of NCV values of WT and Mtmr2 $^{-/-}$mice at P170 after Niacoat-SR treatment from P21. n=10 WT vehicle, n=10 WT Niacoat-SR, n=24 Mtmr2$^{-/-}$ vehicle, n=20 Mtmr2$^{-/-}$ Niacoat-SR, with sex equally distributed within each group. Ordinary ANOVA followed by Dunn's multiple comparison test, ****p<0.0001. Data represent mean± SEM*
*On the right, table showing specific NCV values. Data are indicated as mean± SEM.*

First, neurophysiological results showed that Niacoat-SR treatment was able to significantly ameliorate NCV in *Mtmr2*$^{-/-}$ Niacoat-SR-treated mice compared to *Mtmr2*$^{-/-}$ vehicle-treated mice, which are known to have altered NCV at 6 months (Bolino *et al*., 2004; Guerrero-Valero *et al*, 2021), **(Figure 45 NCV:** WT vehicle 39,15±0,44 m/s *vs*. *Mtmr2*$^{-/-}$ vehicle 30,13±0,25 m/s ****p<0.0001, *Mtmr2*$^{-/-}$ vehicle 30,13±0,25 m/s *Mtmr2*$^{-/-}$ Niacoat-SR 33,94±0,31 m/s, ****p<0.0001, Ordinary ANOVA followed by Dunn's multiple comparison test).

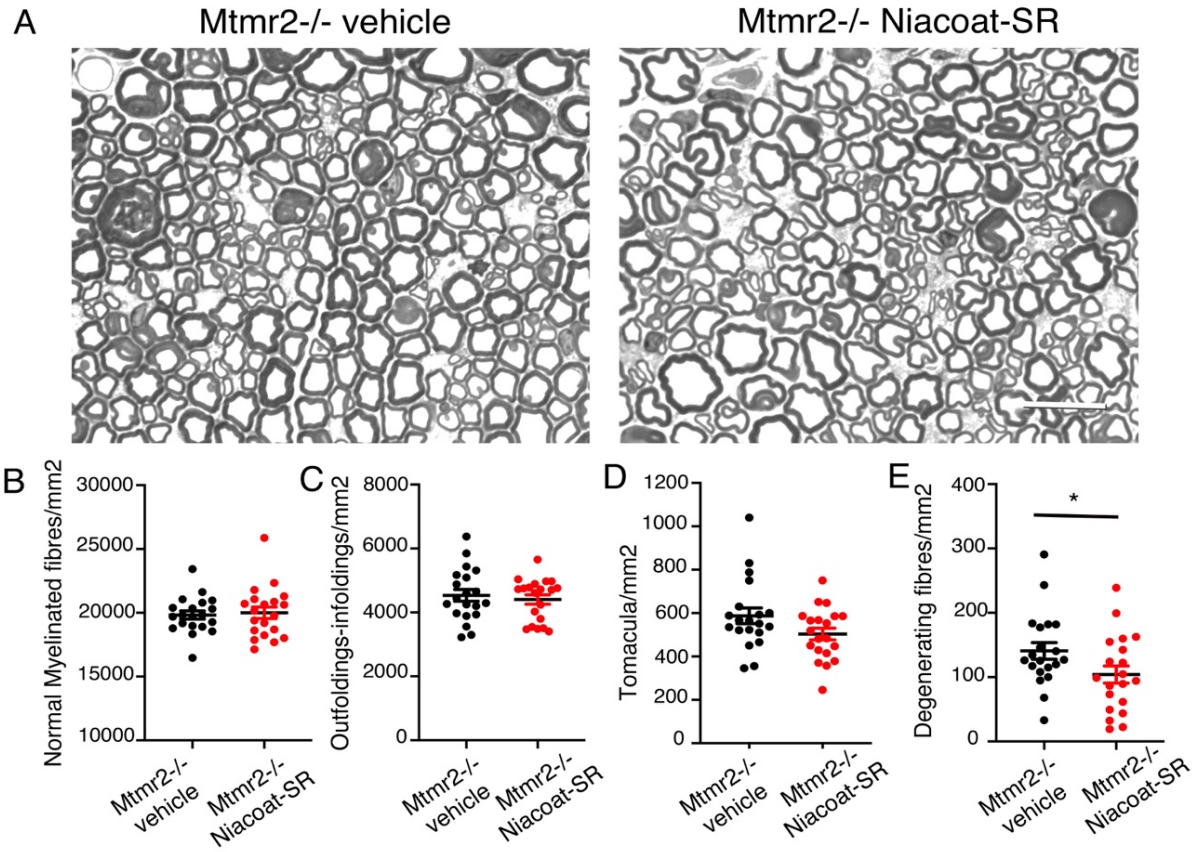


***Figure 46. Niacoat-SR treatment from P21 to P170 partially ameliorates morphology in Mtmr2*$^{-/-}$ *mice sciatic nerves.***

*A) Representative images of sciatic nerve semithin sections analysis of both vehicle and Niacoat-SR-treated Mtmr2*$^{-/-}$ *mice at P170; n=20 Mtmr2*$^{-/-}$ *vehicle, n=20 Mtmr2*$^{-/-}$ *Niacoat-SR; Scale Bar is 14,4 μm; B-E) Quantification of fibres displaying normal myelin structure(B) and aberrant myelin structures(C-E). Aberrant structures have been classified as myelin outfoldings (C), tomacula (D) and degenerations(E); Degenerating fibres: Mtmr2*$^{-/-}$ *vehicle vs. Mtmr2*$^{-/-}$ *Niacoat-SR *p=0.0430; Parametric T-test, Welch's correction. Data represent mean± SEM.*

However, morphological analyses of *Mtmr2*$^{-/-}$ sciatic nerves semithin sections showed that Niacoat-SR treatment did not rescue the number of aberrant fibres (e.g. myelin outfoldings/tomacula) but significantly reduced the number of degenerating fibres **(Figure 46E DEGENERATING FIBRES**: *Mtmr2*$^{-/-}$ vehicle *vs. Mtmr2*$^{-/-}$ Niacoat-SR, *p=0.0430; Parametric T-test, Welch's correction; n=20 per group), without altering the number of normal myelinated fibres. To see if Niacoat-SR treatment had a major effect on large-calibre axons (motor fibres) which express high levels of NRG1 type III, we decided to analyse quadriceps nerve morphology (**FIGURE 47**). Our results show that Niacoat-SR treatment had no effects in the number of aberrant nor degenerating fibres (**FIGURE 47 C,D,E**).

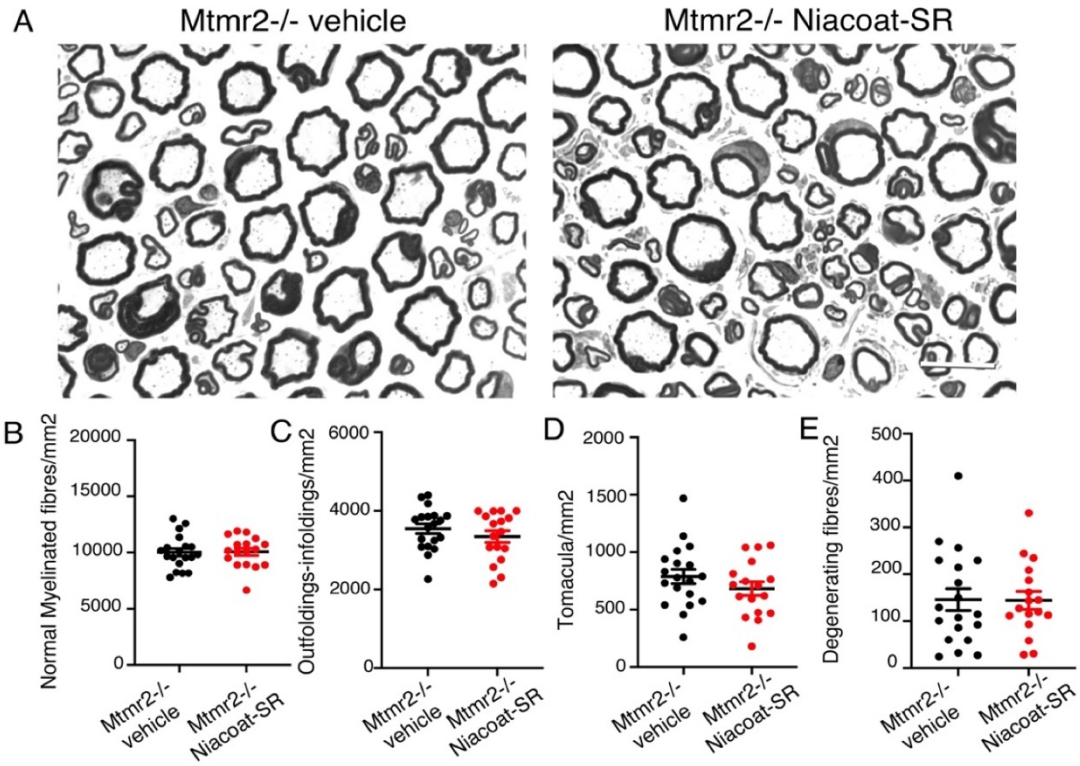


***Figure 47. Niacoat-SR treatment from P21 to P170 does not ameliorate morphology in Mtmr2$^{-/-}$ mice quadriceps nerves.***
*A) Representative images of quadriceps nerves semithin sections analysis of both vehicle and Niacoat-SR-treated Mtmr2$^{-/-}$ mice at P170; n=20 Mtmr2$^{-/-}$ vehicle, n=20 Mtmr2$^{-/-}$ Niacoat-SR; Scale Bar is 14,4 μm; B-E) Quantification of quadriceps fibres displaying normal myelin structure(B) and aberrant myelin structures(C-E). Aberrant structures have been classified as myelin outfoldings (C), tomacula (D) and degenerations(E); Data represent mean± SEM.*

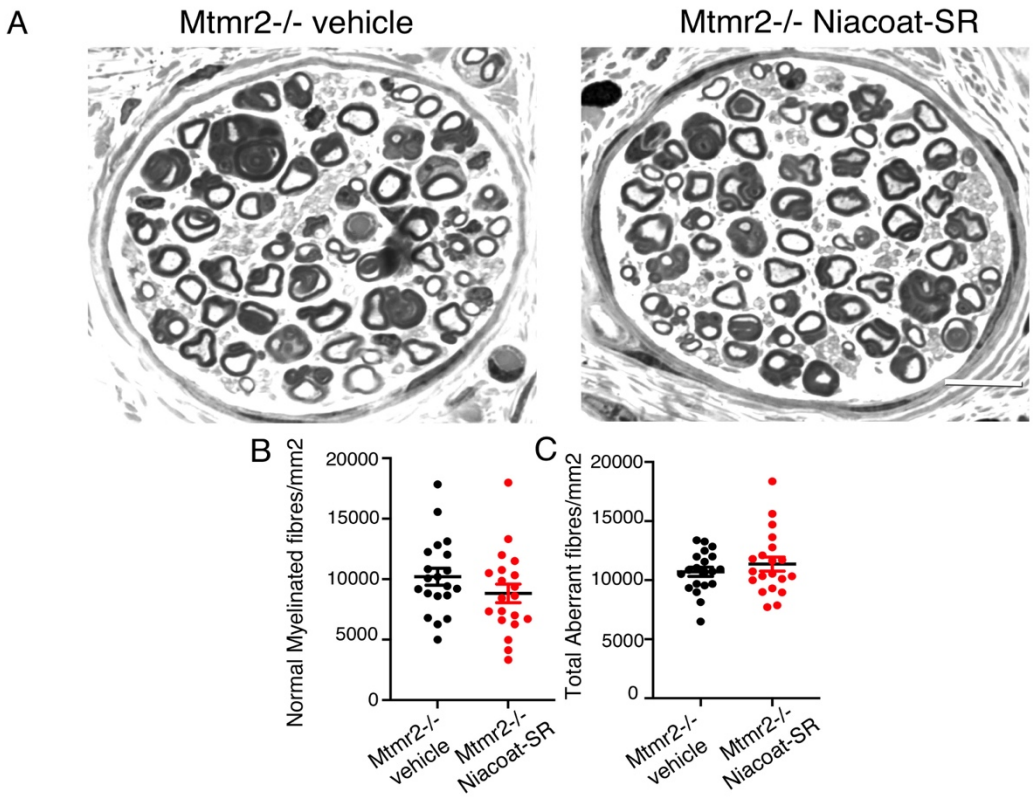


***Figure 48. Niacoat-SR treatment from P21 to P170 does not ameliorate morphology in Mtmr2$^{-/-}$ mice plantar nerves.***
*A) Representative images of plantar nerves semithin sections analysis of both vehicle and Niacoat-SR-treated Mtmr2$^{-/-}$ mice at P170; n=20 Mtmr2$^{-/-}$ vehicle, n=20 Mtmr2$^{-/-}$ Niacoat-SR; Scale Bar is 20 μm; B-E) Quantification of plantar nerve fibres displaying normal myelin structure(B) and aberrant myelin structures(C). Aberrant structures include myelin outfoldings, tomacula and degenerations; Data represent mean± SEM.*

Finally, since CMTs are primarily length-dependent neuropathies, we thought reasonable to investigate Niacoat-SR treatment effect on plantar nerves. In this case also, we found no amelioration of the morphological phenotype for any of the categories scored (**FIGURE 48 B,C**).

Altogether, these results indicate that Niacoat-SR treatment does not rescue the morphological phenotype, but it may have a neuroprotective effect by partially preventing degeneration at least in sciatic nerves.

These findings were corroborated by plasma NF-L (Neurofilament-light) chain levels analysis (performed in collaboration with Dr Amanda Heslegrave, UK Dementia Research, UCL, London), which are an informative biomarker of axonal degeneration

used for a variety of neurodegenerative conditions (including inherited neuropathies) both in human as in mouse models (Rossor & Reilly, 2022). Indeed, NF-L plasma levels were increased in Mtmr2 mutant mice as compared to controls at 6 months and showed a trend for amelioration in *Mtmr2* $^{-/-}$ mice after Niacoat-SR treatment **(Figure 49 NF-L:** WT vehicle *vs Mtmr2* $^{-/-}$ vehicle **p=0.0034; WT vehicle *vs Mtmr2* $^{-/-}$ Niacoat-SR *p=0.0273; Non-parametric ANOVA, Dunn's multiple comparison test).

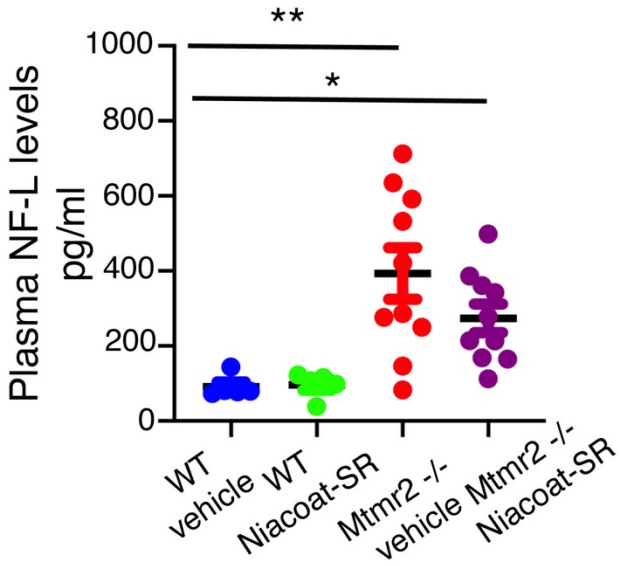


***Figure 49. Niacoat-SR effects on NF-L levels in Mtmr2$^{-/-}$ mice at 6 months.***
*Quantification of plasma NF-L levels (pg/ml) in WT and Mtmr2$^{-/-}$ mice. NF-L is a biomarker of axonal degeneration. Niacoat-SR treatment showed a trend for amelioration of NF-L levels in Mtmr2$^{-/-}$ mice; N=5 WT vehicle, n=5 WT Niacoat-SR, n=10 Mtmr2$^{-/-}$ vehicle, n=10 Mtmr2$^{-/-}$ Niacoat-SR; WT vehicle vs. Mtmr2$^{-/-}$ vehicle **p=0.0034; WT vehicle vs. Mtmr2$^{-/-}$ Niacoat-SR *p=0.0273; ANOVA Parametric T-test, Welch's correction. Data represent mean± SEM.*

Moreover, by closely looking at our data, we also found a correlation between NF-L levels and NCV values, indicating that mice displaying higher NCV also have lower NF-L levels in plasma (**Figure 50)**.

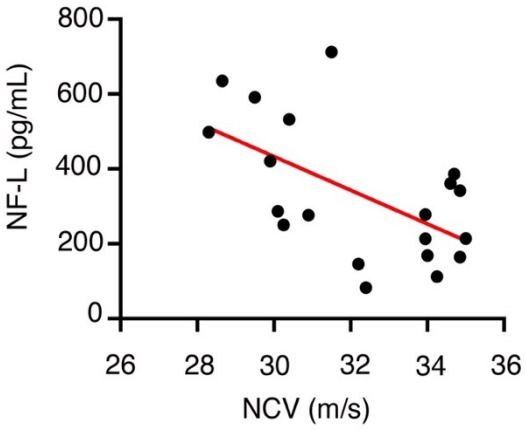


***Figure 50. Correlation between NCV and NF-L values after Niacoat-SR treatment at P170.*** *Graph showing the correlation existing between NCV and NF-L levels after Niacoat-SR treatment: mice with higher NCV also have lower NF-L levels. Pearson correlation test, r=-0.5731, P=0.0083.*

Since we found that Niacoat-SR positively modulated both NCV and NF-L, two crucial functional outcome measures in our model, we decided to further investigate axonal degeneration in *Mtmr2*$^{-/-}$ mice at 12 months of age. We already knew that in this model myelin degenerations and fibres loss progressively worsen with age likely contributing to NCV reduction (Bolis *et al*., 2005). It is possible that myelin degenerations can also result from a MTMR2 cell-autonomous role in neurons, which we have not demonstrated yet. However, recent data performed in our laboratory on full 129Sv/Pas strain *Mtmr2*$^{-/-}$ mice, suggested that with this genetic background, the pathological phenotype is more prominent. For those reasons, we decided to re-evaluate morphological and functional outcome measures at 12 months of age (**Figure 51**).

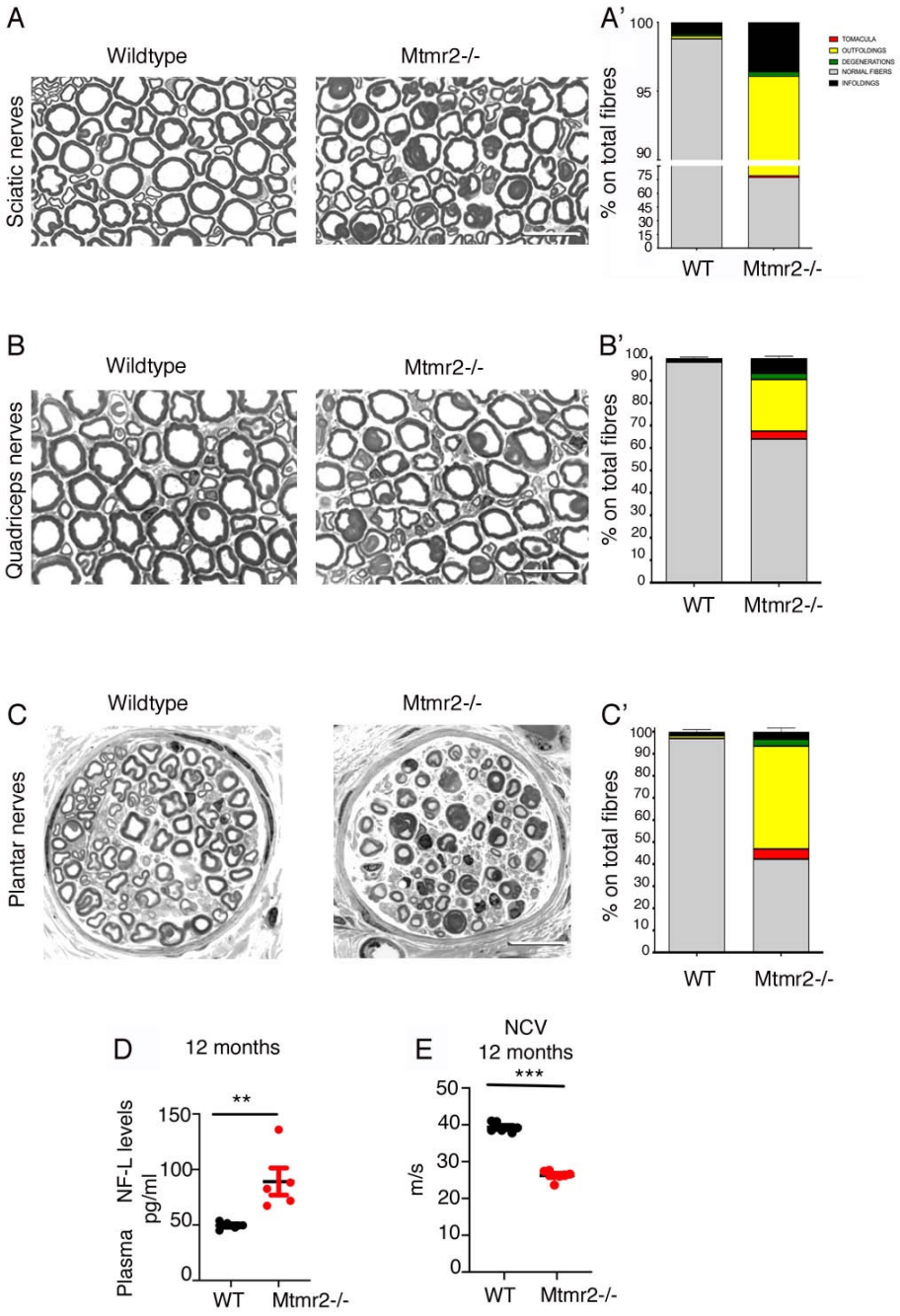


***Figure 51. Mtmr2 $^{-/-}$ mice phenotypic progression at 12 months of age.***

*A-C) Representative images of sciatic (A), quadriceps (B) and plantar (C) nerves semithin sections. Bar is 20 µm; A'-C') Graphs showing the percentage of normal fibres (gray), tomacula (red), outfoldings (yellow), infoldings (black) degenerations (green) on total fibres, n=4 WT and n=4 Mtmr2$^{-/-}$ mice; D) NF-L levels resulted to be increased also at 12 months age in Mtmr2$^{-/-}$ mice, WT vs. Mtmr2$^{-/-}$mice **p=0.0079, Non-parametric Mann-Whitney Student T-test; E) NCV is significantly reduced in Mtmr2$^{-/-}$mice at 12 months; n=7 WT and n=7 Mtmr2$^{-/-}$mice; ***p=0.006, Non-parametric Mann-Whitney Student T-test. Data represent mean± SEM.*

Morphological analyses on sciatic nerves semithin sections showed (**Figure 51 A**) an increased number of aberrant fibres-including tomacula, outfoldings, infoldings and degenerations- [**Figure 51 A'**, **ABERRANT FIBRES** WT= 256,63±21,52 (1,18%) *vs. Mtmr2*$^{-/-}$ = 4488,82±110,84 (22,19%)] associated with a reduction in the number of total fibres compared to WT (**Figure 51 A'TOTAL FIBRES** WT= 22290,03±407,2 *vs. Mtmr2*$^{-/-}$ = 20223,44±602,4: reduction of 10%), suggesting a clear progression of the phenotype. At 6 months indeed there is no evidence of fibres loss.

Then, to specifically evaluate the amount of motor fibres displaying aberrant myelin, we decided to analyse quadriceps nerve morphology (**Figure 51 B**). In line with our previous results, we observed an increased number of aberrant fibres [**Figure 51 B'**, **ABERRANT FIBRES** WT=226,96±83,78(1,35%) *vs. Mtmr2*$^{-/-}$ = 4240,37±567,77 (35,58%)], together with a reduction in the number of total fibres compared to WT (**Figure 51 B', TOTAL FIBRES** WT=16421,61±347,96 *vs. Mtmr2*$^{-/-}$ =11894,29±815,66: reduction of 28%).

Finally, since CMT4B1 like other neuropathies primarily affects distal body districts, we considered to study plantar nerves morphology (**Figure 51 C**). As expected, the pathological phenotype here is even more evident, both in terms of reduction of total fibres (**Figure 51 C' TOTAL FIBRES** WT= 26343,32±2138,66 *vs. Mtmr2*$^{-/-}$ =15156,31±775,23: reduction of 43% ) and number of fibres showing alterations [**Figure 51 C' ABERRANT FIBRES** WT=687,97±43,04 (2,69%) *vs. Mtmr2*$^{-/-}$ = 8674,01±221,68 (57,35%)].

When looking at functional outcome measures, NF-L showed increased levels also at 12 months (**Figure 51 D, NF-L 12 months** WT vs. *Mtmr2*$^{-/-}$**p=0.0079, Non-parametric Mann-Whitney student T-test), while NCV was even more decreased than at 6 months (**Figure 51 E, NCV**: WT 39,3± 0,413 m/s *vs. Mtmr2*$^{-/-}$ 26,27±0,43 m/s, ***P=0.006, Non-parametric Mann-Whitney student T-test).

Taken together, these results indicate a clear progression of Mtmr2$^{-/-}$ mice phenotype from 6 to 12 months, particularly for the significant fibres loss paralleled by a consistent worsening of NCV and NF-L values, which reproduce the human disease evolution. The relevance of these findings consists in highlighting the beneficial effects obtained with Niacoat-SR treatment in limiting axonal degeneration. Axonal loss is indeed the main functional aspect related to disability in different neuropathies and being able to limit its progression is a striking therapeutical point.

Finally, we decided to assess Niacoat-SR safety profile by performing histological and biochemical analyses after five months of daily administrations.

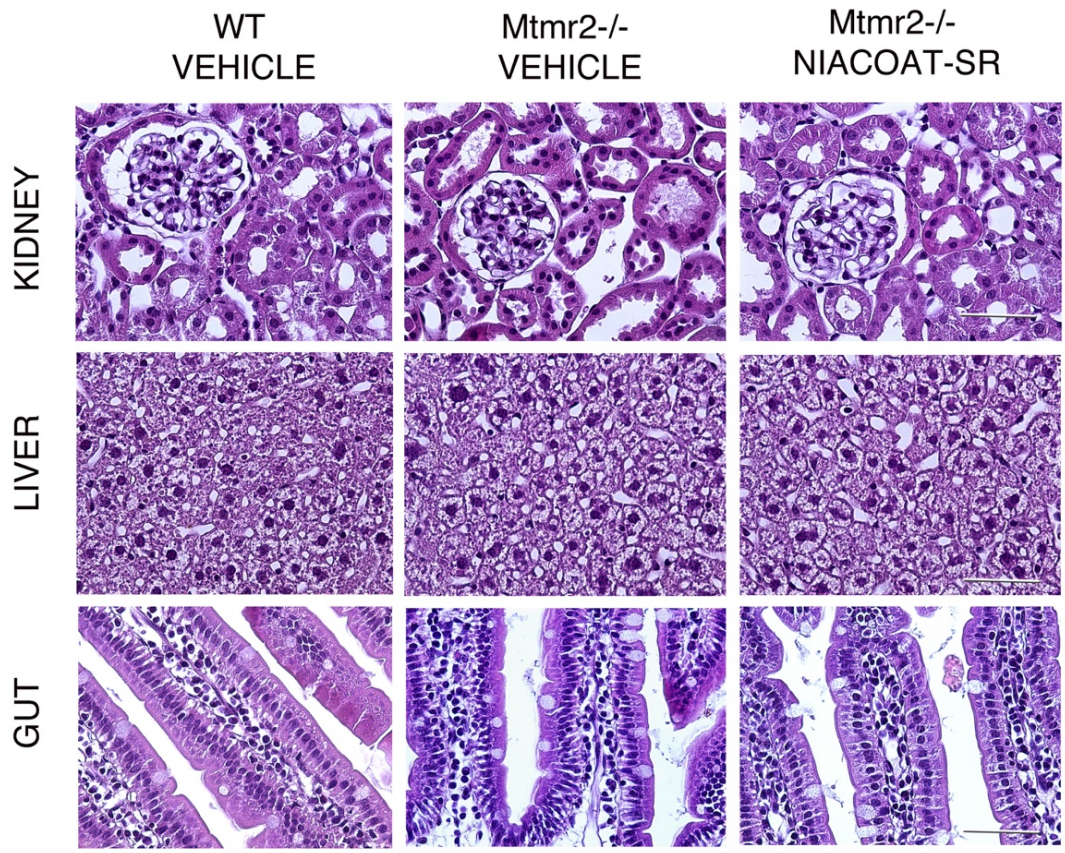


***Figure 52. Niacoat-SR is not toxic and is well-tolerated by mice after 5 months of treatment.*** *Representative images acquired at bright-field microscope showing kidney, liver, and gut sections stained with haematoxylin-eosin staining protocol, n=3 WT animals per condition analysed. No alterations have been found. Magnification is 40x. Bar in all sections is 55 μm.*

In agreement with preliminary results indicating that Niacoat-SR was well-tolerated by wild-type mice when administered from P21 to P50 (see 3.3.2), histological analyses of liver, gut, and kidney (**Figure 52**) and biochemical analyses of serum analytes associated with hepatic, renal, and lipid profiles (**Figure 53)**, (analyses performed in collaboration with Dr.Michele Raso, Animal biochemistry facility, HSR, Milan) showed no pathological alterations.

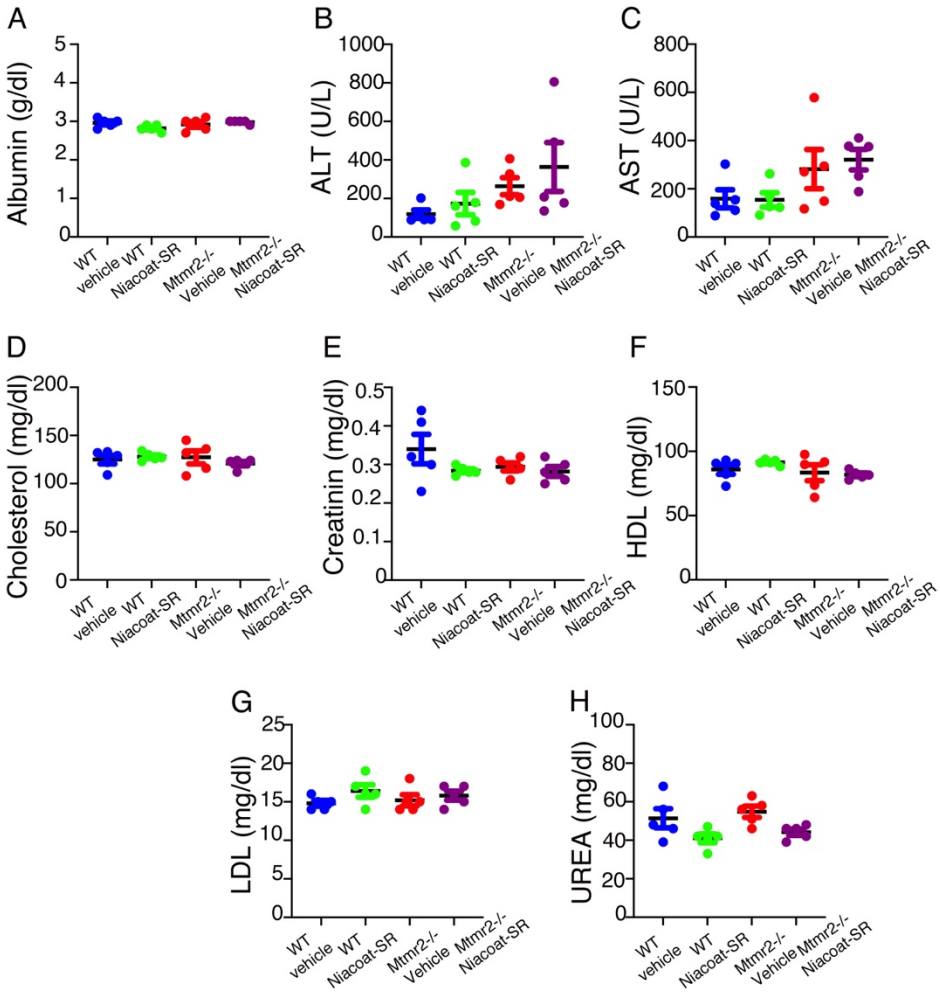


***Figure 53. Niacoat-SR does not alter hepatic, renal and lipid serum profiles of Mtmr2$^{-/-}$ mice after 5 months of treatment.***

*A) Quantification of hepatic-, renal- and lipid-associated analytes levels in WT and Mtmr2$^{-/-}$ mice serum after 5 months-treatment with vehicle or Niacoat-SR. N=5 WT vehicle, n=5 WT Niacoat-SR, n=5 Mtmr2$^{-/-}$ vehicle, n=5 Mtmr2$^{-/-}$ Niacoat-SR; Non-parametric ANOVA, Dunn's multiple comparisons test. Data represent mean± SEM. ALT=alanine transferase; AST=aspartate-amino transferase; LDL=low-density lipoprotein; HDL=high-density lipoprotein.*

Altogether these results suggest that Niacoat-SR is safe and positively regulates different outcome measures (e.g., NCV, NF-L, transcriptome), even if we did not observe amelioration of aberrant myelin in *Mtmr2*$^{-/-}$ mice (model of CMT4B1 neuropathy). Despite its potential application in clinical practice as drug repurposing strategy, some aspects still need to be elucidated.

# 4.DISCUSSION

Charcot-Marie-Tooth neuropathies are one of the most frequent forms of inherited neuromuscular disorders, with a prevalence of 1:2500 people, high heterogeneity, and significant social costs (Rossor *et al*., 2016).

Despite the recent development at the preclinical level of precision medicine tools (e.g., ASO, gene therapy) designed on the specific genetic profile, no treatments are still currently available for these disorders. In addition, the wide range of genetic and clinical manifestations makes difficult to find a unique therapeutical option.

In this work, we aimed to fulfil this unmet clinical need and we aimed at validating a therapeutic strategy based on drug repurposing that ideally can be beneficial to different clinical forms of CMT neuropathies.

More specifically, we pointed our attention on a group of demyelinating CMTs characterized by focal hypermyelination (e.g., CMT4B and HNPP). Despite the different genetic background, these neuropathies are all characterized by the presence of aberrant myelinated structures (e.g., myelin oufoldings/infoldings and tomacula), which partially result from the dysregulation of the PI3K-Akt-mTORC1 axis, downstream NRG1 type III signalling **(**Goebbels *et al*, 2012 Fledrich *et al*, 2014; Guerrero-Valero *et al*., 2021).

NRG1 type III is indeed a master regulator of PNS myelination and its expression levels determine the amount of myelin produced, which is always a function of the axonal diameter (Salzer, 2015). For these reasons, we thought that the modulation of NRG1 type III signal could be a valid strategy to ameliorate CMTs neuropathies with focal hypermyelination. Of note, NRG1 type III levels are regulated by two proteases, namely BACE and TACE, that cleave NRG1 with two opposite outcomes. BACE activates NRG1 type III and allows the molecule to be exposed with the EGF domain extracellularly tethered to the axonal surface. TACE is a negative regulator, as cleaves NRG1 type III and inactivates the molecule which is no longer able to interact with ErbB2/B3 receptors in Schwann cells. Moreover, TACE can be pharmacologically activated by niacin, nicotinic acid.

Thus, we thought that niacin as TACE activator, could downregulate NRG1 type III signalling and lower excessive myelination. Preliminary results obtained in our laboratory demonstrated, as proof-of-principle, the efficacy of this strategy in both *in vitro* and *in vivo* models of CMT4B1 and HNPP neuropathies (Bolino et al.., 2016).

More precisely, niacin given as Niaspan® (FDA-approved, long-lasting release of niacin/nicotinic acid/vitamin B3) was able to reduce the percentage of aberrant myelinated fibres without impacting the myelination process (no negative effects on *g-ratio*).

To better understand how niacin effects on axonal TACE are mediated in the nerve, we decided to investigate its mechanism of action by looking at Gpr109a receptor expression in both PNS (axons) and CNS (motoneurons cell bodies). Niacin interacts with Gpr109a receptor in different tissues, including spleen, adipose tissue, and skin (Offermanns & Schwaninger, 2015), so we thought it could likely be present also in the nervous system. However, we found that Gpr109a is not expressed by motoneurons in both PNS and CNS compartments, indicating that other receptors may be involved. To mention, Gpr81and Gpr109b are other receptors of the HCA2 family which however show higher affinity for other ligands (Blad *et al*., 2011).

Niaspan® is currently used in clinical practice to treat dyslipidemia and recently found to have also anti-atherogenic, neuroprotective and anti-inflammatory effects (Chen *et al.*, 2007; Chen *et al*., 2009; Offermanns & Schwaninger, 2015; Rawji *et a*l., 2020).
Our preliminary results supported Niaspan® repurposing as possible treatment for CMTs neuropathies with focal hypermyelination (Bolino *et al*., 2016).
However, in the perspective of a clinical translation, we needed to refine the treatment protocol by reproducing Niaspan® human kinetics (in 24hrs) and administration *per os* in mice and to investigate both morphological and functional outcome measures after a long period of treatment. To this aim, in collaboration with Dr. Gazzaniga's group (University of Milano, "La Statale") we produced Niacoat-SR, a new long-lasting release formulation of niacin, suitable for gavage administration in mice.
Pharmacokinetics studies demonstrated that Niacoat-SR (960mg/kg, gavage) was able to sustain niacin concentration in the nerve. More specifically, niacin concentration in the nerve peaked at 1h, remained stable until 3hrs and resulted to be detectable until 9hrs after last administration, whereas pure niacin is usually eliminated after 4hrs. Considering that mice digestion takes between 6-9 hours to be completed (Schwarz *et al*.,2002), these data confirmed that Niacoat-SR consistently reproduced Niaspan® human kinetics in mice.

Plasma levels of niacin showed a similar trend to pure niacin, even if the Niacoat-SR 960mg/Kg dose showed higher AUC values compared to pure niacin. This was expected considering the higher dose and the different formulation used.
Accordingly, we decided to test Niacoat-SR toxicity and tolerability in mice, particularly in the perspective of a chronic treatment. High doses of niacin can indeed have side-effects such as flushing, abdominal discomfort and nausea, even if mainly associated with IR (immediate release) formulations (Cooper *et al.,* 2015). In our case, the dose of 960 mg/kg corresponds to 28 mg of niacin in adult mice (30 gr), which is substantially lower than the range of 100-300 mg associated with the anti-dyslipidemic effect (1-3gr/day in humans). In line with that, Niacoat-SR resulted to be well-tolerated by mice.

Considering these results, we decided to set up a long-term pre-clinical trial with Niacoat-SR (960mg/kg, QD, gavage) from P21 to P170 in *Mtmr2* $^{-/-}$ mice (CMT4B1 model). Our data showed that Niacoat-SR was able to significantly increase TACE activity, to ameliorate MNCV and to positively modulate plasma NF-L levels, with the latest two being two functional outcome measures associated with clinical disability and therefore crucial points for translational approval. Moreover, we found them to be mutually correlated and extremely relevant in relation to the phenotypic progression observed in 12-months-old *Mtmr2* $^{-/-}$ mice.
Nevertheless, we did not find a morphological rescue. This was unexpected, particularly in relation to the increased MNCV observed. TACE indeed is the primary target of niacin and axonal TACE expression is reduced after P60 (Bolino *et al*., 2016), thus it is possible that after this age niacin effects on TACE are not as effective as before. Therefore, it could be interesting to investigate Niacoat-SR effects on morphology at an earlier time point. At least, we found a slight reduction in the number of sciatic degenerating fibres which paralleled the trend for reduction of plasma NF-L levels, suggesting that Niacoat-SR treatment for five months mainly exerted a neuroprotective effect by limiting degeneration and preserving axonal integrity. Accordingly, modulation of $NAD^+$ levels represents an interesting therapeutic candidate to counteract axon degeneration in several neurodegenerative conditions (Gerdts *et al*., 2016). We did not look at CMAP amplitudes because at 6 months they are not altered in our *Mtmr2* $^{-/-}$ mouse model (Bolis *et al*., 2005), which is expected, since the degenerative process has just started and then a significant

condition of fibres loss is still not present. It would be interesting instead to see if Niacoat-SR treatment could have a better beneficial effect at a later time-point when axonal loss is more present (e.g., in 12-months-old mice). Motor behavioural performance analyses were not included as well, since they are known to be only mildly impaired in *Mtmr2* $^{-/-}$ mouse model at 6 months of age (Bolino *et al*., 2004). Importantly, these aspects indicate that the murine phenotype is overall less severe than human one and that it could be a partial limit in understanding treatments efficacy from a functional point of view. This difference could be explained by the fact that: 1) mice live less, 2) CMT4B1 is a length-dependent disease and as such, murine nerves are shorter than human ones, 3) other myotubularins/mechanisms can compensate MTMR2 loss in mice.

Considering that 1) both CMT4B1 and HNPP neuropathies are chronic diseases which progress to degeneration and fibres loss with age, 2) nerve regeneration is possible in the PNS and 3) Niacin acts on NRG1, which plays a crucial role also during nerve regeneration, we thought that evaluating niacin impact on PNS physiological ability to regenerate and remyelinate after damage could be an essential point towards clinical application.

Our studies were designed to specifically evaluate niacin impact on NRG1 type I and III which have different roles during the regenerative process. Our findings showed that niacin treatment did not negatively impact on nerve regeneration/remyelination independently from the period of treatment after sciatic nerve crush (T1-T21; T10-T21; T1-T45). The regenerative process does not exactly recapitulate development and remyelination lasts longer, thus we did not really expect to observe a morphological rescue at T45dpsni. It could be interesting to see what happens at a later time-point.

Moreover, our studies on regeneration brought to light the presence of a defective regenerative process in both our mouse models (*Mtmr2* $^{-/-}$ and *Pmp22*$^{+/-}$) which was not previously known. Given the ubiquitous role of MTMR2 in PI (3,5) P2 modulation, associated with both autophagy and cytoskeleton remodelling, we thought that an alteration in the clearance process could likely be the cause. However, we did not find any significant variations in the number of macrophages nor in the autophagy flux, indicating that other mechanisms may be involved. Regarding this, mTORC1 was recently found to orchestrate a metabolic shift towards glycolysis after injury to prevent

axonal loss (Babetto *et al*., 2020). Since mTORC1 pathway is dysregulated in our mouse model (Guerrero-Valero *et al*., 2021), we considered reasonable to evaluate a possible correlation with our condition. Interestingly, we found an increased number of structural preserved axons at 36hours after injury in *Mtmr2* $^{-/-}$ mice, which however was not supported by an increase in PS6 levels. These findings then raise questions on whether some axon-autonomous mechanisms may influence the clearance process and how this initial delay could impact on overall regeneration.

In conclusion, given the positive results obtained in the modulation of different outcome measures in both development and after nerve injury, we can postulate that Niacin/Niaspan® repurposing could be an efficient strategy to exert neuroprotective effects and ameliorate clinical disability due to axonal loss in a variety of CMT neuropathies.

More specifically, the results obtained suggest that an early treatment with Niaspan® would be preferable to limit degeneration and fibres loss which start at 6 months and become prominent at 12 months in our *Mtmr2*$^{-/-}$ mouse model. However, since the human pathology is more severe and already present in childhood, one limit to clinically translate this strategy could be Niaspan® possible detrimental effects on lowering cholesterol levels during growth. An accurate evaluation of the correct dosage is then required if thinking of giving Niaspan® to very young patients while effects on adults are already well-described.

Other than drug repurposing, another interesting therapeutic option could be a genetic therapeutic approach. Gene therapy can indeed overcome problems related to chronic administrations by being a one-off treatment with long-lasting effects (Stavrou *et al*., 2021). The MTMR2 gene is a suitable candidate for gene therapy because of its small dimension (1,932bp), (Bolino *et al*, 2000). In addition, restoration of the 50% of the enzymatic activity would be sufficient to overcome the pathology, since CMT4B1 is a recessive disease and human carriers as well as heterozygous mice are not affected. However, one of the main challenges is to find the best route of administration, suitable for clinical translation while being able to reach a sufficient biodistribution in all the PNS, particularly in Schwann cells. Accordingly, vectors delivery to Schwann cells can be done using systemic delivery (intravenous injection) or restricted/local delivery (intrathecal or

intraneural injection) which show different efficacy and risks of off-side toxicity (Stavrou *et al*., 2021). Even though neurons transduction could be useful as well, we know that CMT4B1 primary target of the disease is myelin. Our previous results reported indeed that Mtmr2 loss specifically in Schwann cells is necessary and sufficient to reproduce the pathology. (Bolis *et al*., 2005).

Another big issue related to gene therapy is the time of delivery. Systemic delivery should be done in mice at two post-natal days when blood-nerve-barrier is still not completely formed, and Schwann cells proliferation is less active. Intrathecal of intraneural injections can be done at older ages but have shown reduced efficacy when compared to systemic delivery, particularly in terms of adequate PNS biodistribution (Stavrou *et al*., 2021).

It is evident then that clinical translation of this strategy could not be so easily done. Niacin/ Niaspan® repurposing would be a safer and quicker strategy to be approved, even though some aspects still need to be clarified.

# 5. MATERIALS AND METHODS

## 5.1 Animals (*Mtmr2*$^{-/-}$, *Pmp22*$^{+/-}$ and *Gpr109a*$^{mRFP}$ mice)

*Mtmr2*$^{fl/+}$ mice were generated by A. Bolino as previously described (Bolino *et al*., 2004). Heterozygous *Mtmr2*$^{fl/+}$ rodents were cross bred with transgenic mice expressing CMV-cre recombinase to specifically remove exon 4 and obtain heterozygous *Mtmr2*$^{+/-}$ mice. These animals were then crossed to obtain full *Mtmr2*$^{-/-}$ mice (*Mtmr2* KO), which ubiquitously lack *Mtmr2* expression. *Mtmr2* $^{+/+}$ were used as Wild-Type (WT) controls.
*Mtmr2* KO mice reproduce Charcot-Marie-Tooth type 4B1 (CMT4B1) neuropathy with myelin outfoldings.
*Pmp22*$^{+/-}$ mice were generated by K. Adlkofer as already described (Adlkofer *et al.,*1995; Adlkofer *et al.,*1997*).* A targeting vector was designed to insert the neomycin phosphotransferase (neo) gene into the first translated exon (exon II) at amino acid eight of the Pmp22 protein. *Pmp22*$^{+/-}$ mice were cross bred with C57/B6 WT to produce litters of around 50% ratio between WT and *Pmp22*$^{+/-}$ genotypes. Animals with Pmp22 gene haploinsufficiency reproduce hereditary neuropathy with liability to pressure palsies (HNPP) with tomacula.
*Gpr109a*$^{mRFP}$ mice (Gpr109a expression reporter mouse line) was generated by replacing the coding sequence of *Gpr109a* gene by a cassette containing the mRFP as described (Hanson *et al.,* 2010). RFP expression was then under the control of *Gpr109a* promoter. Transgenic *Gpr109a*$^{mRFP}$ mice were cross bred with C57/B6 WT to produce litters of around 50% ratio between WT and *Gpr109a*$^{mRFP}$ genotypes.
Mice were housed in a pathogen-free facility in San Raffaele Hospital (Milan, Italy) and cared for following National Health Institute guidelines. All the experiments involving the described animals were performed in accordance with Italian national regulations and covered by experimental protocols reviewed by local Institutional Animal Care and Use Committees (IACUC#701, #1069 and #1070).

## 5.2 Genotyping and Polymerase Chain Reaction (PCR) analysis

Animals genotyping for all lines was performed by genomic DNA isolation from mouse tails at P6-P8. DNA was extracted from fresh caudal biopsies using 300µl of DirectPCR lysis reagent (cat#102-T, Viagen, Biotech) and 15µl of Proteinase K from Tritirachium album (P2308-100mg, SIGMA). Samples were left overnight at 55°C and then at 85°C

for 45 minutes the day after to stop Proteinase K digestion. One or two microliters of DNA were used to carry out Polymerase Chain Reaction (PCR) analysis using GoTaq G2 Flexi DNA Polymerase kit (M7806, PROMEGA) following manufacturer's instructions. Reactions were amplified using Thermal cycler machines (#2720, Applied Biosystems). To discriminate wild-type from heterozygous and mutant mice we used line-specific pairs of primers:

| | |
|---|---|
| *Mtmr2*$^{-/-}$ mice | **Mtmr2 WT (500 bp)**<br>**Lox2P_fw:** 5' TCTTGTGGCTCTTCAGAATTGACC 3'<br>**EX4 REV_:** 5' TCCATGCTCTTGAAATATAACCTG 3'<br><br>**Mtmr2 KO (300 bp)**<br>**Lox3P_fw:** 5' AGCCAGGGCCACTATAGTTCTTAG 3'<br>**FRLT3 _rv:** 5' TGTCAGTTTCATAGCCTGAAGAACG 3' |
| *Pmp22*$^{+/-}$ | **Pmp22 WT (600 bp)**<br>**Ex2_fw:** 5'ATGCTCCTACTCTTGTTGGG 3'<br>**Int2_rv WT:** 5' AGATTAGCCACAGCCATAGTC 3'<br><br>**Pmp22 KO (300 bp)**<br>**Ex2_fw :** 5'ATGCTCCTACTCTTGTTGGG 3'<br>**Neo AS_rv KO:** 5' GCCTTCTATCGCCTTCTTGAC 3' |
| *Gpr109A*$^{mRFP}$ | **Gpr109a$^{mRFP}$ (400 bp)**<br>**404_fw:** 5'ctgcagccttcagaaggaat 3'<br>**405_rv:** 5'cgcatgaactccttgatgac 3' |

To note that transgenic *Gpr109A*$^{mRFP}$ mice show a band only at 400bp which corresponds to the reporter *mRFP* gene, whereas wild-type mice did not show any band.

### 5.3 Sciatic nerve crush and cut

To study Wallerian Degeneration, we performed sciatic nerve crush (axonotmesis) or cut (neurotmesis) to induce acute nerve damage. In both cases, animals were firstly anesthetized with trichloroethanol (SIGMA) 0.02 ml/g of body weight by intraperitoneal injection (i.p.). Sciatic nerves were then exposed after a fine incision between the *gluteus*

and the *femoral* muscles. When performing sciatic nerve crush, nerves were both mechanically and thermically injured with pre-cooled forceps stapling the nerve proximally. The site of damage was marked with carbon powder (SIGMA) in which forceps had been previously immerged. When performing sciatic nerve cut, nerves were proximally severed using fine scissors. In both cases, animals were finally sutured using Monofilament Nylon Dermalon 4.0 (COVIDIEN) and monitored until their recovery form anaesthesia. Nerves were then collected at different time-points in relation to the outcome for both morphological and biochemical analyses.

### 5.4 Niacin *In Vivo* Treatment

To study niacin effect on nerve regeneration/remyelination, we administered 120 mg/kg of Niacin (SIGMA) to both *Mtmr2* $^{-/-}$ and *Pmp22*$^{+/-}$ mice after sciatic nerve crush. Niacin was solubilized in saline (NaCl, 0,9%, SALF) to obtain a final concentration of 5mg/ml. Niacin was daily given to mice by intraperitoneal injection at different time-points and time-windows after sciatic nerve crush, in relation to the experimental rational. Animals were monitored for body weight and clinical signs every day. All treatments have been done following good-practice dose-volumes guidelines (International Consortium for Innovation and Quality in Pharmaceutical Development-IQ 3Rs Leadership Group).

### 5.5 Niacoat-SR Formulation

Niacoat-SR was produced in collaboration with Prof. Andrea Gazzinga and Dr. Matteo Cerea (*Department of Pharmaceutical Sciences, University of Milan "La Statale", Milan, Italy*). Niacin (Ph.Eur grade, Acros Organics) was encapsulated in coated beads microparticles of 200-400 micron in average by applying an ethylcellulose-based membrane (Surelease®, Colorcon) additioned with low-viscosity methylcellulose (Methocel E5 premium LV, Colorcon) to niacin granules, using a fluid bed apparatus (GDPC 1.1, Glatt, D). The beads size limit of 500 micron was imposed to allow gavage administration with feeding tubes of 0,8 mm of internal diameter (FTPU 16-38-50, INSTECH). Stability of the new compound (Niacoat-SR) was then checked and guaranteed at 25°C and 65% relative humidity until 6 months. Niacoat-SR release kinetics was assessed *in vitro* at 37°C (to mimic body temperature) using a water solution and a paddle dissolver device (Sotax AT7, Sotax, CH). Niacoat-SR dissolution in water was

analysed at 1h,3h,6h,9h and 24 hours with both spectrophotometry UV (Lambda 35, Perkin Elmer, USA) and HLPC method (Waters, USA), and finally compared to that of Niaspan® tablets.

## 5.6 Pharmacokinetics Studies (PK)

### *1) Niacin i.p. vs. Niacin gavage*

Five groups of 15 WT 129sv/Pas mice have been daily treated from P30 to P37 by i.p. or gavage with different doses of niacin (nicotinic acid, cell culture grade, N0761-100gr, SIGMA) dissolved in NaCl 0,9% (SALF). Nerves and blood were collected the last day at 0mins, 30mins, 2h, 4h and 6h after last administration (3 animals per time-point). Nerves were immediately snap-frozen in liquid nitrogen, whereas plasma was extracted as described in 5.12. All tissues were then sent to Eurofins (France) for analysis.

### *2) Niacoat vs. Niacin*

A group of 24 WT 129sv/Pas mice was daily treated by gavage from P30 to P37 with the dose of 960mg/Kg, 100mg/ml of Niacoat-SR (lot#191113-E5-60S produced in 2019) to test Niacoat-SR long-lasting release efficacy. Niacoat-SR handling and administration was done as described in 5.7. Nerves and blood were collected on the last day at 0mins, 1h, 3h, 6h, 9h and 12h after last treatment (3 animals per time-point). Nerves were immediately snap-frozen in liquid nitrogen, whereas plasma was extracted as described in 5.12. All tissues were then sent to Eurofins (France) for analysis and results were then compared to those of niacin (point 1).

## 5.7 Niacoat-SR *In Vivo* Treatment

Niacoat-SR aliquots of 175mg were freshly prepared every day by weighing the exact amount of the compound directly into 2 ml Eppendorfs. Tubes were then maintained at room temperature (RT) until use, avoiding direct contact with light. One aliquot for each mouse was daily prepared for the following day.

1ml of High-Viscosity Methylcellulose at 0,75% (4000cP, A4M ID34435, Premium Methylcellulose, VBN n. D180F9E011, COLORCON), used as vehicle solution, was added to each aliquot prior to mice administration. Volumes corresponding to 960mg/kg

dose of Niacoat-SR were administered once a day to mice by gavage, using insulin syringes (#02.071250.300.350, PIKDARE) and feeding tubes (FTPU 16-38-50, INSTECH). In all the experiments, Niacoat-SR administration started after P21 and was done 7days/week, until reaching the scheduled time-point in relation to the outcome analysed.

Animals were monitored for body weight and clinical signs every day and all treatments have been done following good-practice dose-volumes guidelines (International Consortium for Innovation and Quality in Pharmaceutical Development-IQ 3Rs Leadership Group).

Vehicle (Methylcellulose 0,75%) was prepared twice a week following this procedure: approximately 90% of the total volume of sterile deionized (DI) water was put in a becker containing a Polytetrafluoroethylene (PTFE) stir bar and then warmed to approximately 80°C, while stirring on a magnetic stirrer. When temperature was reached, the becker was removed from the heat and methylcellulose (MC) was added to create a 0.75% (w/v) mixture. The mixture was then left to cool to room temperature while stirring. When the MC was completely dissolved, DI water was added to reach final volume. The solution was then stored at 2-8°C, avoiding direct contact with light.

### 5.8 TACE Activity Assay

The SensoLyte 520 TACE (α-Secretase) Activity Assay Kit *Fluorimetric* (ANASPEC, EGT group, Cat. AS-72085) was used to determine TACE activity in mouse sciatic nerves lysates after Niacin/Niacoat treatments. The kit provides a QXLTM520/5-FAM FRET substrate (TACE substrate), derived from a sequence surrounding the cleavage site of TACE, which enables to quantify TACE activity. In the intact FRET peptide, indeed, the fluorescence of 5-FAM is quenched by QXLTM520, whereas in presence of active TACE, the FRET substrate is cleaved into two separate fragments. This results in an increase in 5-FAM fluorescence, which can be monitored at excitation/emission = 490 nm/520 nm. Lysates from sciatic nerves were prepared using kit assay buffer (Component c) with 0,1% Triton X-100 (SIGMA) and manually homogenized with a pestle. Samples were then sonicated for 1 min, left at 4°C for 30mins on a rotating wheel and finally centrifuged at 13,200 rpm for 15mins. The resulting supernatant was collected, and protein concentration was determined using BCA assay (Pierce, Thermo Scientific).

Samples were then loaded on a 96-well black plate together with TACE substrate (diluted 1:100 in assay buffer) and left to gently shake for 1hour at RT, avoiding direct contact with light. Blank and a positive control (rh TACE, recombinant human TACE, R&D System) were also added to the plate and incubated with TACE substrate. After 1 hour, samples fluorescence was recorded using a microplate reader (Victor3, PerkinElmer), detecting emission at 520 nm with excitation at 490 nm. For each sample, fluorescence intensity was normalized for protein concentration and compared to the standard 5-FAM curve. To generate the 5-FAM standard curve, the 5-FAM was diluted from the 1 mM stock to a final concentration of 4 μM, and a standard curve with a range from 2 to 0.03 μM in assay buffer (seven points) was made.

### 5.9 Morphological and Morphometrical analysis

Morphological analysis on sciatic nerves semithin sections was performed at different ages in relation to the outcome. For each experiment, more than n=3 animals were enrolled.

Nerves were collected and immediately fixed with 2,5% glutaraldehyde in 0,12 M phosphate buffer and left at 4°C until use. Samples were then incubated with 1% osmium tetroxide (SIGMA) for 2h at RT to fix lipids, and later embedded in epoxy resin (SIGMA). Semithin sections of 1μm were obtained using Leica Ultracut UCT, followed by staining with toluidine blue and visualization at light microscope (LEICA DFC300F). To perform morphological and morphometrical analyses, digitalized images of nerves cross sections were acquired with a 100x objective and then put together to rebuild the complete section. Morphological analyses were made by scoring the number of aberrant or degenerating fibres on total nerves fibres using Adobe Photoshop CS4 (version 11.0) and Image J (version 1.49) software. Five random images for each sample were taken at 100x objective to score G-ratio, calculated as the ratio between the internal diameter of an axon (without myelin) and total fibre diameter (LeicaQWin software, Leica Microsystem).

### 5.10 Neurophysiology

Neurophysiological analyses were performed in collaboration with Dr. Ubaldo del Carro, Dr. Francesca Bianchi and Dr. Valenzano Serena **(***Clinical Neurophysiology Unit and the Movement Disorders Unit, IRCSS San Raffaele Hospital, Milan*). Mice were anesthetized

with trichloroethanol (SIGMA) 0.02 ml/g of body weight and placed under a heating lamp to avoid hypothermia. The sciatic nerve motor conduction velocity was recorded using steel monopolar needle electrodes. A pair of stimulating electrodes was inserted subcutaneously near the nerve at the ankle and a second pair of electrodes was placed at the sciatic notch, to obtain proximal and distal stimulation, respectively.

## 5.11 Histology

Histological analysis of liver, gut and kidney were performed in collaboration with Dr. Fiocchi A., (*Animal histopathology Unit, HSR, Milan*). Animals were anesthetized with trichloroethanol (SIGMA) 0.02 ml/g of body weight and perfused with 4% paraformaldehyde. Tissues were then collected and left O/N at RT in formalin. The day after, samples were sectioned to fit in plastic capsules (specific for paraffin embedding), and then moved to Ethanol 70% for at least 24h. Tissues were then processed using Leica TP1020 instrument containing an increasing concentration of alcoholic solutions (from 70 to 100%), followed by Bioclear (BioOptica) and paraffin embedding (Bio Plast Plus, BioOptica). Inclusion was performed with Leica EG1150H, whereas sectioning was done using a rotary microtome (Leica RM2235). Sections were then stained with Haematoxylin-Eosin using Leica ST5020 machine following these steps: 1) dewaxing with Bioclear followed by a descending concentration of alcoholic solutions until pure water; 2) staining with Haematoxylin (BioOptica) followed by a cold tap water rinse; 3) staining with Eosin (BioOptica); 4) dehydration with an increasing concentration of alcoholic solutions and Bioclear; 5) Permanent stabilization with a Xylene-based mounting medium. Slides were then kept at RT and images acquired at light microscope (LEICA DFC300F). Clinical interpretation of the results was done by Dr. Francesca Sanvito, MD (*Pathology Unit, IRCCS San Raffaele Hospital, Milan*).

## 5.12 Plasma and Serum collection

Around 500µl of blood were extracted from the cheek of each animal using a hypodermic needle (Gauge G27, PIC solution). To obtain plasma, blood was directly collected in specific tubes containing Lithium Heparin (Microvette®, 500LH, SARSTEDT) while for serum, blood was collected in a 1,5 ml Eppendorf. For both components, samples were left at RT for 30 mins and then centrifuged at 4000rpm for 15 mins. Supernatant was then

moved into a new 1,5ml Eppendorf and kept at -80°C until use. For Pharmacokinetics analyses, plasma samples were sent to *Eurofins*, France (as described in 5.6), whereas for Neurofilament Light-Chain (NF-L) analysis were sent to *UK Dementia Research Institute at UCL, London, United Kingdom* (as described in 5.14). Serum samples were instead analysed at *Animal biochemistry facility, HSR, Milan, Italy,* (as described in 5.13).

### 5.13 Bio clinical analyses

Serum samples of *Mtmr2* KO mice were analysed at *Animal biochemistry facility, HSR, Milan, Italy* by Dr. Raso.

Urea (#0018255440), Crea (#0018255540), AST (#0018257540), ALT (#0018257440), Albumin (#18250040), HDL (#ch2652), LDL (#0018256040) and Cholesterol (#0018250540) were used for the quantitative determination of the serum level with an International Federation of Clinical Chemistry and Laboratory Medicine optimized kinetic ultraviolet (UV) method in an ILab650 chemical analyser (Instrumentation Laboratory), and then expressed as mg/dl. SeraChem Control Level 1 and Level 2 (#0018162412 and #0018162512) were used as quality control.

### 5.14 Plasma Neurofilament Light Chain (NF-L) levels analysis

Plasma samples for Neurofilament Light-Chain (NF-L) analysis were sent to *UK Dementia Research Institute at UCL, London, United Kingdom* and processed by Dr. Amanda Heslegrave. Plasmatic NF-L was measured by single molecule array (SIMOA) on an HD-X analyser (Quanterix), according to manufacturer's instructions. Samples were thawed at 21°C, vortexed, and centrifuged at 13,000 RCF for five minutes at 21°C. On-board the instrument, samples were diluted 1:40 with sample diluent and bound to paramagnetic beads coated with a capture antibody specific for NF-L. NF-L bound beads were then incubated with a biotinylated NF-L detection antibody in turn conjugated to streptavidin-β-galactosidase complex that acts as a fluorescent tag. Subsequent hydrolysis reaction with a resorufin β-D-galactopyranoside substrate produces a fluorescent signal proportional to the concentration of NF-L present. Duplicate measurements were taken of each sample. Sample concentrations were extrapolated from a standard curve, fitted using a 4-parameter logistic algorithm.

## 5.15 Transcriptome analysis

One nerve for each mouse was collected and immediately snap-frozen with 500µl of TRIZOL (Ambion by Life Technologies). Samples were then sent to Professor John Svaren *(University of Wisconsin-Madison, Madison WI, USA*) for the analysis. For *Mtmr2* KO (treated and vehicle) and WT mice, at least 1000 ng total RNA from sciatic nerve was purified and sent to Genewiz (South Plainfield, NJ) for library preparation, after PolyA selection and Illumina sequencing (Illumina HiSeq 2x150bp). Illumina sequencing data were mapped to the GRCm38/mm10 genome using the STAR alignment. Data were analysed using DESeq2 to determine differentially regulated genes (p-value < 0.5), ( Anders *et al*., 2015). The cut-off for determining significantly differentially expressed genes was an FDR-adjusted p-value less than 0.05 (Xie *et al*., 2021). Gene Ontology analysis was performed using Enrichr with all up/down regulated genes with non-adjusted p-value of <0.05, and the Molecular Signature Database (MSigDB) Hallmark gene sets (Liberzon *et al*., 2015).

## 5.16 Immunofluorescence on frozen tissues

Animals were anesthetized using trichloroethanol (SIGMA) 0.02 ml/g of body weight by intraperitoneal injection and then perfused with freshly prepared buffered 4% paraformaldehyde (PFA, SIGMA). Sciatic nerves were collected, embedded in OCT (Killik, Bio-Optica) and then snap-frozen in liquid nitrogen. Spinal cords were collected, finely processed to remove bones and meninges, and then incubated overnight (O/N) in 4% PFA at room temperature (RT). The following day samples were washed with PBS 1X, left O/N at RT in sucrose 30% with 0,1% sodium azide (SIGMA) and finally embedded in OCT. All samples were stored at -80°C until use.

Eight µm-thick sciatic nerve sections were cut transversally or longitudinally at cryostat (LEICA), left to air dry for 2h at RT and then permeabilized for 5 minutes in ice-cold methanol or acetone (Carlo Erba). Slides were blocked for 1h at RT in 1% BSA, 0,05% TRITON, 10% NGS. Incubation with primary antibodies was done for 2h at RT or O/N at 4°C. Sections were then washed with PBS 1X and then incubated with TRITC or FITC secondary antibodies (1:100) for 1h at RT. Slides were finally mounted using DAPI mounting medium (Vectashield) and then acquired at Confocal Microscope SP5 (Leica). Spinal cords staining was performed on 30 µm-thick sections. Samples were cut and left

to air dry O/N, rehydrated in PBS1X for 15 minutes, permeabilized in 50% ethanol (in PBS) for 30 minutes at RT, and then incubated with PBS+ 0.3% triton (PBS-T 0.3%) for 1h30 at RT. Primary antibodies were incubated O/N at RT. After two 10 minutes-washing in PBS-T 0.3%, samples were incubated with Alexa488/Alexa546/FITC or TRITC secondary antibodies for 3h at RT. Slides were finally mounted using DAPI mounting medium (Vectashield) and then Z-stacks acquired at Confocal microscope SP5 (Leica).

### 5.17 Western Blot

Western blot analysis was performed on sciatic nerves of both WT and mutant mice at different time-points in relation to the outcome. Mice were euthanized using carbon dioxide (CO2), nerves collected and then immediately snap-frozen in liquid nitrogen. Samples lysates have been generated using different lysis buffer in relation to the antigen of interest. SDS buffer (2%SDS, 25mM Tris buffer pH8, 95mM NaCl, 10mM EDTA pH8, complete protease inhibitors (ROCHE), phosphatase inhibitor cocktails 2 and 3 (SIGMA), 10mM NaF, 1mM $Na_3VO_4$ and 1mM β-glycerophosphate) was used to reveal PS6 in nerves. RIPA buffer (0,1%SDS, 0,1% Triton X-100, 100mM NaCl, 8,4mM Sodium phosphate dibasic ($Na_2HPO_4$), 1,6mM Sodium phosphate monobasic ($NaH_2PO_4$) and Sodium Deoxycholate) was instead used to detect autophagy markers LC3 and NBR1 in nerves. Protein concentration of lysates was determined using standard BCA assay (Pierce, Thermo Fisher Scientific). SDS-page gels or Bolt Bis-Tris Plus gels (Thermo Fisher Scientific) were used to run samples and then transferred to PVDF membranes (Millipore), pre-activated in pure methanol. Blocking solutions of 5% Milk (Regilat) or Bovine Serum Albumin (SIGMA) in PBS 0,1% tween 20 (SIGMA) were left overnight at 4°C. For phosphorylated proteins, membranes were pre-incubated for 30 mins at RT in BSA 3% before incubation with both primary and secondary antibodies (always in BSA 3%). For non-phosphorylated antigens both primary and secondary antibodies were diluted in 3% Milk. HRP-conjugated (DAKO) secondary antibodies were normally used and immunoblots developed with ECL/ECL-prime system (Amersham) using UVITEC (Cambridge). Washes have been done in TBS-Tween 0,1% or PBS-Tween 0,1% in case of phosphorylated antigens or not, respectively. Densitometry was done with Image J software and statistical analyses were performed with GraphPad Prism 9.0 as described in 5.19.

## 5.18 Antibodies

**Primary Antibodies**

| Antibody | Species | Dilution | | Source | Catalogue Number |
|---|---|---|---|---|---|
| | | IHC | IB | | |
| pS6 rp (Ser 235/236) | Rb | | 1:1000 | Cell signalling | 4858 |
| LC3 | Rb | | 1:1000 | Sigma | L7543 |
| NBR1 | Ms | | 1:250 | Prod.Gianni | AB55474 |
| Vinculin | Ms | | 1:10000 | Millipore | 05-386 |
| Tubulin beta | Ms | | 1:5000 | Sigma | T4026 |
| Neurofilament-M | Ck | 1:2000 | | Biolegend | 822701 |
| MBP | Rat | 1:50 | | Millipore | MAB386 |
| F4/80 | Rat | 1:100 | | Biorad | MCA497 |
| RFP | Rb | 1:100 | | ThermoFisher | R10367 |
| ChAT | Goat | 1:100 | | Millipore | AB144P |
| NeuN | Ms | 1:200 | | Millipore | MAB377 |

**Secondary Antibodies**

| Antibody | Species | Dilution | | Source | Catalogue Number |
|---|---|---|---|---|---|
| | | IHC | IB | | |
| α-Rb Immunoglobulins/HRP | Goat | | 1:10000 | DAKO | P0448 |
| α-Ms Immunoglobulins/HRP | Rb | | 1:5000 | DAKO | P0260 |
| FITC α-Ck | Donkey | 1:100 | | Starfish | 703-095-155 |
| TRITC α-Rat | Donkey | 1:100 | | Starfish | 712-025-150 |
| TRITC α-Rb | Donkey | 1:100 | | Starfish | 711-025-152 |
| FITC α-Rat | Donkey | 1:100 | | Starfish | 712-095-153 |
| Alexa-488 α-Mouse | Donkey | 1:500 | | Invitrogen | A21202 |
| Alexa-488 α-Goat | Donkey | 1:500 | | Invitrogen | A11055 |

### 5.19 Statistical Analysis

All experiments account for at least n=3 animals per group/condition. Normalization is indicated. Statistical analyses were performed using GraphPad Prism version 9. Data are shown as MEAN±SEM and the correct p value is reported under each graph in figure legends. Different tests have been applied in relation to the experimental setting: Mann Whitney non-parametric two-tailed Student's t-test was used to compare two independent groups; One-sample Student's t-test was used to compare different experiments and assess whether the median of ratios was greater than 1; One-way non-parametric ANOVA test followed by Dunn's multiple comparison test was used with more than two groups. Significant results have been displayed in the graphs with asterisks: *p<0.05, **p<0.01,***p<0.001, ****p<.0001.

# REFERENCES


Adlkofer K, Frei R, Neuberg DH-H, Zielasek J, Toyka KV & Suter U (1997a) Heterozygous Peripheral Myelin Protein 22-Deficient Mice Are Affected by a Progressive Demyelinating Tomaculous Neuropathy. *J Neurosci* 17: 4662–4671

Adlkofer K & Lai C (2000) Role of neuregulins in glial cell development. *Glia* 29: 104–111

Adlkofer K, Martini R, Aguzzi A, Zielasek J, Toyka KV & Suter U (1995) Hypermyelination and demyelinating peripheral neuropathy in Pmp22-deficient mice. *Nat Genet* 11: 274–280

Adlkofer K, Naef R & Suter U (1997b) Analysis of compound heterozygous mice reveals that theTrembler mutation can behave as a gain-of-function allele. *J Neurosci Res* 49: 671–680

Anders S, Pyl PT & Huber W (2015) HTSeq--a Python framework to work with high-throughput sequencing data. *Bioinformatics* 31: 166–169

Arthur-Farraj PJ, Latouche M, Wilton DK, Quintes S, Chabrol E, Banerjee A, Woodhoo A, Jenkins B, Rahman M, Turmaine M, *et al* (2012) c-Jun Reprograms Schwann Cells of Injured Nerves to Generate a Repair Cell Essential for Regeneration. *Neuron* 75: 633–647

Attarian S, Fatehi F, Rajabally YA & Pareyson D (2020) Hereditary neuropathy with liability to pressure palsies. *J Neurol* 267: 2198–2206

Babetto E, Wong KM & Beirowski B (2020) A glycolytic shift in Schwann cells supports injured axons. *Nat Neurosci* 23: 1215–1228

Bai Y, Zhang X, Katona I, Saporta MA, Shy ME, O'Malley HA, Isom LL, Suter U & Li J (2010) Conduction Block in PMP22 Deficiency. *Journal of Neuroscience* 30: 600–608

Barter P (2011) HDL-C: Role as a risk modifier. *Atherosclerosis Supplements* 12: 267–270

Benyó Z, Gille A, Kero J, Csiky M, Suchánková MC, Nüsing RM, Moers A, Pfeffer K & Offermanns S (2005) GPR109A (PUMA-G/HM74A) mediates nicotinic acid-induced flushing. *J Clin Invest* 115: 3634–3640

Blad CC, Ahmed K, IJzerman AdP & Offermanns S (2011) Biological and Pharmacological Roles of HCA Receptors. In *Advances in Pharmacology* pp 219–250. Elsevier

Bolino A, Muglia M, Conforti FL, LeGuern E, Salih MAM, Georgiou D-M, Christodoulou K, Hausmanowa-Petrusewicz I, Mandich P, Schenone A, *et al* (2000) Charcot-Marie-Tooth type 4B is caused by mutations in the gene encoding myotubularin-related protein-2. *Nat Genet* 25: 17–19

Bolino A, Bolis A, Previtali SC, Dina G, Bussini S, Dati G, Amadio S, Del Carro U, Mruk DD, Feltri ML, *et al* (2004) Disruption of Mtmr2 produces CMT4B1-like neuropathy with myelin outfolding and impaired spermatogenesis. *Journal of Cell Biology* 167: 711–721

Bolino A, Marigo V, Ferrera F, Loader J, Romio L, Leoni A, Di Duca M, Cinti R, Cecchi C, Feltri ML, *et al* (2002) Molecular characterization and expression analysis of Mtmr2 , mouse homologue of MTMR2 , the Myotubularin-related 2 gene, mutated in CMT4B. *Gene* 283: 17–26

Bolino A, Muglia M, Conforti FL, LeGuern E, Salih MAM, Georgiou D-M, Christodoulou K, Hausmanowa-Petrusewicz I, Mandich P, Schenone A, *et al* (2000) Charcot-Marie-Tooth type 4B is caused by mutations in the gene encoding myotubularin-related protein-2. *Nat Genet* 25: 17–19

Bolino A, Piguet F, Alberizzi V, Pellegatta M, Rivellini C, Guerrero-Valero M, Noseda R, Brombin C, Nonis A, D'Adamo P, *et al* (2016) Niacin-mediated Tace activation ameliorates CMT neuropathies with focal hypermyelination. *EMBO Mol Med* 8: 1438–1454

Bolis A (2005) Loss of Mtmr2 Phosphatase in Schwann Cells But Not in Motor Neurons Causes Charcot-Marie-Tooth Type 4B1 Neuropathy with Myelin Outfoldings. *Journal of Neuroscience* 25: 8567–8577

Bolis A, Coviello S, Visigalli I, Taveggia C, Bachi A, Chishti AH, Hanada T, Quattrini A, Previtali SC, Biffi A, *et al* (2009) Dlg1, Sec8, and Mtmr2 Regulate Membrane Homeostasis in Schwann Cell Myelination. *Journal of Neuroscience* 29: 8858–8870

Brinkmann BG, Agarwal A, Sereda MW, Garratt AN, Müller T, Wende H, Stassart RM, Nawaz S, Humml C, Velanac V, *et al* (2008) Neuregulin-1/ErbB Signaling Serves Distinct Functions in Myelination of the Peripheral and Central Nervous System. *Neuron* 59: 581–595

Brown BG (2005) Can niacin slow the development of atherosclerosis in coronary artery disease patients already taking statins? *Nat Rev Cardiol* 2: 234–235

Cattin A-L & Lloyd AC (2016) The multicellular complexity of peripheral nerve regeneration. *Current Opinion in Neurobiology* 39: 38–46

Chen J, Cui X, Zacharek A, Ding GL, Shehadah A, Jiang Q, Lu M & Chopp M (2009) Niaspan Treatment Increases Tumor Necrosis Factor-α-Converting Enzyme and Promotes Arteriogenesis after Stroke. *J Cereb Blood Flow Metab* 29: 911–920

Chen J, Cui X, Zacharek A, Jiang H, Roberts C, Zhang C, Lu M, Kapke A, Feldkamp CS & Chopp M (2007a) Niaspan increases angiogenesis and improves functional recovery after stroke. *Ann Neurol* 62: 49–58

Chen P, Piao X & Bonaldo P (2015) Role of macrophages in Wallerian degeneration and axonal regeneration after peripheral nerve injury. *Acta Neuropathol* 130: 605–618

Chen Z-L, Yu W-M & Strickland S (2007b) Peripheral Regeneration. *Annu Rev Neurosci* 30: 209–233

Clark AB & Holt JM (1997) Identifying and managing patients with hyperlipidemia. *Am J Manag Care* 3: 1211–1219; quiz 1223–1225

Cooper DL, Murrell DE, Roane DS & Harirforoosh S (2015) Effects of formulation design on niacin therapeutics: mechanism of action, metabolism, and drug delivery. *International Journal of Pharmaceutics* 490: 55–64

Dick J & Thomas PK, (2005) Peripheral Neuropathy. *Elsevier Saunders, fourth edition*. Volume 1. Pages 1-1190.

Di Stefano M, Loreto A, Orsomando G, Mori V, Zamporlini F, Hulse RP, Webster J, Donaldson LF, Gering M, Raffaelli N, *et al* (2017) NMN Deamidase Delays Wallerian Degeneration and Rescues Axonal Defects Caused by NMNAT2 Deficiency In Vivo. *Current Biology* 27: 784–794

Di Stefano M, Nascimento-Ferreira I, Orsomando G, Mori V, Gilley J, Brown R, Janeckova L, Vargas ME, Worrell LA, Loreto A, *et al* (2015) A rise in NAD precursor nicotinamide mononucleotide (NMN) after injury promotes axon degeneration. *Cell Death Differ* 22: 731–742

D'Urso D & M□ller HW (1997) Ins and outs of peripheral myelin protein-22: Mapping transmembrane topology and intracellular sorting. *J Neurosci Res* 49: 551–562

Falls D (2003) Neuregulins: functions, forms, and signaling strategies. *Experimental Cell Research* 284: 14–30
Feltri ML, Poitelon Y & Previtali SC (2016) How Schwann Cells Sort Axons: New Concepts. *Neuroscientist* 22: 252–265

Figley MD, Gu W, Nanson JD, Shi Y, Sasaki Y, Cunnea K, Malde AK, Jia X, Luo Z, Saikot FK, *et al* (2021) SARM1 is a metabolic sensor activated by an increased NMN/NAD+ ratio to trigger axon degeneration. *Neuron* 109: 1118-1136.e11

Figlia G, Gerber D & Suter U (2018) Myelination and mTOR. *Glia* 66: 693–707

Figlia G, Norrmén C, Pereira JA, Gerber D & Suter U (2017) Dual function of the PI3K-Akt-mTORC1 axis in myelination of the peripheral nervous system. *eLife* 6: e29241

Fleck D, van Bebber F, Colombo A, Galante C, Schwenk BM, Rabe L, Hampel H, Novak B, Kremmer E, Tahirovic S, *et al* (2013) Dual Cleavage of Neuregulin 1 Type III by BACE1 and ADAM17 Liberates Its EGF-Like Domain and Allows Paracrine Signaling. *Journal of Neuroscience* 33: 7856–7869

Fledrich R, Stassart RM, Klink A, Rasch LM, Prukop T, Haag L, Czesnik D, Kungl T, Abdelaal TAM, Keric N, *et al* (2014) Soluble neuregulin-1 modulates disease pathogenesis in rodent models of Charcot-Marie-Tooth disease 1A. *Nat Med* 20: 1055–1061

Forese MG, Pellegatta M, Canevazzi P, Gullotta GS, Podini P, Rivellini C, Previtali SC, Bacigaluppi M, Quattrini A & Taveggia C (2020) Prostaglandin D2 synthase modulates macrophage activity and accumulation in injured peripheral nerves. *Glia* 68: 95–110

Fricker FR, Lago N, Balarajah S, Tsantoulas C, Tanna S, Zhu N, Fageiry SK, Jenkins M, Garratt AN, Birchmeier C, *et al* (2011) Axonally Derived Neuregulin-1 Is Required for Remyelination and Regeneration after Nerve Injury in Adulthood. *Journal of Neuroscience* 31: 3225–3233

Ganji SH, Kamanna VS & Kashyap ML (2003) Niacin and cholesterol: role in cardiovascular disease (review). *The Journal of Nutritional Biochemistry* 14: 298–305

Garratt AN, Voiculescu O, Topilko P, Charnay P & Birchmeier C (2000) A Dual Role of erbB2 in Myelination and in Expansion of the Schwann Cell Precursor Pool. *Journal of Cell Biology* 148: 1035–1046

Gerdts J, Brace EJ, Sasaki Y, DiAntonio A & Milbrandt J (2015) SARM1 activation

triggers axon degeneration locally via NAD $^{+}$ destruction. *Science* 348: 453–457

Gerdts J, Summers DW, Milbrandt J & DiAntonio A (2016) Axon Self-Destruction: New Links among SARM1, MAPKs, and NAD+ Metabolism. *Neuron* 89: 449–460

Goebbels S, Oltrogge JH, Wolfer S, Wieser GL, Nientiedt T, Pieper A, Ruhwedel T, Groszer M, Sereda MW & Nave K (2012) Genetic disruption of *Pten* in a novel mouse model of tomaculous neuropathy. *EMBO Mol Med* 4: 486–499

Gomez-Sanchez JA, Carty L, Iruarrizaga-Lejarreta M, Palomo-Irigoyen M, Varela-Rey M, Griffith M, Hantke J, Macias-Camara N, Azkargorta M, Aurrekoetxea I, *et al* (2015) Schwann cell autophagy, myelinophagy, initiates myelin clearance from injured nerves. *Journal of Cell Biology* 210: 153–168

Guerrero-Valero M, Grandi F, Cipriani S, Alberizzi V, Di Guardo R, Chicanne G, Sawade L, Bianchi F, Del Carro U, De Curtis I, *et al* (2021) Dysregulation of myelin synthesis and actomyosin function underlies aberrant myelin in CMT4B1 neuropathy. *Proc Natl Acad Sci USA* 118: e2009469118

Guertin DA, Stevens DM, Thoreen CC, Burds AA, Kalaany NY, Moffat J, Brown M, Fitzgerald KJ & Sabatini DM (2006) Ablation in Mice of the mTORC Components raptor, rictor, or mLST8 Reveals that mTORC2 Is Required for Signaling to Akt-FOXO and PKCα, but Not S6K1. *Developmental Cell* 11: 859–871

Guo J, Wang L, Zhang Y, Wu J, Arpag S, Hu B, Imhof BA, Tian X, Carter BD, Suter U, *et al* (2014) Abnormal junctions and permeability of myelin in PMP22-deficient nerves: Myelin Permeability in HNPP. *Ann Neurol* 75: 255–265

Hanson J, Gille A, Zwykiel S, Lukasova M, Clausen BE, Ahmed K, Tunaru S, Wirth A & Offermanns S (2010) Nicotinic acid– and monomethyl fumarate–induced flushing involves GPR109A expressed by keratinocytes and COX-2–dependent prostanoid formation in mice. *J Clin Invest* 120: 2910–2919

Höke A & Brushart T (2010) Introduction to special issue: Challenges and opportunities for regeneration in the peripheral nervous system. *Experimental Neurology* 223: 1–4

Ilfeld BM, Preciado J & Trescot AM (2016) Novel cryoneurolysis device for the treatment of sensory and motor peripheral nerves. *Expert Rev Med Devices* 13: 713–725

Ino D & Iino M (2017) Schwann cell mitochondria as key regulators in the development and maintenance of peripheral nerve axons. *Cell Mol Life Sci* 74: 827–835

Ito MK (2002) Niacin-based therapy for dyslipidemia: past evidence and future advances. *Am J Manag Care* 8: S315-322

Iwakura Y & Nawa H (2013) ErbB1-4-dependent EGF/neuregulin signals and their cross talk in the central nervous system: pathological implications in schizophrenia and Parkinson's disease. *Front Cell Neurosci* 7

Jacinto E, Facchinetti V, Liu D, Soto N, Wei S, Jung SY, Huang Q, Qin J & Su B (2006) SIN1/MIP1 Maintains rictor-mTOR Complex Integrity and Regulates Akt Phosphorylation and Substrate Specificity. *Cell* 127: 125–137

Jessen KR & Arthur-Farraj P (2019) Repair Schwann cell update: Adaptive reprogramming, EMT, and stemness in regenerating nerves. *Glia* 67: 421–437

Jessen KR & Mirsky R (2005) The origin and development of glial cells in peripheral nerves. *Nat Rev Neurosci* 6: 671–682

Jessen KR & Mirsky R (2016) The repair Schwann cell and its function in regenerating nerves: Repair Schwann cell and its function in regenerating nerves. *J Physiol* 594: 3521–3531

Jessen KR & Mirsky R (2019) The Success and Failure of the Schwann Cell Response to Nerve Injury. *Front Cell Neurosci* 13: 33

Jessen KR, Mirsky R & Lloyd AC (2015) Schwann Cells: Development and Role in Nerve Repair. *Cold Spring Harb Perspect Biol* 7: a020487

Jung J, Cai W, Lee HK, Pellegatta M, Shin YK, Jang SY, Suh DJ, Wrabetz L, Feltri ML & Park HT (2011) Actin Polymerization Is Essential for Myelin Sheath Fragmentation during Wallerian Degeneration. *Journal of Neuroscience* 31: 2009–2015

Kidd GJ, Ohno N & Trapp BD (2013) Biology of Schwann cells. In *Handbook of Clinical Neurology* pp 55–79. Elsevier

Klein D & Martini R (2016) Myelin and macrophages in the PNS: An intimate relationship in trauma and disease. *Brain Research* 1641: 130–138

La Marca R, Cerri F, Horiuchi K, Bachi A, Feltri ML, Wrabetz L, Blobel CP, Quattrini A, Salzer JL & Taveggia C (2011) TACE (ADAM17) inhibits Schwann cell myelination. *Nat Neurosci* 14: 857–865

Li J, Parker B, Martyn C, Natarajan C & Guo J (2013) The PMP22 gene and its related diseases. *Mol Neurobiol* 47: 673–698

Liberzon A, Birger C, Thorvaldsdóttir H, Ghandi M, Mesirov JP & Tamayo P (2015) The Molecular Signatures Database Hallmark Gene Set Collection. *Cell Systems* 1: 417–425

MacKay D, Hathcock J & Guarneri E (2012) Niacin: chemical forms, bioavailability, and health effects. *Nutrition Reviews* 70: 357–366

Manor J, Calame DG, Gijavanekar C, Tran A, Fatih JM, Lalani SR, Mizerik E, Parnes M, Mehta VP, Adesina AM, *et al* (2022) Niacin therapy improves outcome and normalizes metabolic abnormalities in an NAXD-deficient patient. *Brain* 145: e36–e40

Martini R, Fischer S, López-Vales R & David S (2008) Interactions between Schwann cells and macrophages in injury and inherited demyelinating disease. *Glia* 56: 1566–1577

Mei L & Nave K-A (2014) Neuregulin-ERBB Signaling in the Nervous System and Neuropsychiatric Diseases. *Neuron* 83: 27–49

Michailov GV, Sereda MW, Brinkmann BG, Fischer TM, Haug B, Birchmeier C, Role L, Lai C, Schwab MH & Nave K-A (2004) Axonal Neuregulin-1 Regulates Myelin Sheath Thickness. *Science* 304: 700–703

Montani L, Pereira JA, Norrmén C, Pohl HBF, Tinelli E, Trötzmüller M, Figlia G, Dimas P, von Niederhäusern B, Schwager R, *et al* (2018) De novo fatty acid synthesis by Schwann cells is essential for peripheral nervous system myelination. *Journal of Cell Biology* 217: 1353–1368

Mueller M, Wacker K, Ringelstein EB, Hickey WF, Imai Y & Kiefer R (2001) Rapid Response of Identified Resident Endoneurial Macrophages to Nerve Injury. *The American Journal of Pathology* 159: 2187–2197

Nagappa M, Sharma S & Taly AB (2022) Charcot Marie Tooth. In *StatPearls* Treasure Island (FL): StatPearls Publishing

Napoli I, Noon LA, Ribeiro S, Kerai AP, Parrinello S, Rosenberg LH, Collins MJ, Harrisingh MC, White IJ, Woodhoo A, *et al* (2012) A Central Role for the ERK-Signaling Pathway in Controlling Schwann Cell Plasticity and Peripheral Nerve Regeneration In Vivo. *Neuron* 73: 729–742

Nave K-A (2010) Myelination and the trophic support of long axons. *Nat Rev Neurosci.* 11: 275–283

Nave K-A & Salzer JL (2006) Axonal regulation of myelination by neuregulin 1. *Current Opinion in Neurobiology* 16: 492–500

Nikiforov A, Kulikova V & Ziegler M (2015) The human NAD metabolome: Functions, metabolism and compartmentalization. *Crit Rev Biochem Mol Biol* 50: 284–297

Nocera G & Jacob C (2020) Mechanisms of Schwann cell plasticity involved in peripheral nerve repair after injury. *Cell Mol Life Sci* 77: 3977–3989

Norrmén C, Figlia G, Pfistner P, Pereira JA, Bachofner S & Suter U (2018) mTORC1 Is Transiently Reactivated in Injured Nerves to Promote c-Jun Elevation and Schwann Cell Dedifferentiation. *J Neurosci* 38: 4811–4828

Norrmén C & Suter U (2013) Akt/mTOR signalling in myelination. *Biochm Soc Trans* 41: 944–950

Notterpek L, Roux KJ, Amici SA, Yazdanpour A, Rahner C & Fletcher BS (2001) Peripheral myelin protein 22 is a constituent of intercellular junctions in epithelia. *Proc Natl Acad Sci USA* 98: 14404–14409

Offermanns S & Schwaninger M (2015) Nutritional or pharmacological activation of HCA(2) ameliorates neuroinflammation. *Trends Mol Med* 21: 245–255

Pareyson D & Marchesi C (2009) Diagnosis, natural history, and management of Charcot–Marie–Tooth disease. *The Lancet Neurology* 8: 654–667

Pereira JA, Lebrun-Julien F & Suter U (2012) Molecular mechanisms regulating myelination in the peripheral nervous system. *Trends in Neurosciences* 35: 123–134

Peschon JJ, Slack JL, Reddy P, Stocking KL, Sunnarborg SW, Lee DC, Russell WE, Castner BJ, Johnson RS, Fitzner JN, *et al* (1998) An Essential Role for Ectodomain Shedding in Mammalian Development. *Science* 282: 1281–1284

Pieper JA (2003) Overview of niacin formulations: Differences in pharmacokinetics, efficacy, and safety. *American Journal of Health-System Pharmacy* 60: S9–S14

Pirinen E, Auranen M, Khan NA, Brilhante V, Urho N, Pessia A, Hakkarainen A, Kuula J, Heinonen U, Schmidt MS, *et al* (2020) Niacin Cures Systemic NAD+ Deficiency and Improves Muscle Performance in Adult-Onset Mitochondrial Myopathy. *Cell Metabolism* 31: 1078-1090.e5

Previtali SC, Quattrini A & Bolino A (2007) Charcot–Marie–Tooth type 4B demyelinating neuropathy: deciphering the role of MTMR phosphatases. *Expert Rev Mol Med* 9: 1–16

Rao SNR & Pearse DD (2016) Regulating Axonal Responses to Injury: The Intersection between Signaling Pathways Involved in Axon Myelination and The Inhibition of Axon Regeneration. *Front Mol Neurosci* 9

Rawji KS, Young AMH, Ghosh T, Michaels NJ, Mirzaei R, Kappen J, Kolehmainen KL, Alaeiilkhchi N, Lozinski B, Mishra MK, *et al* (2020) Niacin-mediated rejuvenation of macrophage/microglia enhances remyelination of the aging central nervous system. *Acta Neuropathol* 139: 893–909

Rossor AM, Tomaselli PJ & Reilly MM (2016) Recent advances in the genetic neuropathies. *Current Opinion in Neurology* 29: 537–548

Rossor AM & Reilly MM (2022) Blood biomarkers of peripheral neuropathy. *Acta Neuro Scandinavica* 146: 325–331

Salzer JL (2003) Polarized Domains of Myelinated Axons. *Neuron* 40: 297–318

Salzer JL (2015) Schwann Cell Myelination. *Cold Spring Harb Perspect Biol* 7: a020529

Salzer JL, Brophy PJ & Peles E (2008) Molecular domains of myelinated axons in the peripheral nervous system. *Glia* 56: 1532–1540

Sasaki Y, Nakagawa T, Mao X, DiAntonio A & Milbrandt J (2016) NMNAT1 inhibits axon degeneration via blockade of SARM1-mediated NAD+ depletion. *eLife* 5: e19749

Sawade L, Grandi F, Mignanelli M, Patiño-López G, Klinkert K, Langa-Vives F, Di Guardo R, Echard A, Bolino A & Haucke V (2020) Rab35-regulated lipid turnover by myotubularins represses mTORC1 activity and controls myelin growth. *Nat Commun* 11: 2835

Sherman DL & Brophy PJ (2005) Mechanisms of axon ensheathment and myelin growth. *Nat Rev Neurosci* 6: 683–690

Sherman DL, Krols M, Wu L-MN, Grove M, Nave K-A, Gangloff Y-G & Brophy PJ (2012) Arrest of Myelination and Reduced Axon Growth When Schwann Cells Lack mTOR. *Journal of Neuroscience* 32: 1817–1825

Shin YK, Jang SY, Park JY, Park SY, Lee HJ, Suh DJ & Park HT (2013) The Neuregulin-Rac-MKK7 pathway regulates antagonistic c-jun/Krox20 expression in Schwann cell dedifferentiation: Rac in Schwann Cell Responses to Injury. *Glia* 61: 892–904

Stassart RM, Fledrich R, Velanac V, Brinkmann BG, Schwab MH, Meijer D, Sereda MW & Nave K-A (2013) A role for Schwann cell–derived neuregulin-1 in remyelination. *Nat Neurosci* 16: 48–54

Stassart RM, Möbius W, Nave K-A & Edgar JM (2018) The Axon-Myelin Unit in Development and Degenerative Disease. *Front Neurosci* 12: 467

Stassart RM & Woodhoo A (2021) Axo-glial interaction in the injured PNS. *Develop Neurobiol* 81: 490–506

Stavrou M, Sargiannidou I, Georgiou E, Kagiava A & Kleopa KA (2021) Emerging Therapies for Charcot-Marie-Tooth Inherited Neuropathies. *IJMS* 22: 6048

Stierli S, Imperatore V & Lloyd AC (2019) Schwann cell plasticity-roles in tissue homeostasis, regeneration, and disease. *Glia* 67: 2203–2215

Stratton J & Shah P (2016) Macrophage polarization in nerve injury: do Schwann cells play a role? *Neural Regen Res* 11: 53

Taveggia C, Zanazzi G, Petrylak A, Yano H, Rosenbluth J, Einheber S, Xu X, Esper RM, Loeb JA, Shrager P, *et al* (2005) Neuregulin-1 Type III Determines the Ensheathment Fate of Axons. *Neuron* 47: 681–694

Trapp BD & Kidd GJ (2004) Structure of the Myelinated Axon. In *Myelin Biology and Disorders* pp 3–27. Elsevier

Tricaud N & Park HT (2017) Wallerian demyelination: chronicle of a cellular cataclysm. *Cell Mol Life Sci* 74: 4049–4057

Villines TC, Kim AS, Gore RS & Taylor AJ (2012) Niacin: The Evidence, Clinical Use, and Future Directions. *Curr Atheroscler Rep* 14: 49–59

Willem M, Garratt AN, Novak B, Citron M, Kaufmann S, Rittger A, DeStrooper B, Saftig P, Birchmeier C & Haass C (2006) Control of Peripheral Nerve Myelination by the ß-Secretase BACE1. *Science* 314: 664–666

Wolpowitz D, Mason TBA, Dietrich P, Mendelsohn M, Talmage DA & Role LW (2000)

Cysteine-Rich Domain Isoforms of the Neuregulin-1 Gene Are Required for Maintenance of Peripheral Synapses. *Neuron* 25: 79–91

Woodhoo A, Alonso MBD, Droggiti A, Turmaine M, D'Antonio M, Parkinson DB, Wilton DK, Al-Shawi R, Simons P, Shen J, *et al* (2009) Notch controls embryonic Schwann cell differentiation, postnatal myelination and adult plasticity. *Nat Neurosci* 12: 839–847

Xie W, Chen B & Wong J (2021) Evolution of the market for mRNA technology. *Nat Rev Drug Discov* 20: 735–736

Ydens E, Amann L, Asselbergh B, Scott CL, Martens L, Sichien D, Mossad O, Blank T, De Prijck S, Low D, *et al* (2020) Profiling peripheral nerve macrophages reveals two macrophage subsets with distinct localization, transcriptome and response to injury. *Nat Neurosci* 23: 676–689

Zambon AA, Natali Sora MG, Cantarella G, Cerri F, Quattrini A, Comi G, Previtali SC & Bolino A (2017) Vocal cord paralysis in Charcot–Marie–Tooth type 4b1 disease associated with a novel mutation in the myotubularin-related protein 2 gene: A case report and review of the literature. *Neuromuscular Disorders* 27: 487–491